1992

A computational technique for burner balancing in coal-fired power plants

Richard A. Curran
Lehigh University

AUTHOR: Curran, Richard A.

TITLE:

A Computational Technique for Burner Balancing in Coal-Fired Power Plants

DATE: May 31, 1992

A COMPUTATIONAL TECHNIQUE FOR BURNER BALANCING IN COAL-FIRED POWER PLANTS

by

Richard A. Curran

A Thesis

Presented to the Graduate Committee

of Lehigh University

in Candidacy for the Degree of

Master of Science

in

Mechanical Engineering

Lehigh University

April, 1992

CERTIFICATE OF APPROVAL

This thesis is accepted and approved in partial fulfillment of the requirements for the degree of Master of Science.

April 30 1992
Date

Professor Edward K. Levy
Thesis Advisor

Professor Robert P. Wei
Chairman of Department

ACKNOWLEDGEMENTS

I would like to express my gratitude to my advisor, Dr. Edward Levy, for creating the research position which sponsored my graduate studies. I will always be grateful to him for his faith in me.

I would also like to express my gratitude to Mr. Mark D'Agostini for acting as my mentor, and for answering all of my questions.

Thanks to my computer guru, Mr. Chris Muir, for his many helpful programming suggestions.

Thanks to Mr. George Robinson of the Metropolitan Edison Division of General Public Utilities for his hospitality during my visits to Portland Generating Station.

Many thanks to my office comrades, Mr. Gary Schulze, Mr. Xiabo Huang, and my roommate, Mr. Tim Schmitt, for their encouragement and good humor.

I would like to express my sincerest appreciation to my family: Tom, Kathy, Grandmom, Pop, and Aunt Eileen, for all of their love and encouragement. I would especially like to thank my parents for their love and support for as long as I can remember, and for always encouraging me to pursue my dreams.

For Wendy, and our walk in the sun.

TABLE OF CONTENTS

LIST OF FIGURES

NOMENCLATURE

A/F	Air to fuel ratio, by mass flow rate.
C_{DS}	Drag coefficient on a single particle.
D	Pipe diameter (ft).
d_o	Diameter of orifice plate opening (ft).
d_p	Average particle diameter (ft).
dF_d	Drag force on the particles in pipe section dL.
dF_f	Force due to friction acting on the solids in pipe section dL.
dF_g	Net gravitational force acting on the particles in pipe section dL.
dL	Differential length of conveying pipe.
dM_s'	Total solids weight in pipe section dL.
dN	Total number of solid particles in pipe section dL.
e/D	Relative roughness of the pipeline material (dimensionless).
f_g	Gas friction factor.
f_p	Solids friction factor, $f_p=4f_s$.
Fr	Froude number.
g	Gravitational acceleration (ft/sec^2).
i	Pipeline designator.
j	Pipeline section designator.
K, K_e, K_o	Coefficients used in orifice plate calculations.
L	Pipe length (ft).
l	Integration acceleration length, used in

Eqs. (3-25), (3-26), & (3-27).

L_A	Particle acceleration length (ft).
L_e	Effective length, $L_e=L-L_A$.
$m_{a,i}$	Air mass flow rate per pipeline (lbm/sec).
$m_{c,i}$	Coal mass flow rate per pipeline (lbm/sec).
$M_{c,T}$	Total coal mass flow rate in system (lbm/sec).
N	Number of burners supplied by one pulverizer.
ΔP_A	Pressure drop due to acceleration effects (psi).
$\Delta P_{B,T}$	Total pressure drop through a pipe elbow (psi).
$\Delta P_{B,a}$	Pressure drop in elbow due to gas (psi).
$\Delta P_{B,s}$	Pressure drop in elbow due to solid particles (psi).
ΔP_F	Total frictional pressure drop (psi).
ΔP_{Fg}	Frictional pressure drop due to gas flow (psi).
ΔP_{Fs}	Frictional pressure drop due to solid particles (psi).
ΔP_{OP}	Pressure drop across an orifice plate (psi).
ΔP_{Res}	The additional flow resistance which must be added to a pipe to equalize flow (psi).
ΔP_S	Pressure drop due to static head (psi).
ΔP_T	Total pressure drop (psi).
r	Pipe radius (ft).
r_c	Radius of curvature (ft).
Re	Reynolds number.

Re_p	Particle Reynolds number.
Re_t	Terminal Reynolds number, based upon U_t and d_p.
U_f	Actual gas velocity (ft/sec).
U_o	Superficial gas velocity (ft/sec).
U_p	Particle velocity (ft/sec).
U_{p1}	Lower limit of acceleration length integration.
U_{p2}	Upper limit of accleration length integration.
U_t	Terminal velocity of a single particle falling through an infinite fluid (ft/sec).
W_s	Solids mass flow rate (lbm/sec).
y_i	Coal mass flow fraction received by pipeline i.

GREEK

α	Coefficient in orifice plate calculations (see Eq.4-8).
β	Ratio of d_o/D; used in orifice plate calculations.
$\gamma_{B,a}$	Loss factor for air flow through elbow (dimensionless).
$\gamma_{B,s}$	Loss factor for solid particle flow through an elbow (dimensionless).
$\gamma_{B,T}$	Total loss factor for flow through elbow (dimensionless).
γ_c	Coal specific gravity.
ε	Voidage fraction (dimensionless).

η	Orifice plate discharge coefficient.
π	Arccos(-1).
ρ_f	Gas density (lbm/ft^3).
ρ_p	Particle density (lbm/ft^3).
μ	Gas viscosity (lbm/ft/sec).

ABSTRACT

In many coal-fired electric power plants, a single pulverizer supplies fuel to numerous burners. Due to geometrical differences between the pulverized coal transport pipes, the flow of coal and conveying air are usually not equally distributed. The coal flow imbalances result in non-uniform combustion within the furnace, causing a negative impact on unit performance and increased NO_x emissions.

This thesis examines a computational technique for burner balancing based upon pressure losses in pneumatic transport. Utilizing gas-solids pressure drop correlations developed by Yang and Michaelides, a computer code is presented which analyzes the performance of a system of coal pipes.

Using typical power plant operational data, a sample pipeline system is analyzed to determine the orifice plates required to balance the coal flow distribution and determine the unbalanced coal mass flow rates.

The correlations used in the code have a typical accuracy of 30 percent, and the substitution of different elbow correlations into the code produced coal flow deviations of up to 40 percent. The variation of operational parameters such as particle size and pipe roughness generated deviations of up to 7 percent and 15 percent, respectively. Field studies should be performed to ascertain the accuracy of these predictions, and the validity of this balancing technique.

1. INTRODUCTION

1.1 Electric Power Plant Coal Distribution System

When coal arrives at an electric power plant, it is seldom in the optimum condition for combustion. Initially stored in bunkers outside of the plant, it is both too large in size and too high in moisture content to be efficiently utilized. Thus before it is sent to the furnace, it is transported via mechanical conveyor belts to large crushing machines known as pulverizers. The pulverizer reduces the size of the coal particles from inches to particles typically less than 100 microns. As the coal's size is reduced, the surface area available for heat transfer increases, which yields a more efficient combustion process. Figure 1-1 displays a typical pulverizer built by Babcock & Wilcox.

When the coal has been properly sized, it exits the pulverizer and is sent to a large centrifugal fan called an exhauster, diagramed in Figure 1-2. The exhauster transports the coal pneumatically to the furnace in pipes along with primary air. The transport, or primary, air is combined with secondary air (supplied from another fan system) to provide all of the oxygen necessary for complete combustion of the fuel. Many exhausters receive air which has already been preheated by the plant's air heaters, typically to 500 to 600 degrees Fahrenheit, a temperature which is too high to safely transport the potentially volatile coal particles. Therefore,

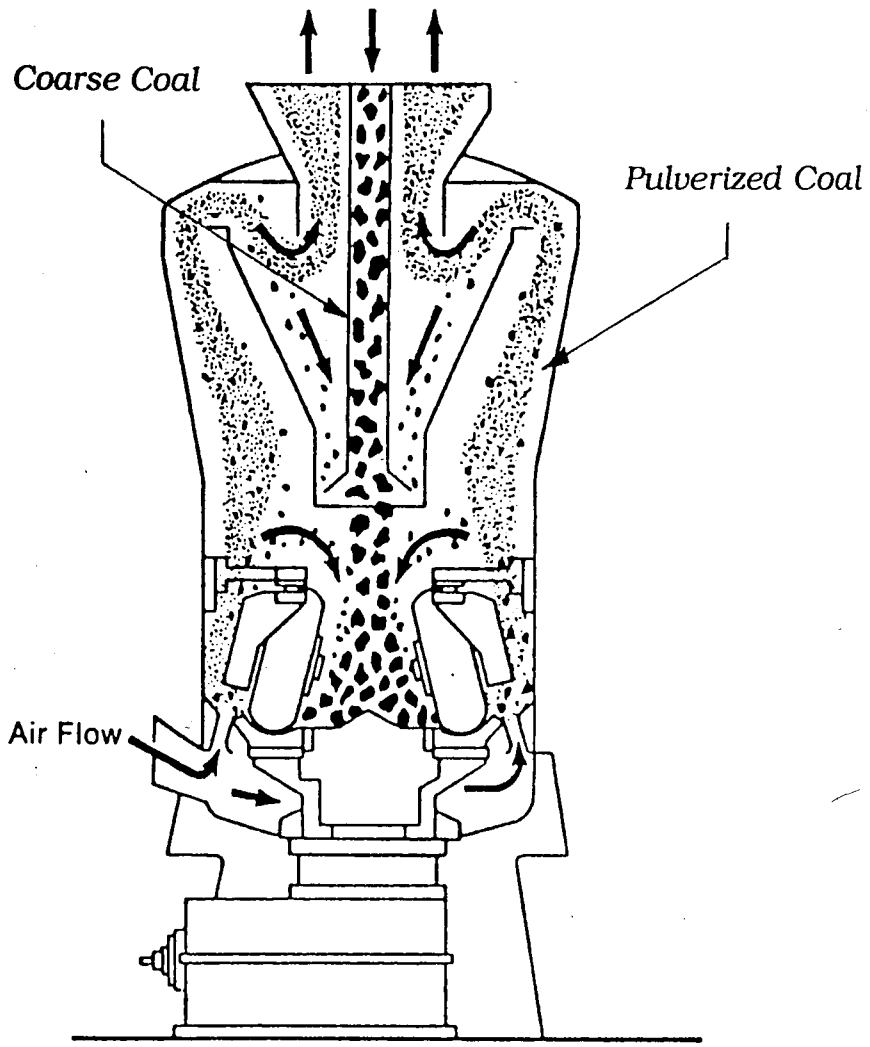

Figure (1-1) Babcock & Wilcox coal pulverizer.

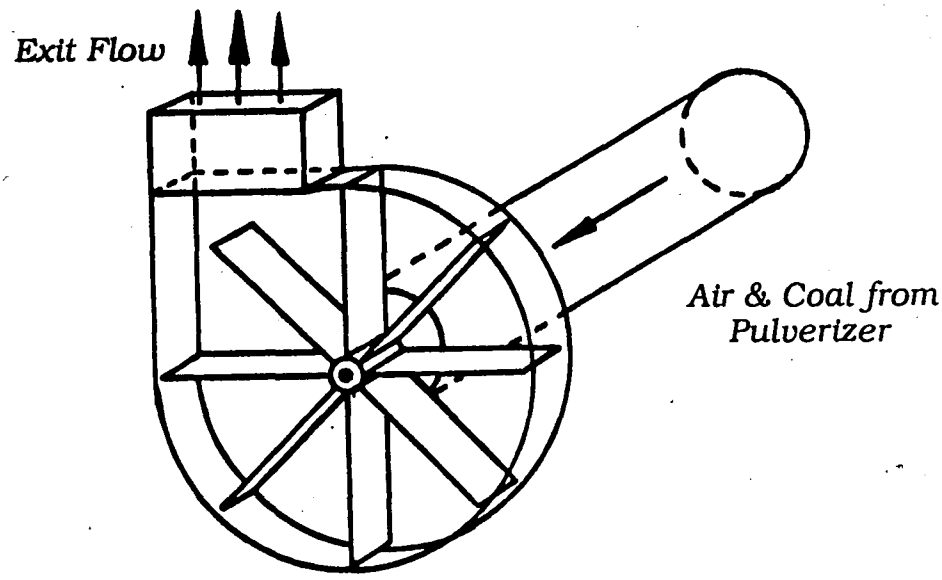

Figure (1-2) Schematic of a typical centrifugal exhauster.

this air is combined with tempering air from the surroundings to achieve an optimum transport temperature, which will serve to evaporate as much moisture from the coal as possible without the threat of spontaneous combustion. Additionally, the preheated air serves to improve the thermodynamic operating efficiency of the overall plant. Transport air temperatures typically are on the order of 150 to 170 degrees Fahrenheit.

Upon exiting the exhauster, the pulverized coal and primary air are transported via cylindrical pipelines to the furnace windboxes, as shown in Figure 1-3. However, one

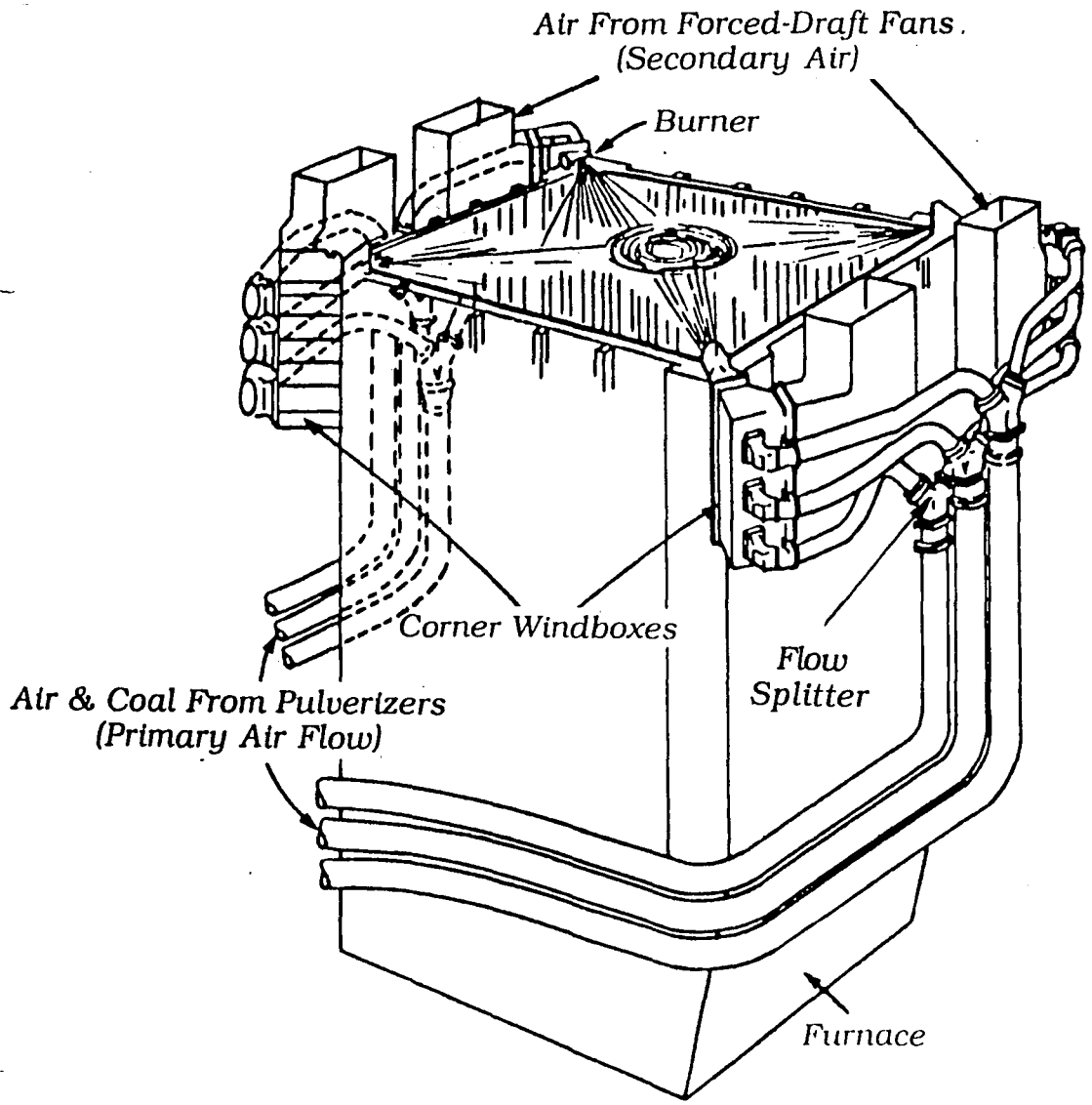

Figure (1-3) Air and coal flow distribution for a tangentially-fired steam generator.

pulverizer-exhauster combination may supply fuel to as many as eight burners at one level in the furnace. This is achieved by utilizing a distribution system which is diagrammed in Figure 1-4. The air-fuel mixture exits the exhauster into a pipe of a given diameter, D_1. This pipe delivers the flow to a device called a coal riffler, which is intended to divide the flow into two equal parts. Figure 1-5 reveals the typical construction of a coal riffler. Upon exiting the riffler, the flow is again transported via pipes whose diameter has been reduced to D_2. Following Figure 1-4, the pipelines again encounter rifflers, splitting the initial flow into four components, each traveling in a pipeline whose diameter has again been reduced, from D_2 to D_3. Having been thus divided, the flow in each pipeline is delivered to the furnace. Due to the complexity of the plant's structure and the varying locations of the individual burners, each pipeline supplied by a pulverizer has a unique shape composed of horizontal, vertical, and elbow sections.

1.2 The Problem of Burner Imbalance

Because of the geometrical differences between the coal pipes supplied by a pulverizer, the coal flow is not equally distributed to the burners. The pipeline which connects the pulverizer to the furthest burner usually receives the least amount of coal, while the shortest pipeline receives the largest coal flow rate. These differences are due to the

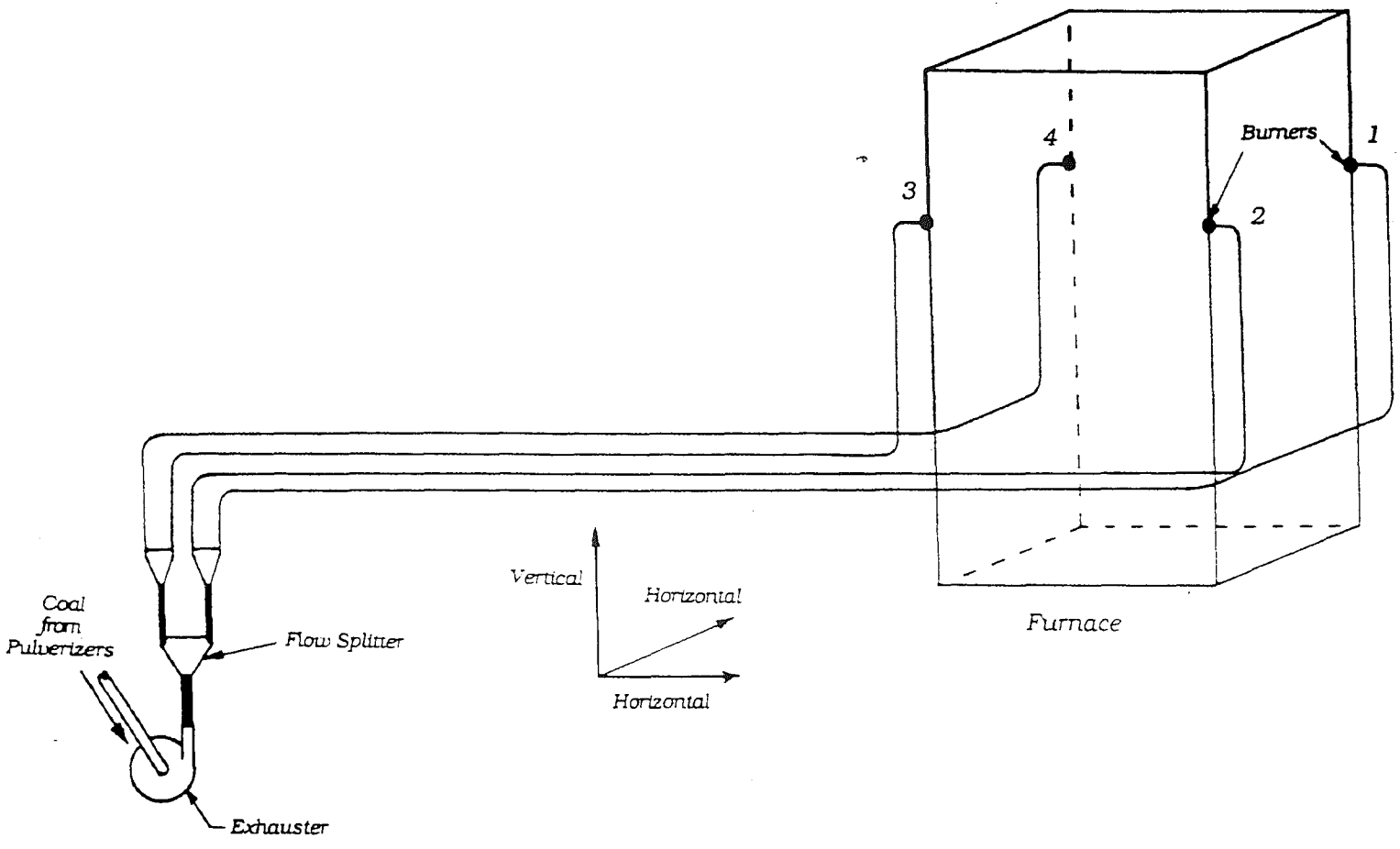

Figure (1-4) Schematic representation of a pulverized coal pipeline system for a tangentially-fired furnace.

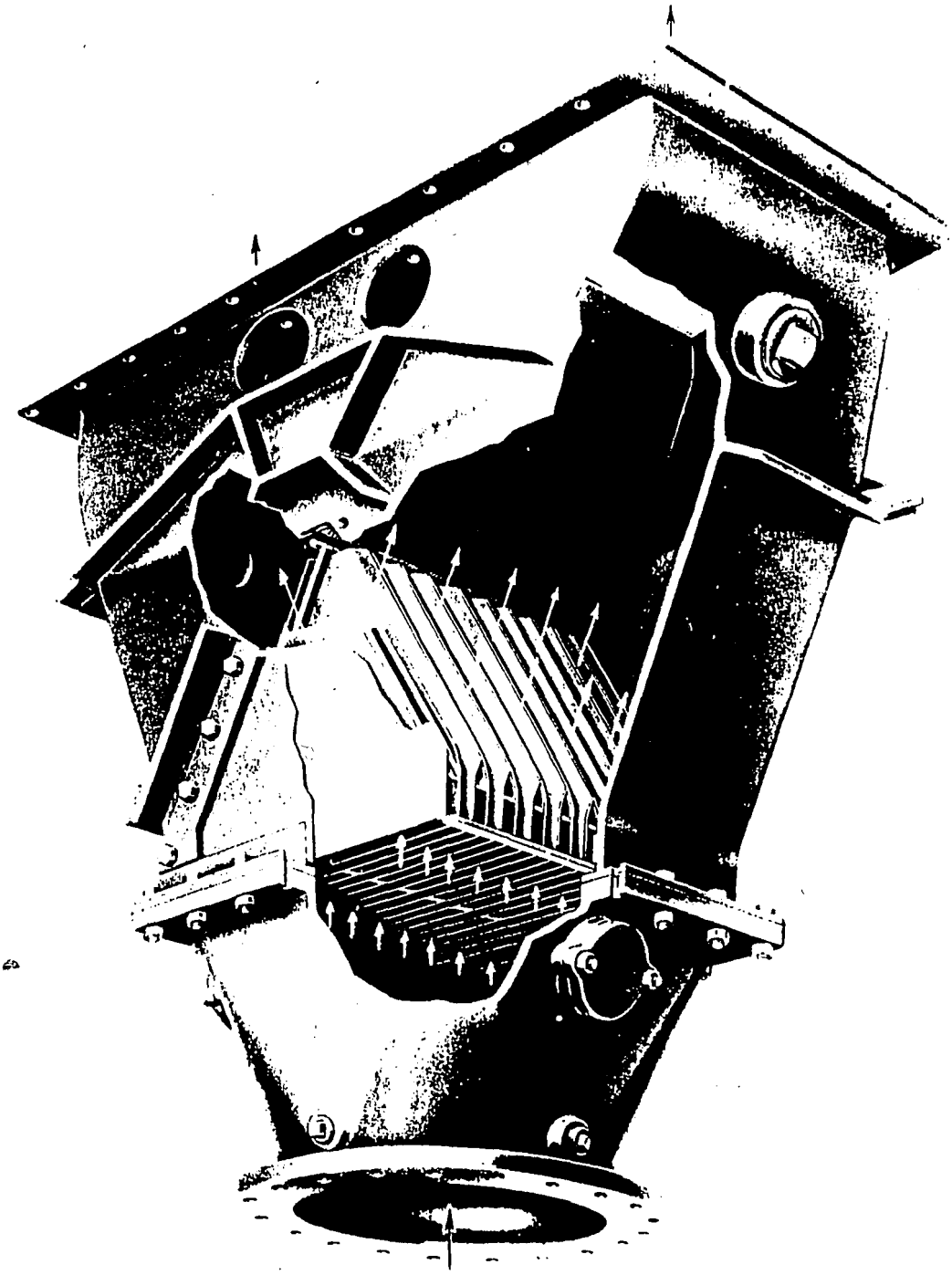

Figure (1-5) Combustion Engineering coal riffler.

different flow resistances presented by the pipelines. This maldistribution results in a different air-fuel ratio for each of the burners at a given level of the furnace, which leads to non-uniform combustion. More specifically, coal flow imbalances are suspected to have the following effects on plant performance:

- Higher unburned carbon levels contained in the flue gas ash, signifying a heat rate penalty. In addition, excessive amounts of carbon in the fly ash render the ash unsuitable for resale.

- Higher levels of thermal nitrous oxides formed due to some burners firing at too high of a temperature.

- Higher levels of reactant nitrous oxides formed due to burners firing above stoichiometric conditions, providing an excess of oxygen to bond with the available nitrogen.

- Burners operating at varying air-fuel ratios produce an uneven temperature distribution in the furnace, resulting in uneven steam temperatures.

- Slag formation, and its resultant fouling of the furnace, has been shown to be greater around the burners which operate fuel-rich.

- Slagging and uneven temperatures can result in steam tube failures.

- Burners operating fuel-lean may experience flame tip instability causing the potential for a "flashback" of fire into the conveying pipelines.

- Pipeline and equipment erosion rates increase in pipelines which receive an excess of coal flow.

Obviously, burner imbalance can become an immense problem for electric utilities due to the heat rate penalties and higher potential for failure outages. In addition, the

Clean Air Act Amendments of 1990 have presented power plants with new standards of combustion performance which must be achieved. Current methods for burner balancing depend heavily upon trial and error procedures and the techniques used do not necessarily result in a well balanced condition.

1.3 Proposed Solution

This thesis presents a computational procedure for balancing the fuel distribution in coal-fired power plants. Using equations which govern the flow of gas-solid mixtures, a computer code is developed which determines the flow resistance of each pipeline in the coal distribution system. A method of equalizing these resistances is presented, as well as a procedure to determine the performance of an existing pipeline system.

A similar computational method based upon pipeline pressure loss is currently utilized by Humbug Mountain Research Laboratories [4] to determine burner balance. This thesis investigates the uncertainties inherent in this technique and provides an assessment of the degree to which burner balance can be achieved by this procedure.

2. GAS-SOLID FLOW

2.1 Fundamentals of Gas-Solid Flow

2.1.1 Flow Qualification

In clean air flow through a pipe, the most common parameter used to describe the flow is the Reynolds number, which is the ratio of the inertial to viscous effects acting upon the flow:

$$Re = \frac{\rho_f V_o D}{\mu} \qquad (2\text{-}1)$$

For the pneumatic transport of coal, Re ranges from 100,000 to 1,000,000, indicating that the flow is in the fully turbulent regime. This allows a one-dimensional (axial) flow assumption. In addition, due to the low air temperature range and air velocities on the order of 100 ft/s, the flow has very low Mach numbers and can be treated as an incomprehensible fluid.

When solid particles are added to the air stream the characteristics of the flow change. The most informative parameter for describing the gas-solid flow is the loading ratio: lbm of solids to lbm of air. Zenz & Othmer [1] provide the following explanation of the effect of the loading ratio upon pneumatic transport. Consider the horizontal pipe flow described in Figure (2-1), where the pressure drop per unit length of pipe is plotted versus the superficial gas

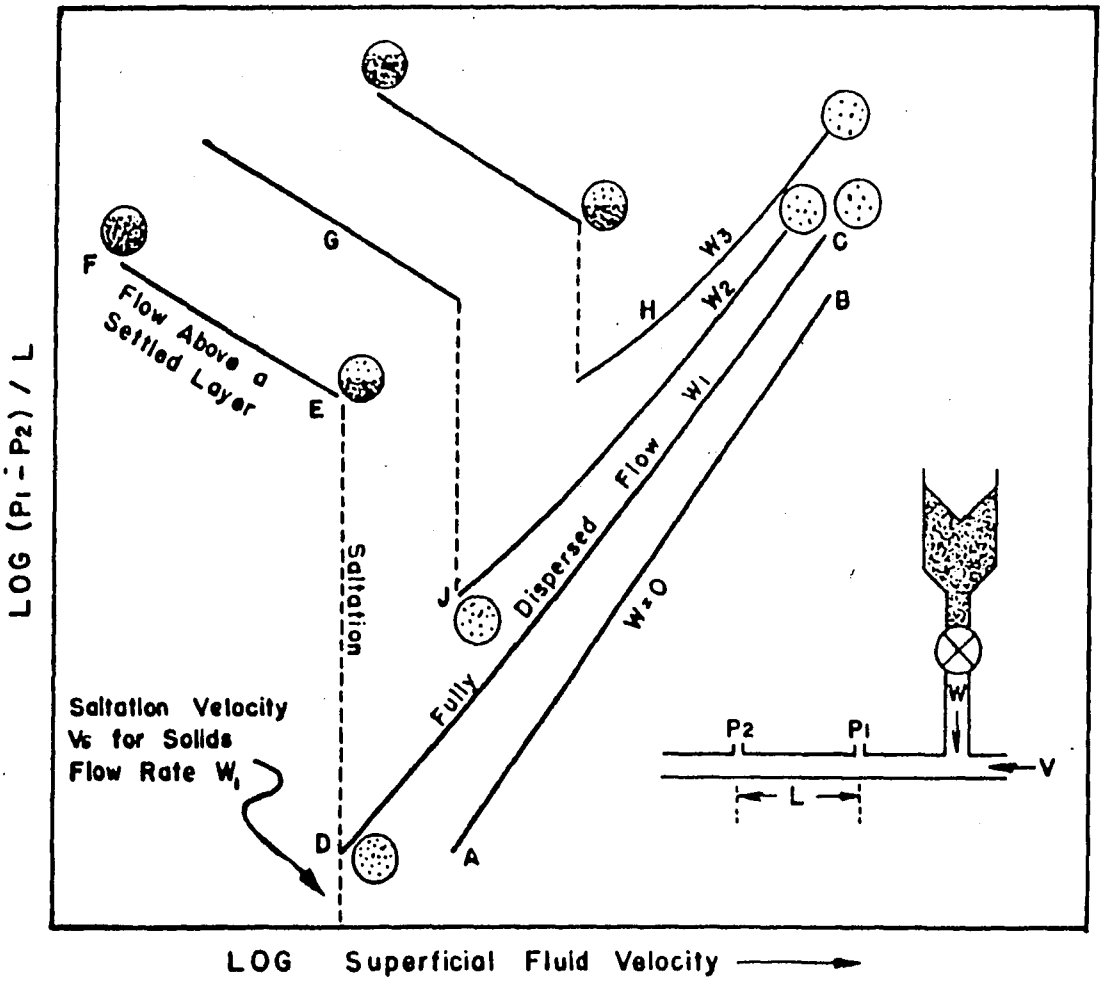

Figure (2-1) Schematic representation of fluid-solids flow characteristics in horizontal transport.

velocity. Line AB represents pipe flow with no solid particles present, i.e. clean air flow. As would be expected, the pressure drop increases as the velocity increases due to frictional losses. However, at identical high velocities, such as points B and C, the addition of solid particles increases the clean-air pressure drop due to the extra energy required to transport the solids.

Now following along line CD, a decrease in flow velocity eventually causes the pressure drop to reach a minimum at which all of the solids will no longer remain entrained in the flow. The velocity at this point (D) is called the saltation velocity. This quantity is highly dependent upon the loading ratio, as shown by the performance of the flows with loadings of W_2 and W_3. Saltation represents a severe discontinuity in the flow due to the fact that it creates an unsteady flow during which some of the solids settles out of the flow stream. Eventually, an equilibrium point is reached, shown as point E on Figure (2-1), where the gas-solid flow now moves above the layer of settled particles. However, further reductions in flow velocity cause the settled layer to grow larger. At this point, the pressure drop begins to increase as the velocity is further decreased, reversing its behavior prior to the onset of saltation. Wen & Simons [2] have presented their visual observations of the progression of saltation from a fully entrained gas-solid flow to one in which the pipe has become fully plugged (See Figure (2-2)).

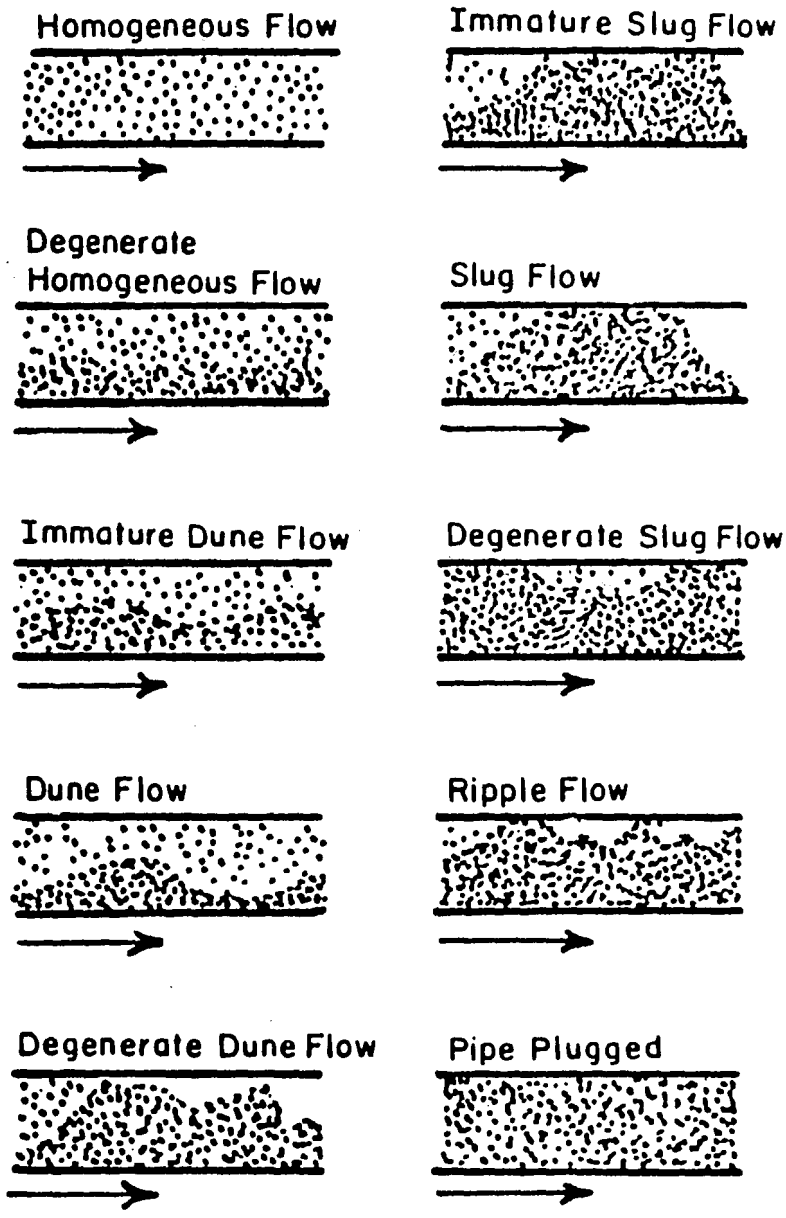

Figure (2-2) Visual observations of saltation patterns.

Vertical pipelines also display a saturation condition which limits their performance in pneumatic transport. Although similar in behavior to horizontal saltation, vertical conveying does not experience the unsteadiness associated with horizontal flow. Figure (2-3), as presented by Zenz & Othmer [1], shows the flow characteristics of vertical pipeline transport. When clean air is flowing, the behavior is identical to that in horizontal clean air flow. And also similar to horizontal flow, the addition of solid particles at a specific high velocity, such as points B and C, causes an increase in pressure drop with an increase in solids loading rate.

However, the similarity ends as the flow velocity is decreased to its minimum pressure loss value. In horizontal transport, this point would indicate the onset of saltation. But in vertical conveying, no flow discontinuity occurs. This point, shown as point D in Figure (2-3), corresponds to a situation in which the loss due to the gravitational static head begins to exceed the frictional losses. Below this velocity, the pressure drop increases with decreasing flow speed, until an absolute minimum velocity is reached. At this point, the fluid can no longer support the flow of solids and the suspension collapses, creating a slug flow regime. The onset of this condition corresponds to a flow speed known as the choking velocity. In Figure (2-3), the loading ratio at point E is the saturation transport capacity of the flow at

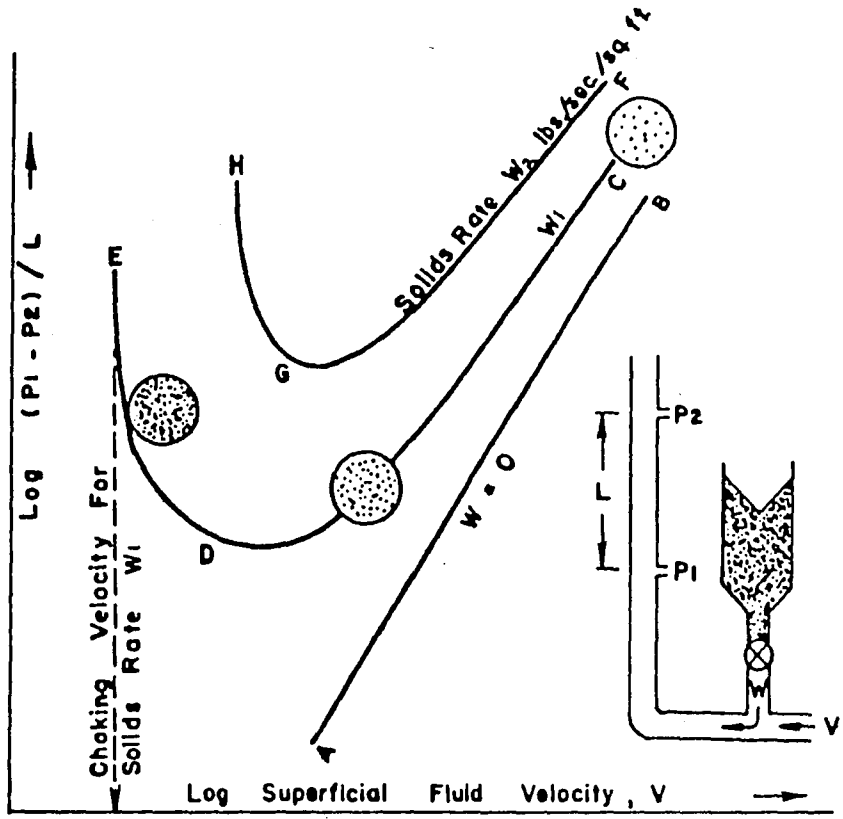

Figure (2-3) Schematic representation of flow characteristics in vertical transport.

It has been shown that for both horizontal and vertical transport, the relationship between pressure drop and flow velocity contains a point where the pressure loss is minimized. Although this point is more distinct in horizontal flow due to the resultant discontinuity, in both cases it indicates the onset of a moving bed of solids rather than a suspension of entrained particles. Klinzing [3] recommends that this minimum pressure drop point be used as the dividing point between dense-phase and dilute-phase pneumatic transport. Accordingly, for this thesis, the term dilute-phase transport will correspond to flow conditions in which the pressure drop per unit length in a pipeline increases as the superficial fluid velocity increases. In Figures (2-1) and (2-3), the region to the right of point D is dilute flow at the solids loading rate of W_1.

2.1.2 Effect of Particles Upon the Flow

In dilute-phase transport, many of the flow qualities, and quantities, depend upon the physical characteristics of the solid particles which are conveyed. One of the most common parameters used to quantify the effect of the solid particle presence is the particle terminal velocity, a measure of the maximum speed a solid particle will attain if allowed to free-fall in an infinite section of the conveying fluid, which is at rest. Several correlations have been published for this velocity and a unified approach was presented by Zenz

& Othmer [1] as

$$U_t = \frac{0.153 d_p^{1.14} g^{0.71} (\rho_p - \rho_f)^{0.71}}{\mu^{0.43} \rho_f^{0.29}} \qquad (2\text{-}2)$$

In addition to the gravitational force which acts upon the particles, there are also collisional forces present. The moving particles possess a momentum which is greater than that of the air they displace, allowing them to leave the main flow and collide with the pipe wall.

The particle Reynolds number, Re_p, is the parameter which describes the region of flow around the solid particles. Thus, it is useful in predicting the overall behavior of the two-phase flow. Yang [5] presents the following expression for this parameter:

$$Re_p = \frac{(U_f - U_p) d_p \rho_f}{\mu} \qquad (2\text{-}3)$$

Several factors, which will be presented later in this Section, cause the particle velocity to differ from the actual air velocity. The particle Reynolds number represents the magnitude of this difference at a given set of flow conditions. When there are small differences between the two velocities, Re_p is low (> 2), and a flow regime develops which is usually present in the dilute-phase transport of very small particles, on the order of less than 1 micron [6].

For intermediate Re_p values, on the order of 2 to 500, the flow around the particle remains laminar, but wakes form behind the moving particle. These wakes represent an inherent energy loss which affects the pressure drop experienced by the flow. The pneumatic transport of pulverized coal in electric power plants usually occurs within this flow regime [6].

Occasionally in pulverized coal transport, Re_p will approach, or even surpass, a value of 500. This value signifies a flow pattern in which the particle begins to shed wakes as vortices. Although the vortices are dampened by the air viscosity, their presence increases the system's losses.

One of the factors affecting the particle Reynolds number is the shape of the solid particles. Generally, the particles are assumed to be spherical and the particle diameter is assumed to be their average value. However, pulverized coal tends to depart from spherical in its shape. These irregular (non-spherical) shapes provide a greater area for fluid shear stresses to manifest themselves and also contribute to the particle's rotational motion. If the rotation becomes appreciable, it creates a lift force (the Magnus force) which acts upon the particle [7]. Quantitatively, the irregular shape is expected to increase the drag coefficient above that of an equivalently sized spherical particle.

2.1.3 Difference Between Gas and Particle Velocities

As mentioned earlier, the actual gas velocity differs

from the particle velocity. By definition, the actual gas velocity is:

$$U_f = U_o/\varepsilon \qquad (2\text{-}4)$$

where the voidage fraction is a measure of how much of the total flow volume is occupied by the conveying fluid. If the solid particles were moving in an infinite flow field in the absence of gravity, they would eventually reach an equilibrium velocity equal to that of the conveying gas. But in actuality, the flow field is confined by the pipeline walls and the particles collide with it. Due to these inelastic collisions, the particles lose some of their kinetic energy. In addition, gravity forces act upon the particle, along with the possibility for Magnus forces and wake-induced turbulence diffusion forces. Thus, the particle motion is continuously being retarded due to the cycle of frictional collisions and subsequent reacceleration into the flow.

2.1.4 Gas-Solid Flow Through Pipe Bends

In the flow of clean air, a pipe bend creates complicated flow patterns. The air near the center of the pipe has the highest velocity and experiences a higher centrifugal force than the fluid closer to the walls of the pipeline. This creates a secondary flow, shown in Figure (2-4), in the plane perpendicular to the pipe axis. The addition of solid

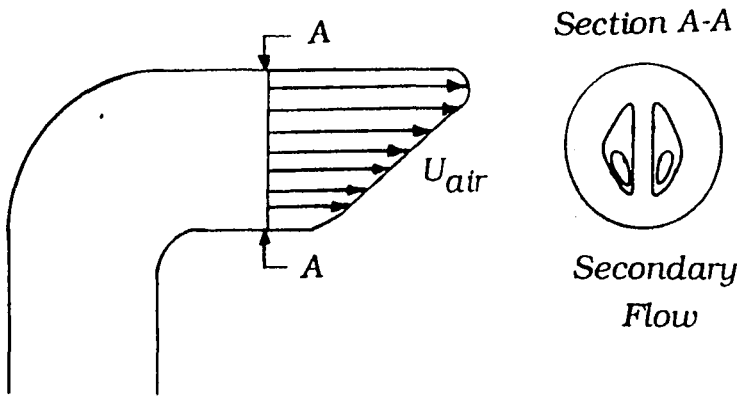

Figure (2-4) Schematic of a secondary flow pattern created by air flow through a pipe bend.

particles to this flow regime creates additional losses for the system due to the momentum lost by the particles as they collide with the pipe walls, and the energy required to reaccelerate them.

The flow of particles through a bend may be achieved in several modes. In the first, the particles follow the gas streamlines until they collide with the bend wall, losing all of their momentum. They are then re-entrained into the flow where they are accelerated back to their steady velocity. This mode is shown schematically in Figure (2-5). The second possible mode of travel is that some particles impinge upon the pipe wall and then slide around the outside of the bend, without losing all of their momentum. However, other

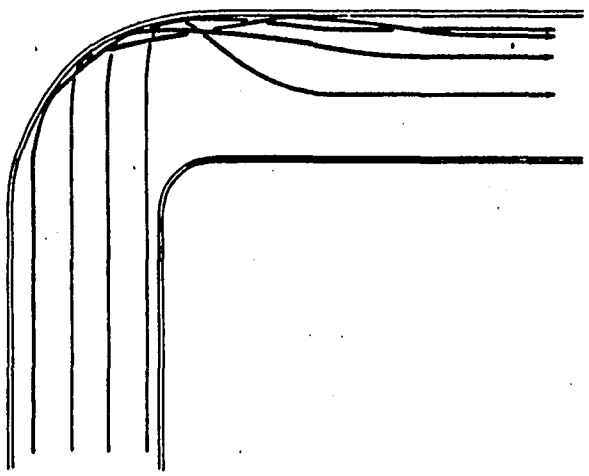

Figure (2-5) Particles may travel a variety of flow paths through a pipe bend.

particles never become displaced from the gas stream and simply follow the stream as it traverses the bend. Due to the secondary flow created by the air flow through the bend and the numerous forces acting upon the particles, it is probable that pneumatic flow through a bend is actually a combination of both of these modes of transport.

2.2 Overview of Gas-Solid Flow Research

Pneumatic transport research has not yet developed a precise, well-founded, scientific theory to encompass all modes of gas-solid flow. Rather, a variety of empirical correlations have been developed to correspond to certain experimental conditions. Obviously, this imposes limits upon

their range of applicability. Furthermore, discrepancies exist among the data of various researchers.

Perhaps the single most complicating factor hindering the growth of a unified pneumatic model is the difficulty encountered in measuring flow properties such as particle velocity. The variety of methods used by researchers, combined with differing flow parameters, has resulted in numerous mathematical expressions for the particle velocity, yielding diverse results.

Similarly, the friction factor related to the flow of solid particles has been investigated with a variety of results. Due to its inherent dependence upon the particle velocity, the mathematical expressions developed by various researchers differ in their results and range of application.

Thus, the design and analysis of pneumatic transport systems has remained an art form, relying upon limited scientific information. This section of the paper provides an overview of the research work which has been performed with the goal of scientifically developing a practical and useful engineering model. As the most readily measurable and identifiable flow variable is the pressure drop, only research studies which sought to relate gas-solids transport to pressure drop were investigated in this thesis. The total pipeline pressure drop has been typically expressed as

$$\Delta P_{TOT} = \Delta P_{ACCN} + \Delta P_{STAT} + \Delta P_{FRIC} \qquad (2\text{-}5)$$

where ΔP_{ACCN} is caused by the energy lost in accelerating the gas and the solid particles to their fully-developed velocities. Figure (2-6) diagrams the additional effect of acceleration losses upon the pressure drop per unit length, as measured experimentally for a given piece of straight pipeline. ΔP_{STAT} develops from supporting the weights of the solids and the gas in vertical transport, and ΔP_{FRIC} results from the frictional flow resistance experienced by both the gas and the particles. The following investigations attempt to develop expressions for ΔP_{TOT} in terms of relevant flow properties.

2.3 Early Research in Horizontal and Vertical Transport

2.3.1 Vogt & White (1948)

Perhaps the earliest documented attempt to formulate a numerical model for gas-solid flow was performed by Vogt & White [8] in 1948. Aware of the lack of quantitative, practical information regarding pneumatic transport, they utilized an experimental facility composed of 0.5 inch diameter iron piping in a circuit of horizontal and vertical pipes. Water manometers connected to pressure taps in the piping were used to record data. The materials used were sand, steel shot, clover seed, and wheat, with mean particle diameters ranging from 0.008 to 0.158 inches.

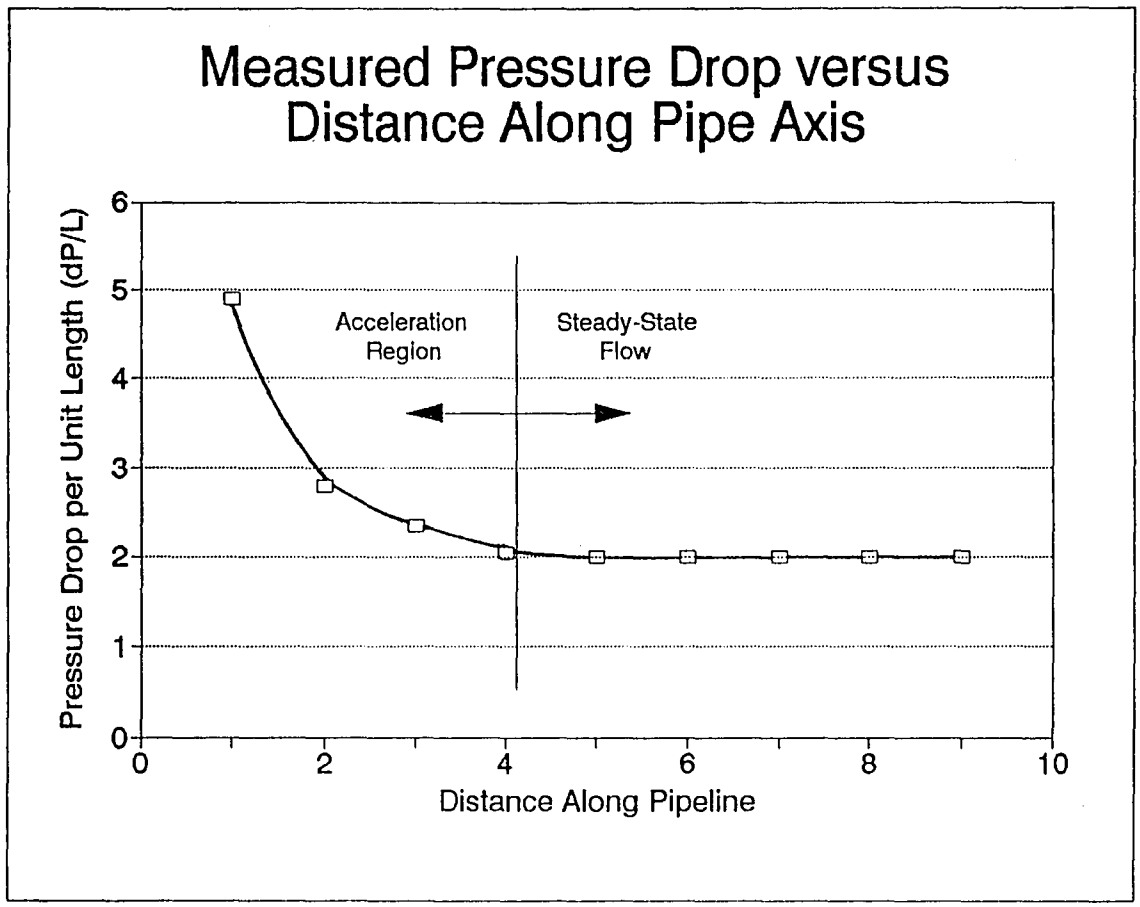

Figure (2-6) Particles have reached a steady-state velocity when the pressure drop per unit length becomes constant.

Due to the large number of variables involved in developing a strictly empirical flow correlation, Vogt & White attempted to develop a theoretical framework to apply to their experimental work. They generated an equation for both horizontal and vertical flow in terms of a ratio of the total pressure drop to the pressure drop experienced by a flow of pure fluid at the same velocity. Their correlation was dependent upon two variables which were empirical functions of the following flow parameters: air density, particle diameter, particle density, and fluid viscosity.

Upon analyzing their data, Vogt & White determined that they did not allow sufficiently for the effects of the pipe bends in their experimental piping circuit. Although their data matched the predictions reasonably well, the behavior of some upstream pressure taps in the system could not be properly accounted for, and the absence of sufficient acceleration regions was suspected. Furthermore, they were unable to explain the effect of particle shape and roughness, which was a factor stressed in their theoretical derivations. However, through manipulation of data, they were able to obtain an empirical correlation. In conclusion, Vogt & White advise the use of their correlation only in situations similar to those in which their work was performed.

2.3.2 Hairu & Molstad (1949)

Due to the absence of a method for estimating the

pressure drop due to solids static head and solids friction pressure drop, Hairu & Molstad [9] performed experiments upon a system composed of 0.267 and 0.532 inch diameter glass tubing in which air transported sand and alumina-silica particles. In addition, they paired their data with a theoretical analysis which utilized a dispersed-solids-density and an expression for pressure drop which included the following assumption. To account for friction losses arising from the presence of solid particles, a Fanning friction factor was employed, in the same way in which it is used to quantify frictional losses due to gas flow alone. Additionally, the analysis was concerned only with flows which were fully accelerated, allowing the associated pressure drop term to be neglected.

However, due to the presence of an acceleration pressure drop over an unexpectedly large distance along the test section, Hairu & Molstad were unable to accurately measure the solids frcition loss. Utilizing their theoretical derivations, they were able to predict only the order of magnitude of the solids friction factor. Realizing the obvious limitations of their work, they concluded that to extend the state-of-knowledge in pneumatic transport further, experiments needed to be performed to isolate the effects of the multitude of phenomena occurring.

2.3.3 Wen & Simons (1959)

Horizontal transport was experimentally investigated by Wen & Simons [2] in 1959. Although they utilized conditions which were applicable only to dense-phase flow, this work produced important insight into saltation in horizontal pipelines.

2.3.4 Barth (1962)

The pneumatic transport of coal in electric power plants was examined by Barth [10] in 1962. Barth recognized that the behavior of the mixture of air and coal is fundamentally different from that of a homogeneous fluid medium, as it had previously been treated by other researchers. Utilizing similarity conditions for the mixture of gas and solid particles in his analysis, Barth proposed a number of requirements which must be fulfilled. Specifically, he mentions the loading ratio of weight of transported material to weight of air, the Froude number[1], and the Reynolds number for flows in the absence of any solid material.

In developing an expression for pressure drop, Barth proposed that the pressure loss of a gas-solid flow consists of two terms: a pressure loss for pure gas flow and an additional loss to account for the presence of solid particles. These two variables are presented in the form of two simple equations as functions of flow specific

[1] The Froude number is the ratio of inertial forces to gravitational forces acting upon the flow.

coefficients. For air flow alone, the pressure drop is easily calculated via the familiar Fanning equation of fluid mechanics

$$\Delta P = f \frac{\rho_f V^2}{2} \qquad (2\text{-}6)$$

with f being the flow friction factor. However, the coefficient for the solids pressure drop is presented in graphical format as a function of the Froude number and is based upon experimental data which were not included in the paper.

Barth also recognized the contribution of static head to the total pressure drop and presented a simple expression for its determination. Experimental data, which were not included in the paper, were employed to develop a coefficient representing the pressure loss due to particle acceleration. The experiments, whose procedure was not given, were also coupled with a thorough theoretical explanation of gas-solid flow through pipe bends and branches.

2.3.5 Jones, Braun, Daubert, and Allendorf (1967)

The estimation of the pressure drop in vertical transport was next investigated by Jones, Braun, Daubert, and Allendorf [11]. They sought to develop a vertical pressure drop expression which would be dependent only upon easily

determined physical properties. Following a common procedure, they separated the total pressure drop into acceleration, static head, and friction terms, where each has a constituent due to the gas and another due to the solid particles. Using test sections composed of 0.305, 0.402, and 0.870 inch diameter steel tubes, the air-transport of a variety of particles, with varying diameters, was investigated. Since the measured pressure drops between equally spaced pairs of pressure taps along the test section were almost always equal, the flow in the section was considered to be fully accelerated. Thus, the pressure drop due to acceleration was subsequently neglected in the data analysis.

The experimental data were used to develop an expression for the solids friction factor, since all other contributions could be easily determined (static head and gas friction factor were presented as explicit equations). However, the resultant correlation was unable to be verified accurately with any data accept that from which it was derived. In addition, the method of determination of the particle velocity, necessary for the static head and acceleration equations, is not explained. In conclusion, Jones et. al. recommended that a comparison with more complete data be performed to properly validate their correlations.

2.3.6 Konno & Saito (1969)

Konno & Saito [12] performed experiments upon both

horizontal and vertical glass pipes of 26.5 and 46.8 mm diameters. They observed two types of flow: one in which the flow was relatively parallel to the pipe axis and the other in which a random flow caused the particles to violently collide with the pipe wall. These two types of flow produced large differences in pressure drop measurements. Due to the difficulty of reproducing the experimental conditions of the random flow, they limited their investigation to only data which were recorded during parallel flow.

The total pipeline pressure drop was divided into its individual components, and the contribution due to static head was neglected during horizontal transport. Particle velocity was expressed as the difference between the gas velocity and the terminal velocity of a single particle

$$U_s = U_{air} - U_t \qquad (2\text{-}7)$$

where U_t is as defined in Equation (2-2). In addition to their development of a pressure drop correlation for fully accelerated flow, Konno & Saito also presented their findings on air velocity profiles through the use of pitot probes. For vertical transport, the air velocity profile was the same as that of pure air flow. However, for horizontal transport, there existed an asymmetrical profile with respect to the pipe axis and it was found to depend upon the particle diameter, density, and mass loading.

During the vertical transport experiments, observations were made of particle concentrations which were higher near the pipe wall when the particles were made of copper or glass. However, polystyrene particles tended to be in higher concentrations near the pipe axis. Although the cause of this difference was not explained, it was proven that higher particle concentrations yield more uniform distributions, and the most important parameter affecting their dispersion is the mass loading. Additionally, it was noticed that there was an additional pressure drop in horizontal pipelines beyond that of vertical transport under similar conditions. They postulated that this phenomena could be attributed to the collisions between particles and the surface of the pipe wall.

2.4 Recent Advances in Horizontal and Vertical Transport

2.4.1 Rose & Duckworth (1969)

One of the most widely referenced research works is that of Rose & Duckworth [13]. Their method paired experimental data with a dimensional analysis derived from first principles. Experimental copper pipelines of 1.26 inch diameter were constructed to allow for the simulation of both gas-solid and liquid-solid transport. The following information will pertain to their findings on gas-solid transport.

The principle of conservation of momentum was employed to develop a series of non-dimensional equations. Specifically,

the forces a volume element of flow experiences due to pressure, gravity and friction are summed and set equal to the net efflux of momentum, which arises from the motion of the gas and the particles:

$$\delta F_p + \delta F_g + \delta F_f = M_a \delta V_a + M_s \delta V_s \qquad (2\text{-}8)$$

where
- δF_p = Force due to pressure drop
- δF_g = Gravitational force
- δF_f = Frictional force due to shear stress at pipe wall
- M_a = Mass of fluid in volume element
- M_s = Mass of solids in volume element
- δV_a = Velocity of fluid in element
- δV_s = Velocity of solids in element

This formulation can be rearranged to produce the familiar relationship of the flow pressure drop being equal to the summation of the gravitational, frictional, and accelerational effects. Dimensional analysis is then performed for both accelerating and fully established flow. For established flow, the pressure drop is dependent upon the usual parameters of velocity, density, loading, and diameter as well as a dimensionless friction coefficient λ_m .

$$\lambda_m = \frac{\Delta P_m}{\frac{\rho_f V^2}{2}\frac{L}{D}} - 2\left(\frac{gD}{V^2}\right)\sin\theta\left[1 + M^*\left(\frac{V}{V_s}\right)\left(1 - \frac{\rho_f}{\rho_s}\right)\right] \qquad (2\text{-}9)$$

with ΔP_m = Total pressure drop in the fully-accelerated region

V = Gas velocity

V_s = Solids velocity

ρ_s = Particle solid density

M^* = Mass loading ratio

θ = Pipe inclination above horizontal

The coefficient is the sum of the friction coefficient due to gas flow, λ_f and the coefficient due to the presence of solid particles, λ_s .The solids friction coefficient is a function of 13 flow variables and parameters which are represented by 10 dimensionless groups which depend upon empirical correlation.

$$\lambda_s = \Psi\left\{\left(\frac{\rho_f VD}{\mu}\right),\left(\frac{V^2}{gD}\right),\left(\frac{M_s}{M_f}\right),\left(\frac{\rho_s}{\rho_f}\right),(\varepsilon),\left(\frac{d}{D}\right),\left(\frac{k}{D}\right),(Z),(\beta),(\theta)\right\} \quad (2\text{-}10)$$

where ε = Coefficient of restitution for particle collisions

k = Pipe roughness coefficient

Z = Particle shape factor

β = Parameter for particle size distribution

Obviously, the determination of such a variable depends upon accurate, flow-specific experimental data.

For accelerating flow, the pressure drop is represented

as a function of 8 dimensionless groups, which again hinge upon empirical correlation. Similar groups were also developed to determine the solids velocity and length of pipeline needed to fully accelerate the particles.

The analysis of experimental data was then combined with the dimensionless groups to produce the following results. Holding the parameters of k/d, Z, and β constant, it was determined that the acceleration length is independent of the pipeline inclination and can be estimated by the following expression:

$$\left(\frac{L_A}{D}\right) = 6\left[\left(\frac{M_s}{\rho_f g^{0.5} D^{2.5}}\right) \times \left(\frac{D}{d}\right)^{0.5} \times \left(\frac{\rho_s}{\rho_f}\right)\right]^{1/3} \qquad (2\text{-}11)$$

where the parentheses do not indicate dimensional analysis but are used for mathematical clarity. Similarly, the acceleration pressure drop was reduced to a usable equation with the inclusion of two graphed functions of dimensionless variables: Ψ_4 and Ψ_5. Thus, the expression for the acceleration pressure drop becomes:

$$\left(\frac{\Delta P_{A,s}}{\frac{\rho_f V^2}{2}}\right) = 1.12 M^* \times \Psi_4\left(\frac{V^2}{g d \rho^{*2}}\right) \times \Psi_5(\theta) \qquad (2\text{-}12)$$

with Ψ_4 and Ψ_5 provided by graphs produced by Rose & Duckworth.

When this technique is applied to determining the solid fictional coefficient, six graphical functions are developed to quantify the influence of the effective dimensionless groups. However, size distribution and non-sphericity effects were not examined and the effect of pipe roughness was assumed to be adequately accounted for in the gas friction coefficient. Thus, to determine the pressure drop which occurs in fully accelerated flow, the numerical values for the six functions are determined from their graphs and summed to provide the friction coefficient needed in Equation (2-9).

In summary, the application of the Rose & Duckworth method requires a knowledge of the following information:

1. The gas friction coefficient
2. The dimensionless functions of the flow parameters, which depend upon flow specific information
3. The solids velocity which can be obtained via several dimensionless functions and a derived equation

This information then allows the total pipeline pressure drop to be determined from the equation

$$\Delta P_{TOT} = \Delta P_m + \Delta P_{A,s} + \frac{\rho_f V^2}{2} \qquad (2\text{-}13)$$

where ΔP_m is as described in Equation (2-9), $\Delta P_{A,s}$ is given in Equation (2-12) and the final term on the right-hand side of Equation (2-13) accounts for the loss due to fluid

acceleration.

2.4.2 Capes & Nakamura (1973)

Extensive experimental work was performed by Capes & Nakamura [14] and the resultant data have been utilized in many subsequent research efforts. Using 3 inch diameter plexiglass tubing, they studied the vertical flow of a variety of particle materials and sizes. In addition, they presented a slightly modified (using their data) form of the particle friction factor which was originally proposed by Konno & Saito [12].

An analysis of their data revealed that the assumption of the particle velocity equaling the difference of the fluid velocity and the terminal velocity of a single particle (see Eq. (2-7)) is incorrect, and the increased "slip" velocity is due to particle-wall friction and, at lower gas velocities, particle recirculation effects. Although an expression for the flow pressure drop was not presented, Capes & Nakamura provided profiles of pressure drop versus pipe distance for a variety of flow conditions. Their success in isolating particle acceleration effects allowed them to determine that the correlation developed by Rose & Duckworth for the acceleration length consistently overestimated the actual acceleration zone.

2.4.3 Khan & Pei

In attempt to decipher the differences among the various vertical transport pressure drop data and correlations published at the time, Khan & Pei [15] presented an analysis of the various equations and performed experimental work to develop their own expression. They proposed that the pressure drop in vertical transport depends upon seven distinct parameters:

1. Mass loading ratio of solids to gas
2. Density ratio of solid to gas (the buoyancy effect)
3. Diameter ratio of particle to pipe
4. Reynolds number
5. Froude number
6. Ratio of drag coefficient of solids to pipe friction factor $C_D/f(\lambda)$
7. Shape factor of the solids used ϕ

These parameters were used in a dimensional analysis to produce the following correlation for pressure drop:

$$\frac{\Delta P_s}{\Delta P_f} = 2.66\left[\left(\frac{C_D}{\lambda}\right)\times\left(\frac{\rho_f}{\rho_s}\right)\times\left(\frac{D_p}{D_t}\right)^2\times\left(\frac{Re}{Fr}\right)^{0.5}\times\left(\frac{\theta}{\phi^{0.5}}\right)\right] \qquad (2\text{-}14)$$

In comparison with other researchers' data and correlations, this expression was found to predict experimentally observed pressure drops more consistently than any of the others. However, no information was provided concerning the acceleration length or its associated pressure drop.

2.4.4 Michaelides (1987)

Aside from the works published by Yang [5,16-19], which will be discussed in Chapter 3, the next advances in the field of pneumatic transport and pressure drop correlations were presented in 1987 by Michaelides [20]. He developed a highly mathematical dynamic model of particle motion and combined it with a "single-fluid" assumption concerning the pneumatic flow. However, the resultant expression for pipeline pressure drop is based upon a ratio of the pressure drop due to the solid particles to the pressure drop due to the gas flow. This representation does not identify the effects of acceleration and static head upon the pressure drop, nor does it provide a straight-forward description of the solid particle velocity expression. Rather, the derivations are based upon a parameter which represents the time between particle collisions.

2.4.5 Michaelides & Roy (1987)

In that same year, Michaelides & Roy [21] published a comparison and evaluation of the various correlations for pneumatic transport which were currently available. Specifically, they pooled together the published experimental data and developed a large data bank with which to compare the various expressions, including that of Michaelides [7]. However, rather than interpret the variations in each of the pressure drop relations, they decided to compare resultant

friction factors. Thus, variations in acceleration length, particle velocity, and static head were not examined.

The correlation put forth by Michaelides [7], which was derived using most of the information in the data bank, was recommended as the best choice in evaluating gas-solid transport. In addition, Michaelides & Roy stated that the work of Rose & Duckworth [13] is considered to be acceptable for the prediction of the general pressure drop.

2.5 Research on Pneumatic Transport through Pipe Bends

In contrast to the amount of work performed on the area of vertical pneumatic transport, gas-solid flow through pipe bends has received very little attention, despite the fact that almost all pipelines experience bends along their flow path. Much of the early design procedures for pneumatic conveying systems relied upon using an equivalent length of straight pipe to account for the bend, in exactly the same manner used for single-phase flow. Other systems simply relied upon the experience of past designs to guide the installation of new systems.

2.5.1 Schuchart (1968)

The first attempt at an experimental scientific study of the pressure drop resulting from pipe bends was Schuchart [22] in 1968. Utilizing quartz beads and granular polyamide plastic, he experimented with bend diameter-to-pipe diameter

ratios ranging from 3.5 to 21.5. Analysis of his data provided an expression for the pressure drop experienced by a flow through a bend:

$$\frac{\Delta P_b}{\Delta P_{stl}} = 210\left(\frac{D_b}{D_t}\right)^{-1.15} \qquad (2\text{-}15)$$

where ΔP_b = Pressure drop in bend

ΔP_{stl} = Pressure drop in pipe of equivalent length

D_b = Diameter of bend curvature

D_t = Pipe diameter

This equation states that the total pressure loss due to the bend is inversely proportional to the radius of curvature. In addition, he provided an expression for the pressure drop encountered in the equivalent straight section of pipe, which depends upon numerous experimentally determined constants. Schuchart also warned of the correlations' limitations for very fine particle sizes and recommended that experimental work be performed to determine the exact effect of particle size.

2.5.2 Rose & Duckworth (1969)

Rose & Duckworth [13] proposed the idea that the majority of the energy loss experienced by the flow in a bend is due to re-accelerating the particles which collide with the pipe wall. Thus, they recommended using their acceleration

pressure drop expression along with their equation for acceleration length to calculate the pressure drop due to pipe bends. However, they predicted that this will overestimate the actual loss since it assumes that all of the solid particles collide with the wall of the bend and come to rest, requiring a complete re-acceleration to the steady state velocity.

2.5.3 Mason & Smith (1971)

Fine powder-sized particles were experimentally studied by Mason & Smith [23] in a system composed of 1, 2, and 3 inch diameter pipes with a 90 degree bend. The single ratio of bend diameter-to-pipe diameter used was 20. Their data were analyzed to produce a bend particle resistance coefficient which is a function only of the mass loading

$$\psi_{bp} = 0.027 m^{*} - 0.0025 m^{*2} \qquad (2\text{-}16)$$

This coefficient was combined with the factor arising from the flow of air, which is a nearly constant value of 0.025, to produce the following expressions for the total bend resistance number and the resultant pressure drop:

$$\psi_{bt} = 0.025 + 0.027 m^{*} - 0.0025 m^{*2} \qquad (2\text{-}17)$$

$$\Delta P_b = \psi_{bt} \frac{\rho_f V_f^2}{2} \qquad (2\text{-}18)$$

The use of this one expression to quantify the flow through the bend renders it something of a "black-box". In addition, an analysis of the flow data reveal that this correlation does not properly account for the subsequent downstream acceleration effects of the bend upon the flow. Rather, this equation only accounts for the fraction of the total re-acceleration pressure drop which occurs within the actual bend.

2.5.4 Klinzing (1980)

In 1980, Klinzing [24] published a comparison of the pressure losses in bends between the recorded data and the subsequent correlations for gas-solid flow. Citing the complex phenomena occurring in pipe bend flow, Klinzing termed variations between calculated and experimental values of 50% as being reasonable. He concluded that the model put forth by Schuchart was best suited to predict the pressure drop experienced by a two-phase flow. In addition, he speculated that the overprediction of data by several of the other correlations may be due to the possible occurrence of drag-reduction by the presence of the particles.

2.5.5 Michaelides (1987)

The various limitations of the existing correlations for

pressure drop in bends were examined by Michaelides [20] in an attempt to utilize all of the existing data and information to develop a more accurate and complete expression. A discussion of this work and its resultant equation for pressure loss will be deferred until Chapter 3.

2.6 Summary of Gas-Solid Research

The variety of work performed in the field of pneumatic transport has yet to produce an accurate, applicable method for predicting the behavior of gas-solid systems. Differences among recorded data have led to varying empirical correlations. In addition, the laboratory apparatus employed rarely mimics that used in industrial applications, further hindering the usability of empirical correlations. However, selected research works have been assembled into several handbooks for the design and operation of gas-solid transport systems.

Zenz & Othmer [1] recommended the correlations developed by the extensive experimental work of Hinkle [25], the premier data source at the time. However, the numerous works published since then have revealed inconsistencies in Hinkle's methods.

More recently, Soo [26], in *The Handbook of Multiphase Systems*, chose to develop a hybrid formula for pressure loss based upon the data and correlations of Rose & Duckworth [13] and the work of Dogin & Lebedev [27]. His derivation centered

upon calculating a friction factor which would account for the flow of both the gas and solid. However, the presence of acceleration effects is not mentioned, and the accuracy of the final expression is not demonstrated.

In summary, the manuals available for pneumatic transport are limiting both in their scope of analysis and range of applicability. In addition, the published correlations for pressure loss which were described in this chapter suffer from the following drawbacks:

- The acceleration length expression derived by Rose & Duckworth, though widely utilized, has been proven to overestimate its actual value.
- Pressure loss expressions which are in the form of a ratio of the mixture loss to the loss for air alone, as in Khan & Pei [15], conceal the effect of static head upon the flow.
- Some parameters rely upon the accuracy of information which is not readily available, such as the coefficient of restitution for particle collisions.
- The development and use of certain factors, such as the particle drag coefficient, is unclear.

The methods described in Chapter 3 attempt to account for the drawbacks listed above and provide an accurate method for predicting the performance of pneumatic transport systems.

3. SELECTED PRESSURE DROP CORRELATIONS

3.1 Vertical and Horizontal Transport

All of the research work discussed in Chapter 2 possesses limitations that limit its value in the analysis of the pulverized coal flow in an electric power plant. Specifically, none of the authors cited provide all of the necessary information needed to accurately use their equations. For example, parameters such as the particle drag coefficient are needed for the calculations, but information on their derivation is not provided. Due to the absence of a unified calculation procedure for the pressure loss, the works described in Chapter 2 will not be utilized in this thesis, deferring instead to the method which will now be discussed.

Recognizing the absence of a complete approach to analyzing dilute-phase pneumatic transport systems, Yang [5] presented a unified theory in 1976. He sought to develop a correlation between known operating conditions (the independent variables) and the resultant behavior (the dependent variables). Specifically, the independent variables are:

- Type of particles which are conveyed, and their properties: size, shape, density, and roughness.
- Solids loading (or, conveying) rate.
- Properties of the conveying fluid such as density and viscosity at the operating conditions.

- Fluid conveying velocity.
- Pipe geometry and material.

Similarly, the dependent variables are the phenomena which result from a set of independent variables:

- Pressure drop in transport line.
- Acceleration length and pressure drop.
- Particle velocity and potential choking in vertical lines or saltation in horizontal lines.

Based upon this distinction, Yang performed a detailed derivation to account for each of the independent variables in a form which allows the dependent variables to be calculated.

3.1.1 Solid Particle Velocity and Solid Friction Factor

In developing an expression for the particle velocity, Yang utilized a force balance on a differential section of pipe length, dL. He then paired this with the mass continuity equation to account for the total amount of material flowing through this section. Assuming spherical particles, the total number of particles present in the section dL is

$$dN = \frac{6W_s}{(\rho_p - \rho_f)\pi d_p^3 U_p} dL \qquad (3\text{-}1)$$

Thus, the voidage coefficient, which is the ratio of the volume of pure fluid to the total volume in section dL, is given by

$$\varepsilon = 1 - \frac{4 W_s}{\left(\rho_p - \rho_f\right)\pi D^2 U_p} \qquad (3\text{-}2)$$

Since both of the above equations rely upon the particle velocity, an expression for it was next presented. The net force in an acceleration region acting upon particles in a given section dL is equal to the product of the mass of the particles and their rate of acceleration. For vertical flow:

$$dM_s \frac{dU_p}{dt} = dF_d - dF_g - dF_f \qquad \textit{Vertical} \quad (3\text{-}3)$$

and for horizontal flow:

$$dM_s \frac{dU_p}{dt} = dF_d - dF_f \qquad \textit{Horizontal} \quad (3\text{-}4)$$

The difference between vertical and horizontal transport is the additional effect of a gravitational static head upon vertical flows. But beyond this acceleration zone, the particles travel at a relatively constant velocity and the dU_p/dt term in Eqs. (3-3) and (3-4) becomes equal to zero. Thus, for fully accelerated vertical flow:

$$dF_d = dF_g + dF_f \qquad \textit{Vertical} \quad (3\text{-}5)$$

and fully accelerated horizontal flow:

$$dF_d = dF_f \qquad \textit{Horizontal} \quad (3\text{-}6)$$

Within this fully accelerated region, the total drag force upon the number of particles dN is simply the sum of the drag force exerted upon each particle:

$$dF_d = \tfrac{3}{4} C_{DS} \varepsilon^{-4.7} \frac{\rho_f \left(U_f - U_p\right)^2}{\left(\rho_p - \rho_f\right) d_p} dM_s \qquad (3\text{-}7)$$

with U_f as defined by Eq. (1-4). The term of $\varepsilon^{-4.7}$ serves as a dense-phase correction factor for the single particle drag coefficient, C_{DS}, which is correlated for relatively dense mixtures as:

$$C_{DS} = \frac{24}{Re_p} + \frac{3.6}{Re_p^{0.313}} \qquad (3\text{-}8)$$

The particle Reynolds number used above is the same as described in Eq. (1-3).

Similarly, the gravitational force equation becomes:

$$dF_g = g \times dM_s \qquad (3\text{-}9)$$

In order to quantify the effect of solid friction, the

Fanning equation for fluid flow is utilized in conjunction with a particle friction factor to produce:

$$dF_f = \frac{f_p U_p^2}{2D} M_s \qquad (3\text{-}10)$$

The force balance developed in Eqs. (3-5) and (3-6) can now be written in terms of Eqs. (3-7), (3-9), and (3-10) to provide expressions for the particle velocity in vertical

$$U_p = U_f - \sqrt{\left(1 + \frac{f_p}{D}\frac{U_p^2}{2g}\right)\frac{4}{3}\frac{(\rho_p - \rho_f)d_p g}{\rho_f C_{DS}}\varepsilon^{4.7}} \qquad \textit{Vertical} \quad (3\text{-}11)$$

and horizontal transport

$$U_p = U_f - \sqrt{\left(\frac{f_p}{D}\frac{U_p^2}{2g}\right)\frac{4}{3}\frac{(\rho_p - \rho_f)d_p g}{\rho_f C_{DS}}\varepsilon^{4.7}} \qquad \textit{Horizontal} \quad (3\text{-}12)$$

These expressions are very similar to Eq. (2-3), having modified the equation for the terminal velocity of a single particle moving in an infinite fluid (Eq. (1-2)).

The expressions developed rely upon a particle friction factor, f_p . Initially, Yang [18] presented correlations for both horizontal and vertical flow which were based upon a correlation of the experimental data which had been published as of that time (1973). The vertical correlation was a function of the voidage coefficient, the particle Reynolds number, and the terminal Reynolds number, defined as

$$Re_t = \frac{d_p U_t \rho_f}{\mu} \qquad (3\text{-}13)$$

However, the horizontal expression also depended upon the actual gas velocity and the pipe diameter. This dependence is due to the radial distribution of particles (arising from gravity force) which tends to occur in horizontal transport. Prior to the onset of saltation, solid particles may slide, or even roll, along the bottom of the pipe. Determining whether this occurs, or if the particles ricochet off of the pipe walls, or are simply conveyed in a uniform suspension depends upon the particle material properties, the conveying velocity of the gas, the fluid's properties, and the pipe diameter.

Utilizing additional data, Yang [19] developed more accurate empirical coefficients for the vertical friction factor expression and he proposed the following correlations for vertical

$$f_p = 0.0126 \frac{(1-\varepsilon)}{\varepsilon^3} \left[(1-\varepsilon) \frac{Re_t}{Re_p} \right]^{-0.979} \qquad Vertical \; (3\text{-}14)$$

and horizontal flow

$$f_p = 0.117 \frac{(1-\varepsilon)}{\varepsilon^3} \left[(1-\varepsilon) \frac{Re_t}{Re_p} \frac{U_f}{\sqrt{gD}} \right]^{-1.15} \qquad Horizontal \; (3\text{-}15)$$

Examination of the expressions for particle velocity and

friction factor reveal an interdependence of variables such as the voidage factor and the particle drag coefficient which demands an iterative solution procedure. In comparison with the range of values represented by the available data for particle velocity, the performance of the velocity equations to within ± 30% is considered to be of good engineering accuracy. Figures (3-1) and (3-2) plot comparisons between experimental and predicted particle velocities, based upon the data of several researchers. In reference to the criterion mentioned above, the ability of the equations to predict the velocity to within 30% is achieved.

3.1.2 Estimation of the Particle Acceleration Length

The derivation of the expression for the acceleration length hinges upon the relation:

$$dL = U_p dt \tag{3-16}$$

This relation is paired with Eqs. (3-7), (3-9), and (3-10) to produce the following expressions for vertical flow:

$$L_A = \int_{U_{p1}}^{U_{p2}} \frac{U_p}{\frac{3}{4} C_{DS} \varepsilon^{-4.7} \frac{\rho_f \left(U_f - U_p\right)^2}{\left(\rho_p - \rho_f\right) d_p} - \left(g + \frac{f_p}{2} \frac{U_p^2}{D}\right)} dU_p \quad \textit{Vertical} \tag{3-17}$$

and for horizontal flow:

$$L_A = \int_{U_{p1}}^{U_{p2}} \frac{U_p}{\frac{3}{4} C_{DS} \varepsilon^{-4.7} \frac{\rho_f \left(U_f - U_p\right)^2}{\left(\rho_p - \rho_f\right) d_p} - \left(\frac{f_p}{2} \frac{U_p^2}{D}\right)} dU_p \qquad \textit{Horizontal} (3\text{-}18)$$

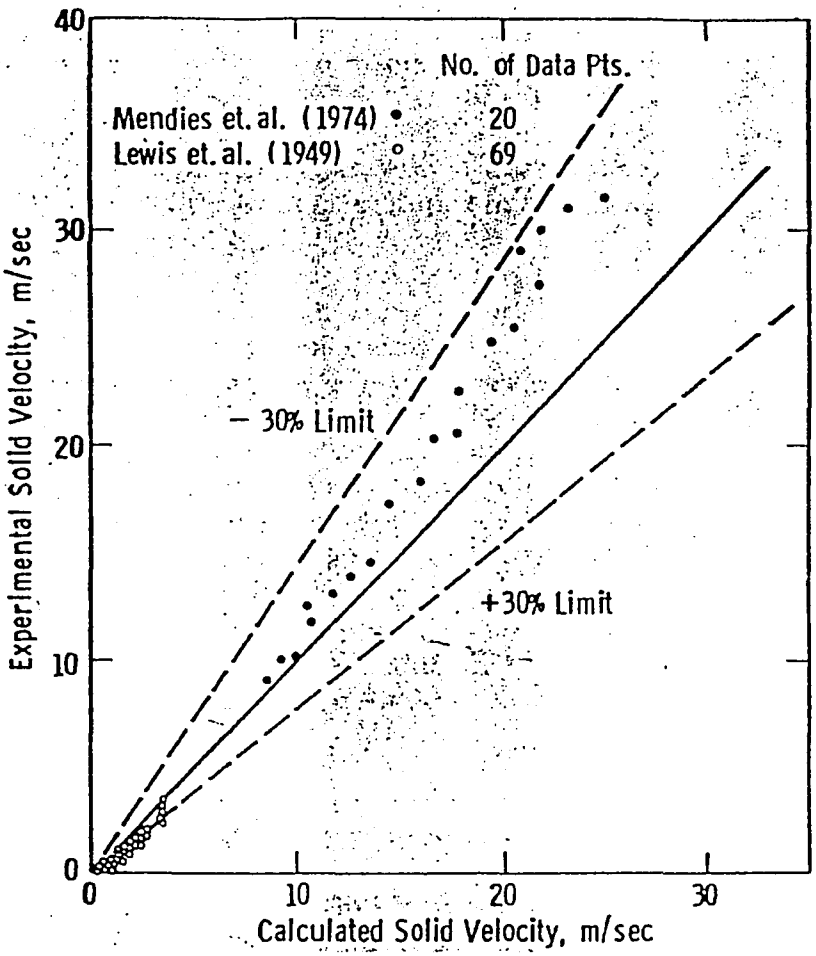

Figure (3-1) Comparison of calculated solid particle velocities with the experimental data of Mendies and Lewis (vertical transport).

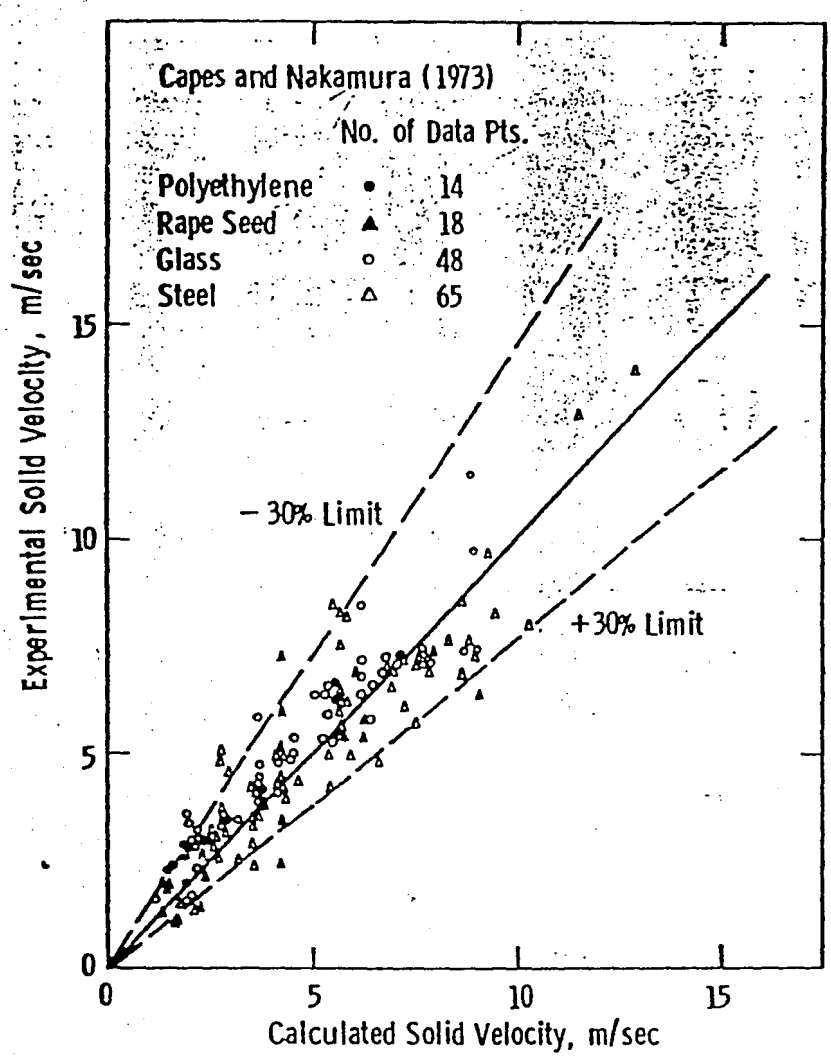

Figure (3-2) Comparison of calculated solid particle velocities with the experimental data of Capes & Nakamura (vertical transport).

The lower limit of integration, U_{p1}, is obtained from Eq. (3-2) with an assumed voidage of 0.65, which pertains to packed bed flow. The upper limit of integration, U_{p2}, is simply the value for the steady-state particle velocity obtained from Eqs. (3-11) and (3-12). To solve this integral, a uniform particle velocity profile is assumed and a standard numerical integration scheme is utilized.

3.1.3 Pressure Drop Equations

Following the standard practice of separating the total pipeline pressure loss into its components (see Eq. (2-1)) Yang [5] developed expressions for the pressure drop due to acceleration, friction and static head. Within these equations, the term L_e is the effective steady-state length, defined as:

$$L_e = L_A - L \tag{3-19}$$

If the acceleration length is greater than the pipe length, the effective length becomes zero.

The pressure loss which arises from the effects of static head is expressed as:

$$\Delta P_S = \rho_p g(1-\varepsilon)L_e \tag{3-20}$$

During horizontal transport, this pressure drop value is zero.

Frictional losses can be separated into two terms: one due to the flowing fluid and the other due to the effect of solid particles.

$$\Delta P_F = \Delta P_{Fg} + \Delta P_{Fs} \tag{3-21}$$

The Fanning equation is utilized to determine the frictional effects of the fluid flow alone. Yang presents it in the form:

$$\Delta P_{Fg} = \frac{2 f_g \rho_f U_f^2}{D} L_e \tag{3-22}$$

where the friction coefficient f_g is a function of the Reynolds number and the pipe material. This value can be obtained from a source such as the Moody diagram, commonly found in fluid mechanics textbooks such as Fox & McDonald [28].

The expression for particle frictional losses is similar to Eq. (3-22), but it includes the voidage effect. Based upon the particle velocity obtained from Eqs. (3-11) or (3-12), the friction equation for both vertical and horizontal transport is:

$$\Delta P_{Fs} = \frac{2 f_s \rho_p (1-\varepsilon) U_p^2}{D} L_e \tag{3-23}$$

For this equation, $f_p = 4f_s$. Eqs. (3-14) and (3-15) provide the friction coefficients for the solid particles.

Within the acceleration region, the acceleration pressure drop is itself composed of several factors,

$$\Delta P_A = R_1 + R_2 + R_3 + R_4 \tag{3-24}$$

The four components are expressed as follows:

$$R_1 = \int_0^l \rho_p (1-\varepsilon) g \, dl \tag{3-25}$$

$$R_2 = \int_0^l \frac{2 f_g \rho_f U_f^2}{D} dl \tag{3-26}$$

$$R_3 = \int_0^l \frac{f_p \rho_p (1-\varepsilon) U_p^2}{2D} dl \tag{3-27}$$

$$R_4 = \left[\rho_p (1-\varepsilon) U_p^2\right]_{@l} \tag{3-28}$$

The upper limit of integration for these equations is the acceleration length, calculated from Eq. (3-17) or (3-18). The static head is represented by Eq. (3-25), which drops to zero for horizontal transport. Using a numerical integration

technique, the acceleration pressure drop can be determined via the sum of its components.

Thus, the total pressure drop experienced by the flow as it travels through a pipeline is determined by the summation of Eqs. (3-20), (3-22), (3-23), and (3-24). Comparisons of this completed model with experimental data reveal an accuracy to within ± 30 to 35%. This range is considered to represent a good correlation due to the wide scatter among the experimental data utilized. Figure (3-3) shows the experimental glass bead data of Jones, et.al., plotted against the values predicted by Yang's model. The 30% criterion is achieved for both the particle velocity and the pressure drop. In Figure (3-4) the data for alumina particles are presented and Yang's calculations are consistently lower than the experimental values by more than 35%, exceeding the bounds of "good engineering accuracy." However, the model does achieve better than 30% accuracy in predicting the behavior of the flow of zircon silica and steel shot, as shown in Figures (3-5) and (3-6).

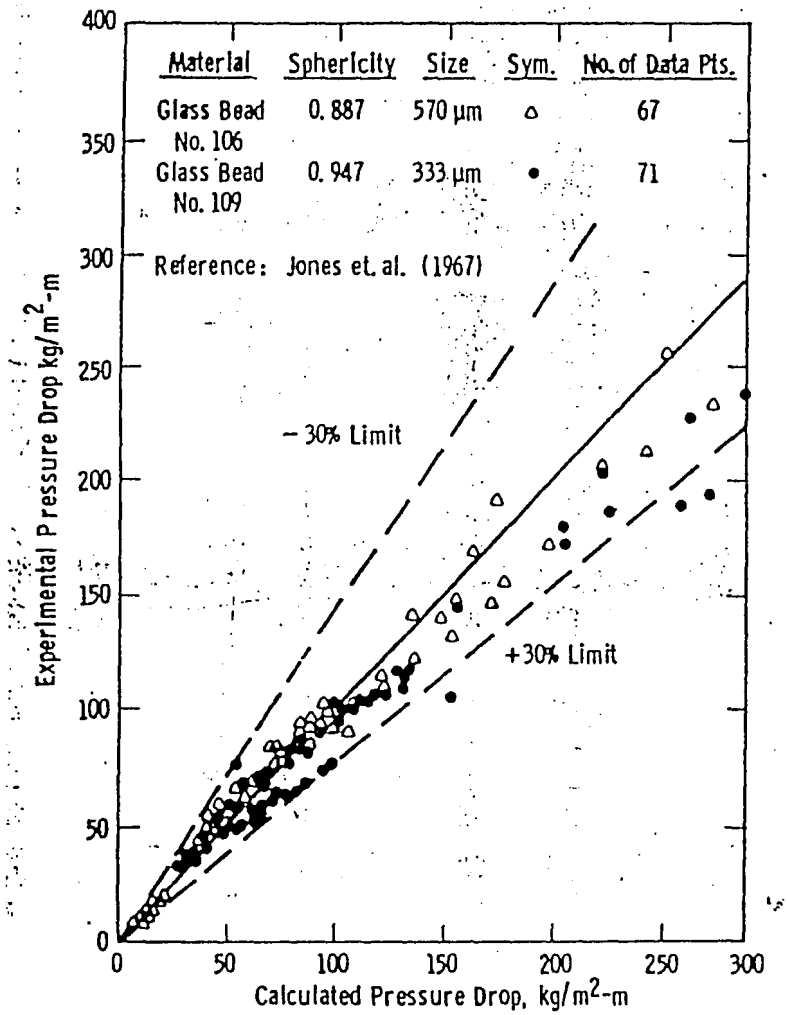

Figure (3-3) Comparison of vertical pressure drop calculations with the glass bead experimental data of Jones, et.al.

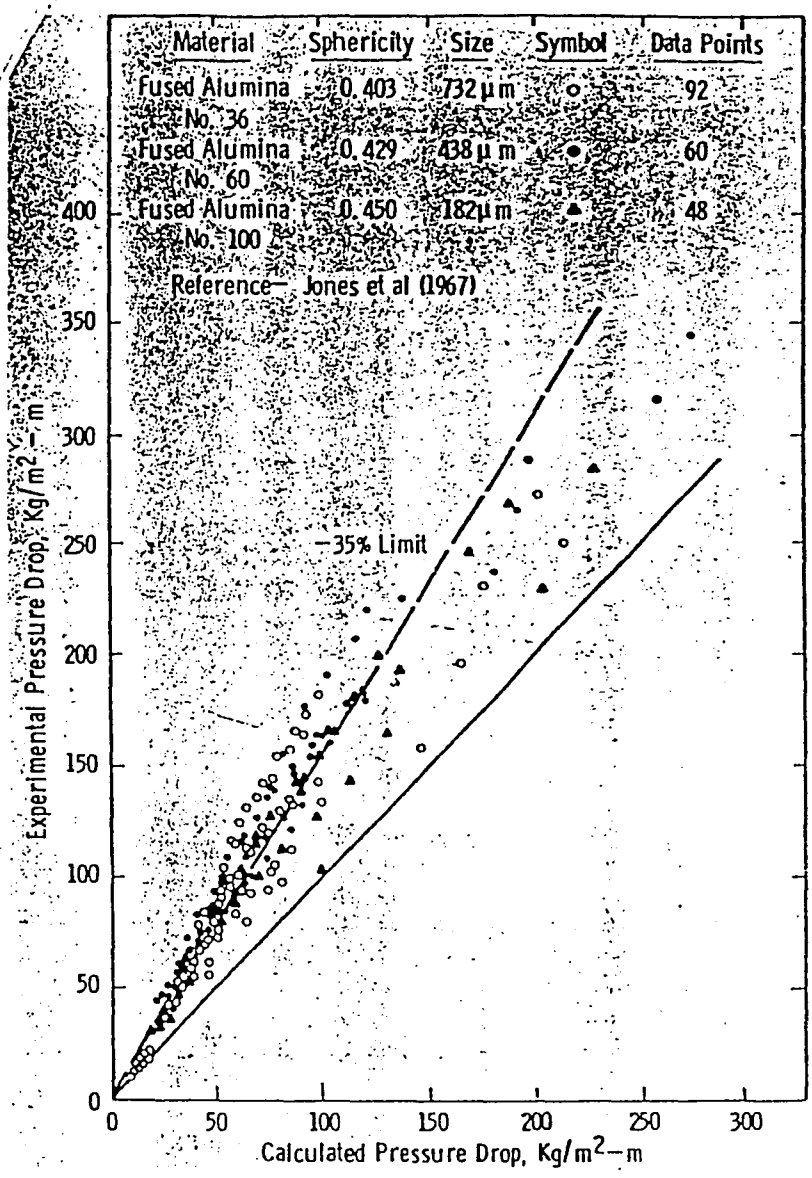

Figure (3-4) Comparison of vertical pressure drop calculations with the alumina particle experimental data of Jones, et.al.

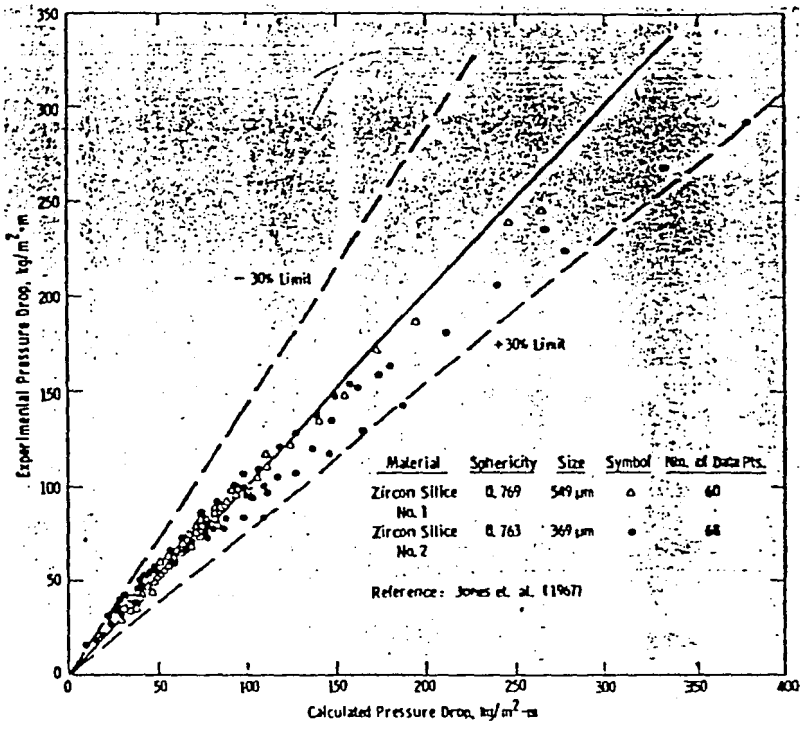

Figure (3-5) Comparison of vertical pressure drop calculations with the zircon silica experimental data of Jones, et. al.

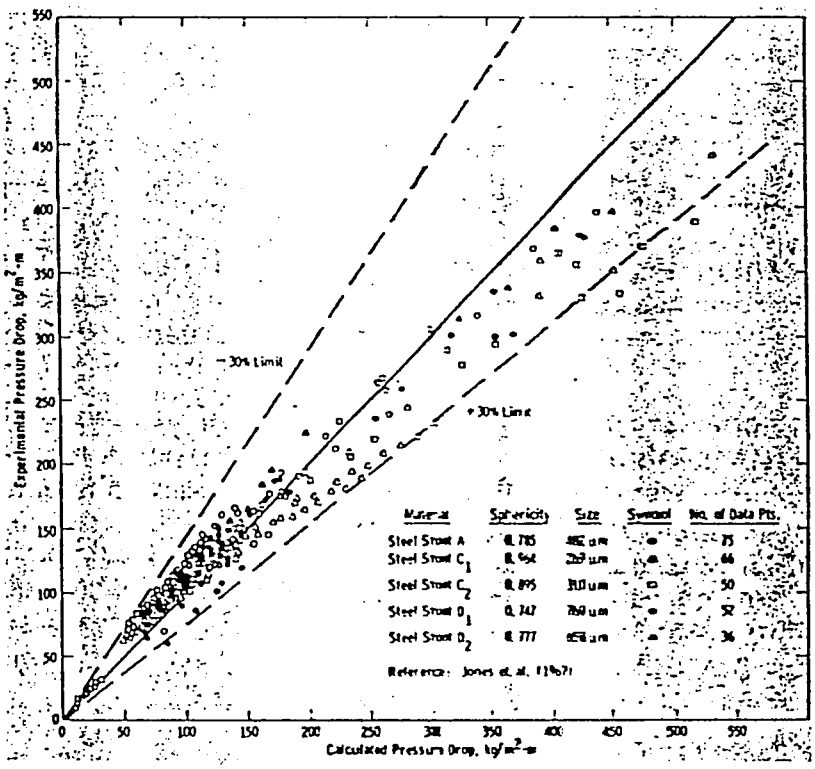

Figure (3-6) Comparison of vertical pressure drop calculations with the steel shot experimental data of Jones, et.al.

3.2 Gas-Solid Flow Through Pipe Bends

The most comprehensive work done to develop an expression for the pressure drop encountered in a pipe bend was performed in 1987 by Michaelides [20]. A system of 4.026 inch diameter piping was used to record data for several bend diameters at various levels of solids loading and air velocity.

A sample of the data recorded is shown in Figure (3-7), where a relative distance value of 0.00 feet corresponds to a point in the flow section where the solids have been fully accelerated to their steady-state velocity. Each of the data points corresponds to a pressure tap located along the pipelines upstream and downstream of the bend. The plot

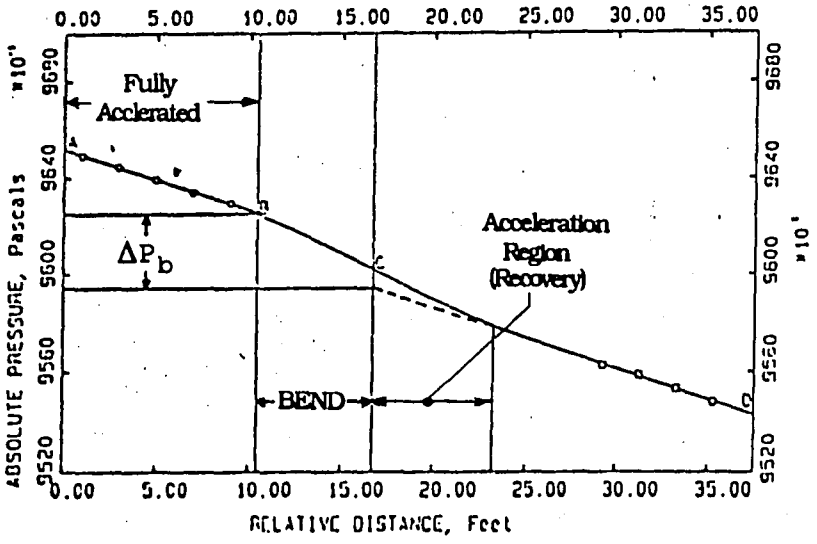

Figure (3-7) Experimental bend pressure gradient data of Michaelides, with designated nomencalture.

clearly reveals the downstream re-acceleration effects of the bend upon the flow, which were neglected in the Mason & Smith [23] analysis. Thus the total contribution of the bend to the pressure loss experienced is given by ΔP_b in Figure (3-7). In addition, the straight-line gradients upstream and downstream of the bend indicate that the solids were completely accelerated, as defined in Figure (2-5).

The analysis of the data revealed that the total pressure drop caused by the bend is best represented as the sum of the contribution due to the air flow and that due to the presence of solid particles:

$$\Delta P_{B,T} = \Delta P_{B,a} + \Delta P_{B,s} \tag{3-29}$$

This equation can better be examined in the dimensionless form of:

$$\gamma_{B,T} = \frac{\Delta P_{B,T}}{\frac{\rho_f U_o^2}{2}} = \gamma_{B,a} + \gamma_{B,s} \tag{3-30}$$

The variables used in Eqs. (3-29) and (3-30), along with those that follow, are defined in the Nomenclature section of this paper.

The two loss coefficients were derived from experimental data:

$$\gamma_{B,a} = 0.167\left[1 + 17.062\left(\frac{r_c}{r}\right)^{-1.219}\right] \times (Re)^{-0.17} \times \left(\frac{r_c}{r}\right)^{0.840} \qquad (3\text{-}31)$$

$$\gamma_{B,s} = \frac{5.4 m^{*1.293}}{Fr^{0.84}\left(\frac{r_c}{r}\right)^{0.39}} \qquad (3\text{-}32)$$

In these equations, both the Reynolds number and the Froude number are calculated based upon the superficial air velocity, U_o, and the pipe diameter, D.

The comparison of the experimental data with the derived correlations is plotted in Figure (3-8), along with the data and equations of Schuchart [22] and Morikawa, et. al. [29]. According to Michaelides, the complexity involved in measuring gas-solid flow, the agreement between calculated and experimental results is considered good, with the absolute average deviation of the results reported to be 17%.

In addition, the resultant expression from the present work was compared to the equations developed by Schuchart, Morikawa, and Mason & Smith at a given operating condition, as shown in Figure (3-9). The Morikawa expression clearly overpredicts the other equations, due to the fact that it is only accurate over a limited range of Froude numbers, which are not encountered for these experimental conditions. Schuchart's correlation matched that of the present study well, but the Mason & Smith equation produced very low values.

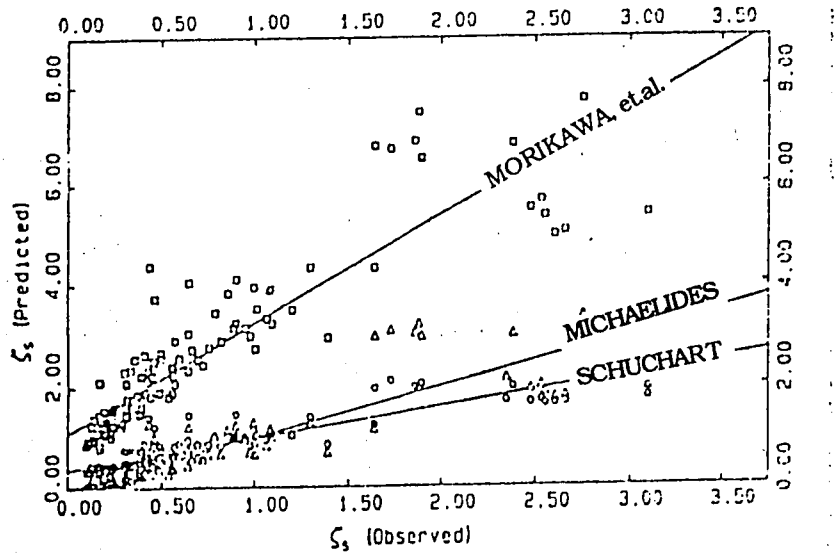

Figure (3-8) Comparison of the Michaelides' solids pressure drop coefficient with those of Schchart and Morikawa.

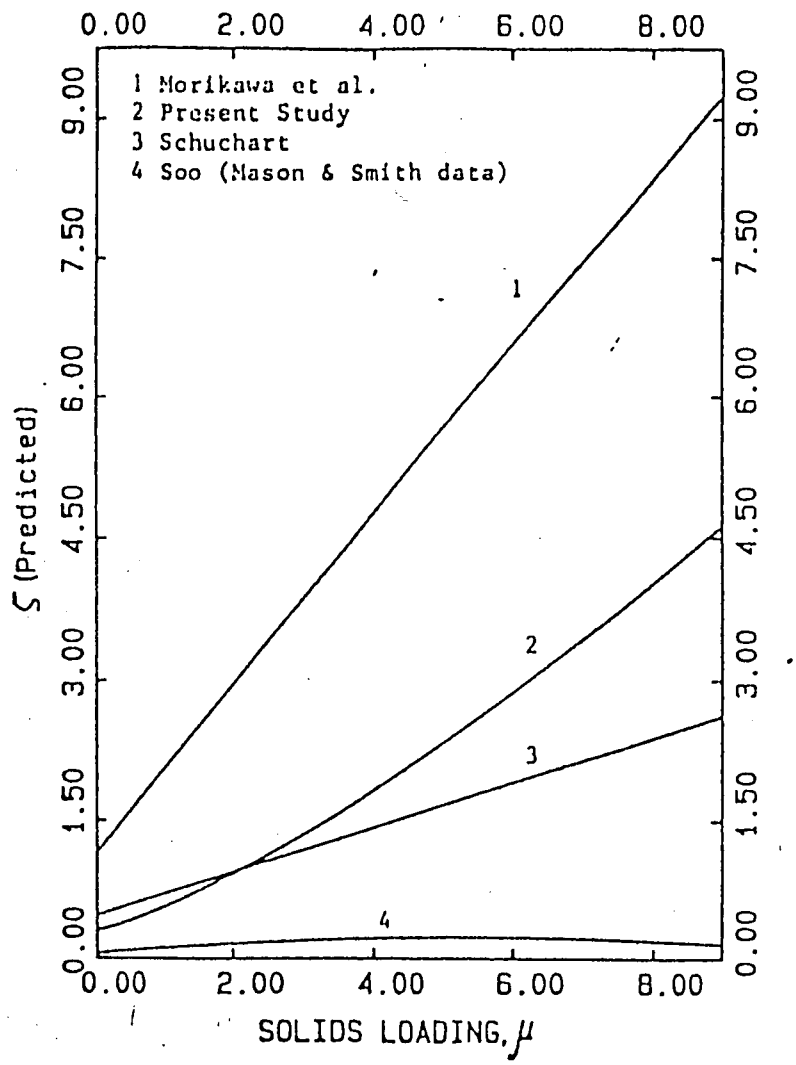

Figure (3-9) Variation of Michaelides' total pressure loss coefficient with solids loading, in comparison with the methods of Morikawa, Schuchart, and Mason & Smith.

This underprediction is due to the derivation of the Mason & Smith expression from data obtained at a single bend diameter, which did not equal that used in the current experiments. The recommendation of Schuchart's expression in 1980 by Klinzing [24], which preceded the development of the Michaelides correlation, would also indicate an endorsement of Eq. (3-30) due to the similarities displayed in Figure (3-9).

Based upon the expressions derived by Michaelides, pipelines with long radii bends will experience overall lower pressure drops than small ones. Combined with the superior erosion performance of long radii bends reported in [30], this work provides strong evidence for their use.

4. BURNER BALANCING METHOD

4.1 Application of Pressure Drop Equations to a Pipeline

The expressions for pressure drop presented in Chapter 3 can be utilized to analyze the flow of pulverized coal in electric power plants by using the additive property of pipeline pressure drop. For example, the flow through the pipeline shown in Figure (4-1) will experience a pressure loss as it travels from point A to point B, designated as ΔP_{AB} . However, this total value can be expressed as the sum of the pressure drops developed in each of the pipeline's sections. This can be written as:

$$\Delta P_{AB} = \Delta P_1 + \Delta P_2 + \Delta P_3 + \Delta P_4 + \Delta P_5 \qquad (4\text{-}1)$$

Each of the sectional pressure drops can then be subdivided into their own contributing components, such as:

$$\Delta P_1 = \Delta P_{1,A} + \Delta P_{1,S} + \Delta P_{1,Fg} + \Delta P_{1,Fs} \qquad (4\text{-}2)$$

If the operating parameters of the flow are known, then these individual pressure losses can be calculated using the equations specified in Chapter 3. Specifically, sections 1 and 5 would be accounted for with Eqs. (3-11), (3-14), (3-20), and (3-21). In addition, since section 1 represents the entrance of the flow, Eqs. (3-17) and (3-24) would be used to

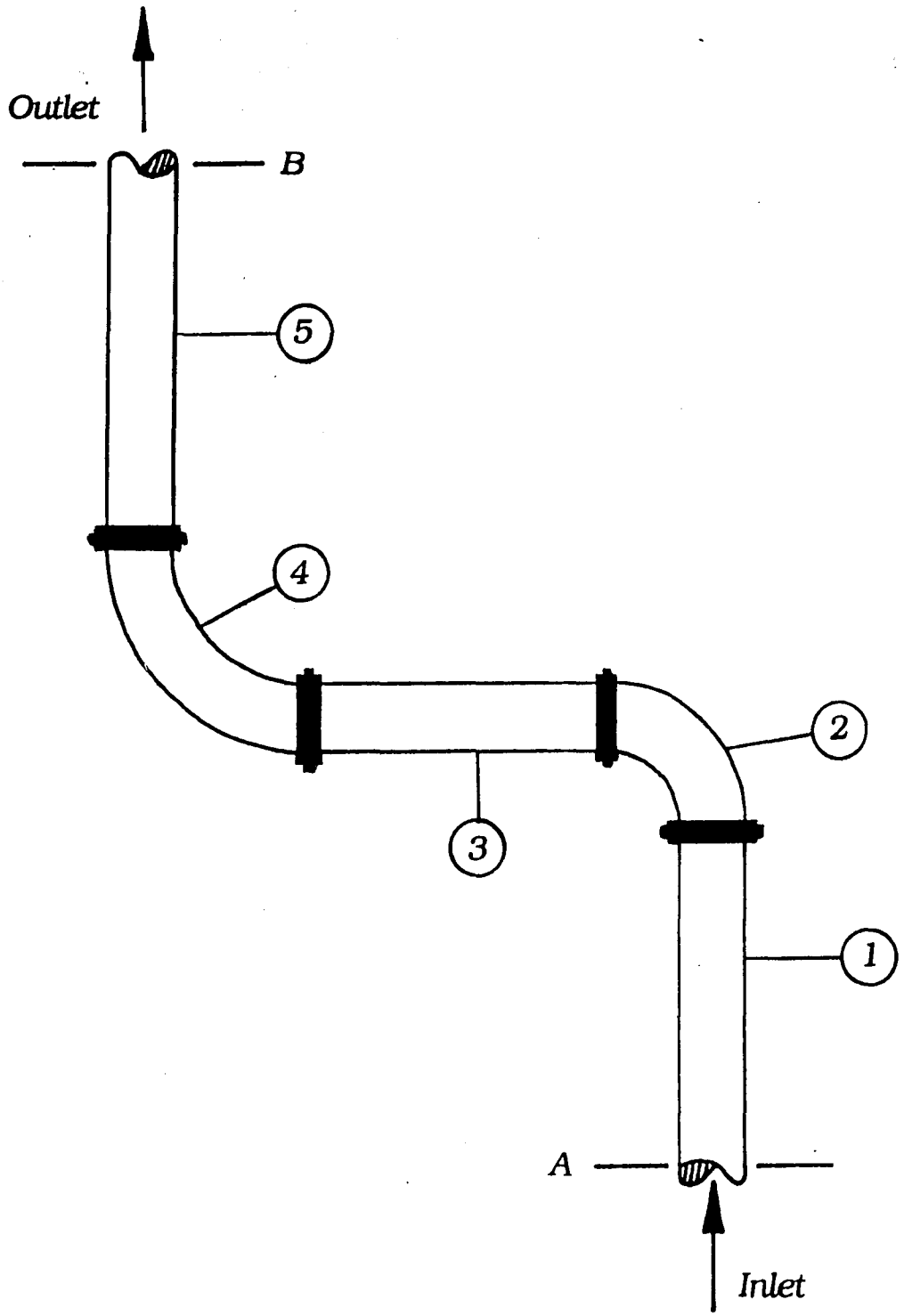

Figure (4-1) Representation of a pipeline as the sum of the individual pipe sections.

determine the acceleration effects. And in similar fashion, sections 2 and 4 would require the use of Eq. (3-32), and section 4 would utilize Eqs. (3-12), (3-15), and (3-21).

4.2 Application to a Simple Pipeline Distribution System

The procedure used in analyzing the flow in Figure (4-1) can be extended to distribution systems in which a single pipe flow is used to supply several others. Figure (4-2) diagrams a simple flow division system in which the entering pneumatic flow is divided into 2 separate flows through the use of a solids riffler (shown previously in Figure (1-5)). Thus, there are two pipelines to be examined, each composed of numerous distinct piping sections, but which also share several sections. To determine the pressure losses of the system, each pipeline is considered separately and its associated pressure drop is calculated via the same method used for Figure (4-1).

Under the assumption that the riffler divides the flow equally and each pipeline receives the same amount of air and solids, pipeline 1 will be examined first. As shown in Figure (4-2), this line is composed of 7 separate sections. Given the system's operating information and flow parameters, the pressure drop correlations of Chapter 3 can be used to calculate the loss resulting from each of these sections, and these individual pressure drops can be summed to yield the total pressure drop for the whole pipeline.

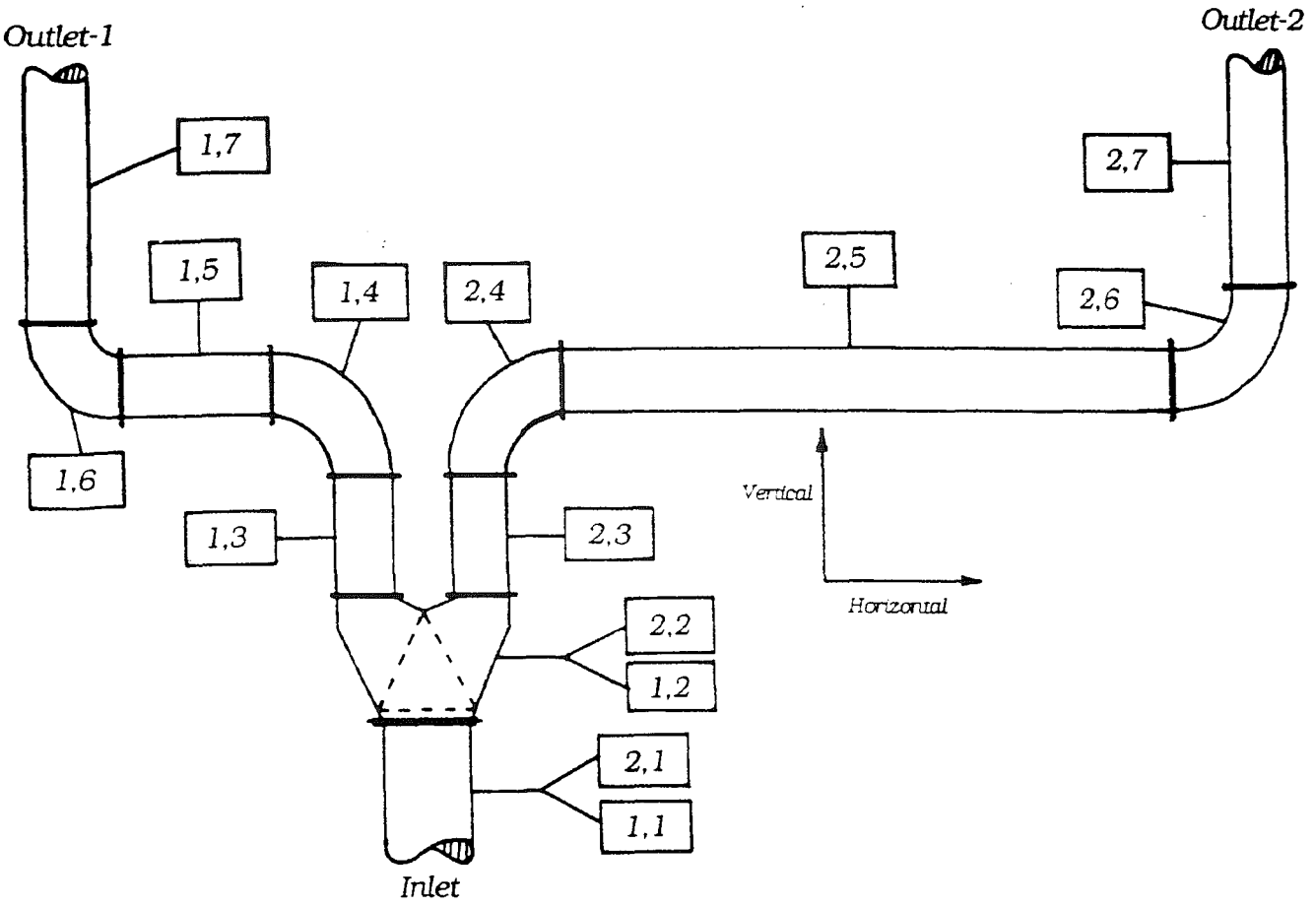

Figure (4-2) A pipe section is assigned two numbers (i,j) to define its location in the system.

The pressure loss experienced in Pipeline 2 can then be calculated in the same manner. Since both pipelines share sections (1,1) and (1,2), the losses developed in those regions are identical. Thus, the pressure drop calculated for section (1,1) is identical to that experienced in section (2,1), and the calculation need only be performed once. As shown in Figure (4-2), Pipeline 1 travels a shorter distance than Pipeline 2 which results in $\Delta P_1 < \Delta P_2$ (with the air and solid flows equally divided).

In conclusion, given the operating conditions and flow parameters, it has been shown that the behavior of a pipeline flow distribution system can be numerically analyzed. The contribution of the solids riffler to the system pressure loss will be discussed in another section of this chapter.

4.2.1 Distribution of Coal in Electric Power Plants

The piping system utilized in electric power plants to deliver coal to the furnace operates under specific boundary conditions. Since all of the pipelines which supply fuel to a given furnace level originate at a common point (the exhauster) and terminate at a common point (the furnace windboxes), they each must experience the same pressure loss. However, the variations in the total lengths of the pipelines, coupled with differing bend diameters, should produce larger pressure drops in some pipelines than in others, as in the situation described for Figure (4-2). The only way that the

identical pressure drop boundary condition can be fulfilled is if the gas-solid flow does not divide equally as it passes through the coal riffler.

Referring again to Figure (4-2), if Pipelines 1 and 2 are considered to terminate at furnace windboxes, then they will experience identical pressure losses:

$$\Delta P_{1,T} = \Delta P_{2,T} = \Delta P_{i,T} = [P, abs]_{@Exhs.} - [P, abs]_{@Furnace} \qquad (4\text{-}3)$$

Since Pipeline 2 is longer than Pipeline 1, it presents a greater resistance to the gas-solid flow. Thus, when the flow passes from section (1,1) into the coal riffler, it "sees" an easier path to the furnace provided by Pipeline 1. This results in a larger amount of coal being sent to Pipeline 1, and a smaller amount being received by Pipeline 2, and the ideal 50-50 division for balanced burners is not achieved. Rather, the flow divides in such a way to equalize the pressure losses experienced by the two pipelines. Since gas-solid flow pressure drop increases with an increase in solids loading, the smaller pressure loss arising from the shorter distance covered by Pipeline 1 will increase as it receives a greater amount of coal than Pipeline 2. Similarly, the higher pressure loss experienced by Pipeline 2 will decrease as the amount of its solids loading decreases, in accordance with Pipeline 1.

4.2.2 The Addition of a Resistance to Balance the Flow

Since the coal flow will not divide evenly for a system of pipelines which traverse different distances, a method of equalizing the flow resistance of each pipeline is needed. Then, when the gas-solids flow enters a riffler, it "reads" identical resistances for each exiting pipeline and the flow divides equally. The equations developed in Chapter 3, along with the method for analyzing pipeline systems previously developed in this chapter, allow for the magnitude of the necessary flow resistances to be calculated.

The methods developed in the previous sections of this chapter are used to determine the size of the flow resistances which are needed to provide balanced fuel distribution. The procedure is as follows:

1. Analyze each pipeline as though it operates independently of any others.

   i. Assume the fuel supplied by the exhauster divides equally, and that each pipeline receives:

$$\dot{m}_{c,i}^{b} = \frac{\dot{M}_{c,T}}{N} \qquad (4-4)$$

   ii. Assume the air supplied by the exhauster divides equally, so that each pipeline has the same superficial air velocity.

   iii. Assume the air and coal material properties are identical in each pipeline.

   iv. Calculate the resultant pressure drop for

each pipeline, $\Delta P_{i,T}$.

2. Determine which pipeline experiences the largest pressure loss, and then calculate the difference for each of the other pipelines:

$$\Delta P_{i,Diff} = \Delta P_{max} - \Delta P_{i,T} \qquad (4\text{-}5)$$

3. To each pipeline, add a flow resistance element whose resultant pressure loss will be:

$$\Delta P_{i,Res} = \Delta P_{i,Diff} \qquad (4\text{-}6)$$

After the flow resistances are added, when the gas-solid stream enters a coal riffler, it will "see" identical paths presented by both of the exiting pipelines.

For example, assume that the pipelines shown in Figure (4-2) are analyzed by the method presented in the balancing algorithm, with the following results:

Pipeline	$\Delta P_{i,T}$	$\Delta P_{i,Res}$
1	10.0 psi	2.0 psi
2	12.0 psi	0.0 psi

Then, for this pipeline system to be used for power plant coal distribution, a flow resistance device must first be added to Pipeline 1. A properly sized device will produce identical pressure drops (12.0 psi) in each of the pipelines, and the flow will divide equally as it passes through the riffler.

4.3 Use of an Orifice Plate as the Flow Resistance

A commonly used device for balancing pipe flows is the concentric orifice plate, shown in Figure (4-3). This thin plate has a hole which is concentric with respect to the pipe axis of flow. The amount of flow resistance presented by an orifice plate depends directly upon the diameter of its opening, d_o. Expressions for calculating the pressure drop a flow experiences as it passes through an orifice plate are derived from experimental data. However, correlations vary depending upon the experimental method employed. Figure (4-4) shows how the location of the pressure taps affects the pressure drop value obtained.

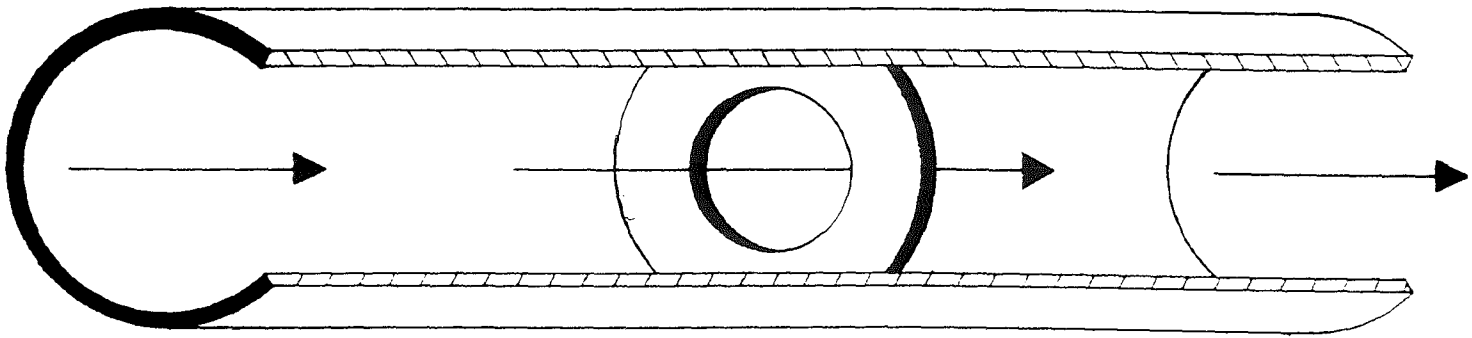

Figure (4-3) Diagram of a concentric orifice plate within a pipe.

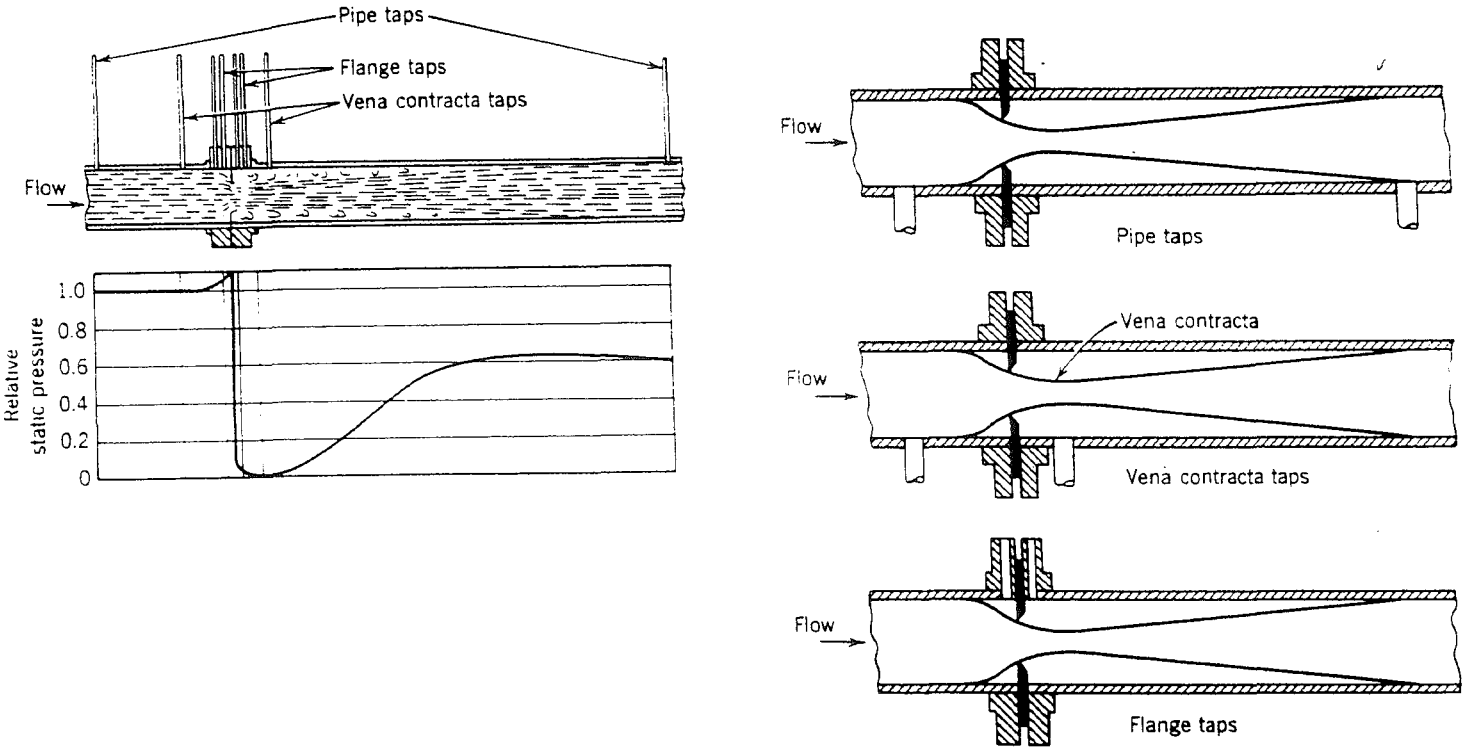

Figure (4-4) The measured pressure drop across an orifice plate depends upon the location of pressure taps.

4.3.1 *Expression for Pressure Drop Across Orifice Plates*

The balancing algorithm presented in Section 4.2.2 requires an expression for the flow resistance which accounts for its overall effect upon the flow. Thus, an equation based upon pipe-tap data will be utilized. Benedict [31] presents an equation for calculating the pressure drop across orifice plates which is based upon a method recommended by the American Society of Mechanical Engineers [32]. Starting with a dimensionless coefficient representing the ratio of the orifice opening diameter to the pipe diameter, the method is as follows:

$$\beta = \frac{d_o}{D} \tag{4-7}$$

$$\alpha = d_o\left(905 - 5000\beta + 9000\beta^2 - 4200\beta^3 + {}^{875}\!/_{D}\right) \tag{4-8}$$

$$K_e = 0.5925 + \frac{0.0182}{D} + \left(0.44 - \frac{0.06}{D}\right)\beta^2 + \left(0.935 + \frac{0.225}{D}\right)\beta^5 + 1.35\beta^{14} + \left(\frac{1.43}{D^{0.5}}\right)(0.25 - \beta)^{2.5} \tag{4-9}$$

$$K_o = K_e\left(\frac{10^6 d_o}{10^6 d_o + 15\alpha}\right) \tag{4-10}$$

$$K = K_o\left(1+\frac{\beta\alpha}{R_D}\right) \tag{4-11}$$

$$\eta = K\left(1-\beta^4\right)^{0.5} \tag{4-12}$$

where η is the flow discharge coefficient, and the Reynolds number used is based upon the pipe diameter and superficial air velocity. The pressure loss is then calculated as:

$$\dot{m}' = \rho_f U_o\left(\frac{\pi D^2}{4}\right) \tag{4-13}$$

$$\dot{m} = \frac{\dot{m}'}{\eta} \tag{4-14}$$

$$\Delta P_{OP} = \left(\frac{4\dot{m}}{\pi D^2}\right)^2 \frac{\left(1-\beta^4\right)}{2\rho_f} \tag{4-15}$$

These expressions pertain only to single-phase flow. At this time, there have been no correlations published which account for the flow of a gas-solid mixture through an orifice plate. However, due to the nature of the flow stream as it approaches and passes through the orifice plate, the use of the one-phase flow correlation is valid. Since the plate represents a very sudden area change, its only effect upon the

solid phase of the flow is the loss of momentum experienced by the particles which collide with the plate. But due to the very dilute conditions used in the pneumatic transport of pulverized coal, the number of particles which hit the plate is very small and the plate's effect is overwhelmingly enacted upon the gas phase of the flow.

Although several studies have been performed for pneumatic flow through a Venturi meter, it represents a distinctly different phenomenon than that occurring in the flow through orifice plates. Figure (4-5) displays this difference through the use of solid particle streamlines. Since the two-phase flow encounters a smooth, gradual area change as it moves through the Venturi, the resistance effect is manifested on both the solids and the air. However, the sudden area change of an orifice plate allows the majority of the particles to move through the plate without "noticing" its presence. A comparison of the gas-solid flow regimes in orifice plates and Venturi meters, which verifies this concept, is presented by Carlson, Frazier, & Engdahl [33].

4.3.2 Use of the Orifice Plate Pressure Drop Equations

Returning to the flow distribution example examined in Section 4.2.2, the resistance which must be added to Pipeline 1 needs to produce a pressure drop of 2.0 psi. The series of equations presented in Section 4.3.1 can be used to calculate

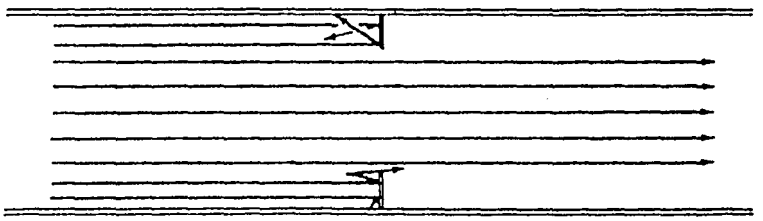

Orifice Plate

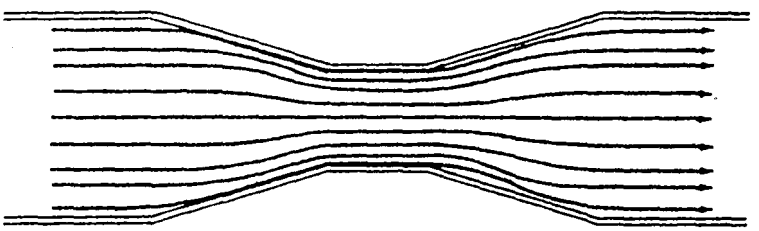

Venturi Meter

Figure (4-5) Diagram of particle flow paths through an orifice plate and a Venturi meter.

the orifice opening diameter required to produce this additional flow resistance. Using an initial guess for d_o, an iterative procedure will generate the actual value of d_o which produces the necessary pressure drop. Thus, for each value of $\Delta P_{i,Res}$ needed to balance a system of pipelines, Eqs. (4-7) through (4-15) can be utilized to calculate the orifice plate size needed by each pipeline.

4.4 Calculation of Imbalanced Flows

As discussed in Section 4.2, the coal distribution system in an electric power plant is governed by the boundary condition that the total pressure drop must be equal in each of the pipelines fed by a single pulverizer, as given by Eq. (4-3). Therefore, if the pipelines are not equipped with correctly sized orifice plates, the system must compensate for the unbalanced pressure drops with an addition or reduction in the mass loading of coal and air which a pipeline receives. Thus, the coal burners which are supplied by the pipelines receive varying amounts of fuel and consequently they operate at differing air-to-fuel ratios.

The computation of fuel distribution will involve an iteration of mass fractions until the pipeline pressure drops are equalized. The solution of the series of pressure drop equations requires the determination of 3N unknowns (N is the number of pipelines). For example, an analysis of the system shown in Figure (1-4) will require the determination of 12

unknowns: the 4 coal mass flow rates, the 4 air mass flow rates, and the 4 pipeline pressure drops. However, the burner balancing routine only provides 9 equations, as shown in Figure (4-6). Thus, an assumption must be made for 3 of the variables. Based upon the dilute nature of pulverized coal transport, the air mass flow rates will function as the assumed variables. Two methods are now presented for determining coal flow distribution, each based upon a distinct assumption regarding the distribution of air mass flow rates.

4.4.1 Determining Actual Fuel Distribution - Method I

To determine the amount of coal which each pipeline receives, an iterative procedure is used. An initial guess for the mass fraction of the total coal flow which each pipe receives is needed to begin the process. From the mass fraction, the amount of coal flowing through each pipe is calculated as:

$$\dot{m}^{u}_{c,i} = y_i \times \dot{M}_{c,T} \qquad (4\text{-}16)$$

This method is based upon the assumption that the air flow divides equally among the pipelines. Along with this information, these initial coal flow rate values are used to calculate the total pressure loss in each pipeline, following the method of Section 4.1. The pressure drop values are then compared to each other to determine if they are equal. If

UNKNOWN VARIABLES

Coal Mass Flow Rates:	$\dot{m}_{c,1}$, $\dot{m}_{c,2}$, $\dot{m}_{c,3}$, $\dot{m}_{c,4}$	[4]
Air Mass Flow Rates:	$\dot{m}_{a,1}$, $\dot{m}_{a,2}$, $\dot{m}_{a,3}$, $\dot{m}_{a,4}$	[4]
Pipeline Pressure Drop:	$\Delta P_{1,T}$, $\Delta P_{2,T}$, $\Delta P_{3,T}$, $\Delta P_{4,T}$	[4]

Total Number of Unknowns = 12

EQUATIONS

Conservation of Coal Mass:	$\dot{m}_{c,1} + \dot{m}_{c,2} + \dot{m}_{c,3} + \dot{m}_{c,4} = \dot{M}_{c,T}$	[1]
Conservation of Air Mass:	$\dot{m}_{a,1} + \dot{m}_{a,2} + \dot{m}_{a,3} + \dot{m}_{a,4} = \dot{M}_{a,T}$	[1]
Pipeline 1 Pressure Drop:	$\Delta P_{1,T} = f\,(m_{c,1}, m_{a,1})$	[1]
Pipeline 2 Pressure Drop:	$\Delta P_{2,T} = f\,(m_{c,2}, m_{a,2})$	[1]
Pipeline 3 Pressure Drop:	$\Delta P_{3,T} = f\,(m_{c,3}, m_{a,3})$	[1]
Pipeline 4 Pressure Drop:	$\Delta P_{4,T} = f\,(m_{c,4}, m_{a,4})$	[1]
Equalized Pressure Drops:	$\Delta P_{1,T} = \Delta P_{2,T} = \Delta P_{3,T} = \Delta P_{4,T}$	[3]

Total Number of Equations = 9

Figure (4-6) The unknown variables and the governing equations for a system of 4 pipelines.

they differ from each other, the coal mass fraction values are changed and the procedure is repeated until a set of coal mass fractions produces equalized pressure drops. The air mass flow rates remain constant throughout this procedure.

4.4.2 Determining Actual Fuel Distribution - Method II

The second method of determining fuel distribution does not assume that the air mass flow is divided equally among the pipelines. Rather, air mass fractions are determined by analyzing the piping system under clean air flow conditions. With the coal mass flow set to zero, the system reduces to 2N unknowns and 2N equations and the amount of air flow in each pipeline can be determined. When coal is added to the air flow, it is assumed that the air flows continue to be distributed in the same manner as for clean air flow. The coal mass fractions are then varied until the pipeline pressure drops are equalized, as in Section 4.4.1. Throughout this iterative procedure, the air mass flow rates remain constant.

The procedures outlined above (Methods I & II) are used to determine how a given flow system is *actually* performing. Conversely, Sections 4.2 and 4.3 present a method for determining what alterations must be made on the same flow system to provide a uniformly distributed flow. A calculation routine for these two procedures is presented in Chapter 5.

4.5 Effect of Coal Riffler Upon the Flow

Referring to Figure (4-2), the second flow section encountered by both pipelines is a coal riffler. This device (see Figure (1-5)) is composed of a series of parallel flow passages which serve to split the inlet flow into two outlet flows. Thus, the continuity equation (conservation of mass flow) governs the flow of both the air and the coal through the riffler. For Figure (4-2):

$$\dot{m}_{c,in} = \dot{m}_{c,1} + \dot{m}_{c,2} = \dot{M}_{c,T} \tag{4-17}$$

$$\dot{m}_{a,in} = \dot{m}_{a,1} + \dot{m}_{a,2} = \dot{M}_{a,T} \tag{4-18}$$

Since no procedure has yet been published for gas-solids flow through a riffler, an analysis of the pressure drop across such a device was performed by the author using several different methods. The first approach assumed the flow could be treated as a fully-developed, one-phase, steady flow between two stationary plates. The continuity and momentum equations for fluid flow were then simplified to produce the simple relation:

$$\overline{V} = \frac{Q}{A} = \frac{a^2}{12\mu}\frac{\Delta P}{L} \tag{4-19}$$

As can be seen, this equation assumes a uniform velocity profile for the air flow which is given by:

$$\overline{V} = \frac{2}{3} U_{max} \qquad (4\text{-}20)$$

Using typical values for flows in power plant systems, this equation yielded pressure losses which were less than 1% of the pressure drop encountered in a 20 foot section of horizontal pipe. Thus, the pressure loss due to the coal riffler is negligible in comparison to those generally encountered in the other pipeline sections.

A second approach utilized a combination of head loss coefficients which were presented by Idelchik [34] for one-phase flows through a series of flat, parallel plates. This method additionally accounts for the entrance effects of the flat plates. Once again, typical operating values were used to evaluate the resulting pressure drop. As before, its value was negligible (< 1%) in comparison to those usually obtained for power plant fuel distribution systems.

Thus, in absence of a two-phase flow correlation and based upon the results of simplified, one-phase, air flow calculations, the pressure drop across a coal riffler will be neglected in the procedures presented by this paper. Although this assumption is inherently incorrect, it is considered to be of minor importance with regard to the overall objective of balancing coal flow distribution in electric power plants.

5. CALCULATION PROCEDURE

5.1 Computer Code

A computer code, written in FORTRAN, has been developed to perform the series of calculations described in Chapter 4. Part I of the program calculates the orifice plates which are needed to balance the coal distribution in a given system. The actual fuel distribution of the system is determined in Part II. As input, the program requires information about the air and coal flow and the exact geometry of the piping system. The code is designed for fuel distribution systems with 2, 4, or 8 pipelines.

5.2 Part I - Calculation of Orifice Plates

A flow chart schematic of the procedure used in Part I of the balancing program is given in Figure (5-1). For reference purposes, each individual section of the pipeline system is assigned a label consisting of two numbers: (i,j), as in Figure (4-2). The first number, i, indicates to which pipeline the section belongs. This value ranges from 1 to N, where N is the number of burners supplied by a single exhauster. The second number, j, corresponds to the location of the section in the pipeline i. Pipe sections are numbered successively, starting with j=1 as the first section downstream of the exhauster and ending with $j=j_{max}$ for the

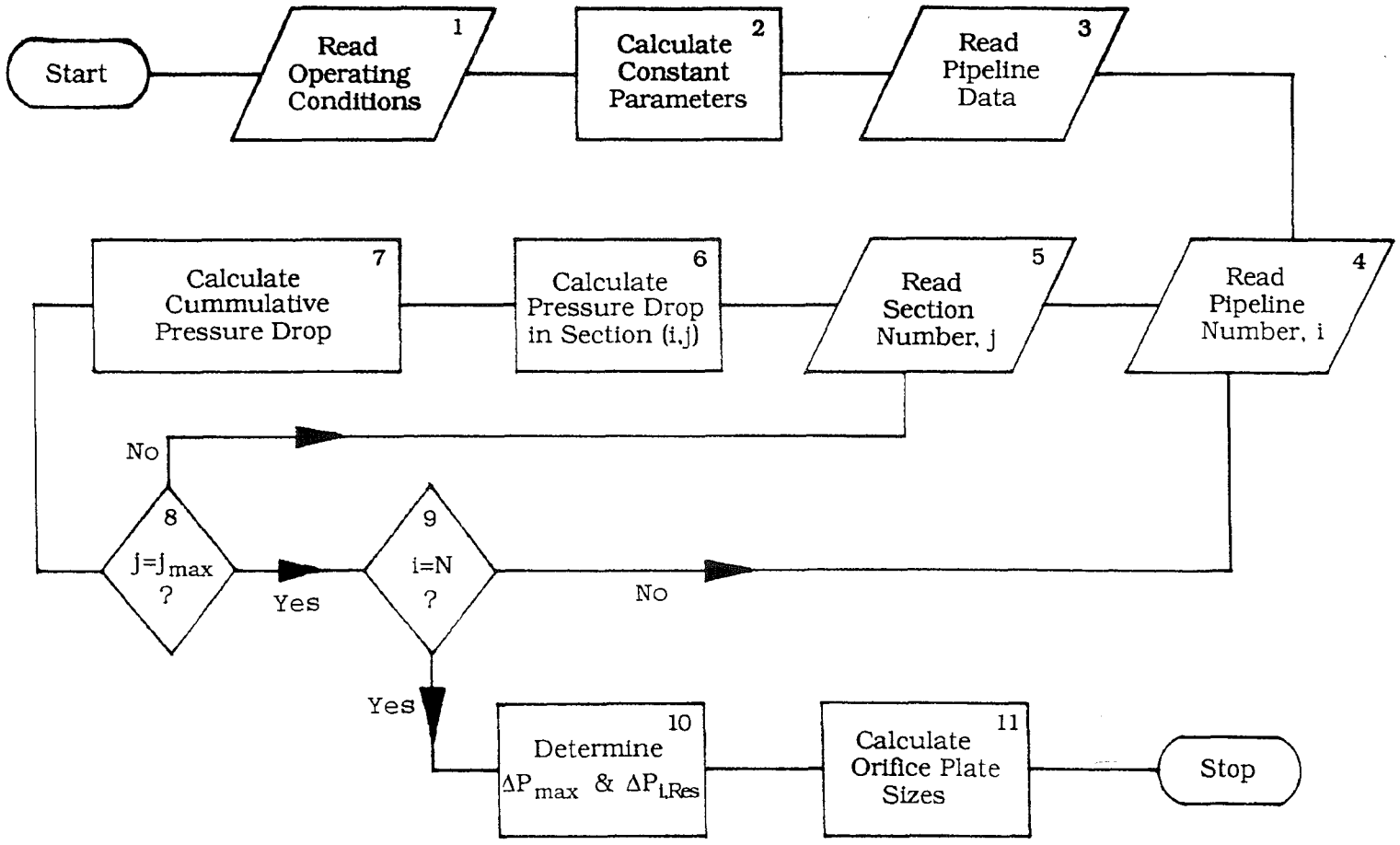

Figure (5-1) Flow chart describing Part I of the computer code.

final section before the burner.

5.2.1 Operating Conditions

In Figure (5-1), the first step in the flow chart reads the operating conditions of the current system. Specifically, the following information is needed:

1. The air temperature, T, of the conveying air as it exits the exhauster (in degrees Fahrenheit).
2. The atmospheric pressure, P_{atm} (in psia).
3. The average diameter of the pulverized coal particles, d_p (in feet).
4. The specific gravity of the coal, γ_c .
5. The coal mass flow rate supplied by the exhauster (in lbm/minute).
6. The superficial air output of the exhauster (in cfm).

As shown in Figure (5-1), this information is then used to calculate several constant flow parameters. The mass density of the conveying air, in units of (lbm/ft^3), is calculated as:

$$\rho_{air} = \rho_f = \frac{28.97 lb_m}{lb_{mol}} \times \frac{(P_{atm}) psia}{(T+460)^\circ R} \times \frac{1 lb_{mol}{}^\circ R}{10.73 psia \times ft^3} \qquad (5\text{-}1)$$

The air viscosity, in units of (lbm/feet/sec), is next determined. However, the correlation is in metric units and the air temperature must first be converted to units of Kelvin.

$$T_K = (T - 32)\left(\frac{5}{9}\right) + 273 \qquad (5\text{-}2)$$

$$\mu = \left| \frac{\left(1.458 \times 10^{-6}\right) T_K^{0.5}}{1 + \frac{110.4}{T_K}} \right| \frac{kg}{m*sec} \times \frac{2.205 lb_m}{1kg} \times \frac{0.3048 m}{1 foot} \qquad (5\text{-}3)$$

Using the specific gravity, the mass density of the coal particles, in ($lbm/feet^3$), can be calculated as:

$$\rho_{coal} = \rho_p = \gamma_c \times 62.4 \frac{lb_m}{feet^3} \qquad (5\text{-}4)$$

The initial calculations conclude with the determination of the terminal velocity for a single particle moving in an infinite flow field, U_t, in units of (feet/sec):

$$U_t = \frac{0.153 d_p^{1.14} g^{0.71} \left(\rho_p - \rho_f\right)^{0.71}}{\mu^{0.43} \rho_f^{0.29}} \qquad (5\text{-}5)$$

This equation is identical to Eq. (2-2) and has been rewritten here for convenience.

5.2.2 Geometry of Pipeline Distribution System

Step 3 of Figure (5-1) involves the storage of pipeline structural information by the program. Initially, the following two parameters are input:

1. N, the total number of burners (and pipelines) supplied by a single exhauster.

2. The pipeline material: Commercial Steel, Wrought Iron, Galvanized Iron, Cast Iron, or Asphalted Cast Iron.

The material specification is needed to determine the pipe surface roughness, a contributor to the gas friction factor, f_g.

The entry and storage of the distribution system geometry is performed for each pipeline via a DO LOOP, which runs at steps of i=1 to N. Within each step of this loop, a second DO LOOP is carried out, running for steps of j=1 to j_{max}. The inner loop steps along an individual pipeline and records the data which is specific to that pipe section. When the current pipeline reaches the furnace windbox at $j=j_{max}$, the outer loop steps forward to the next value of i. In this successive manner, the data needed for each section of each pipeline is recorded.

The following information is recorded for each pipe section type:

1. Horizontal or Vertical Pipe: Pipe diameter, D, and pipe length, L (in feet).

2. Coal Riffler: Inlet, A_{in}, and outlet, A_{out}, cross-sectional area (in square feet).

3. Pipe Bend: Pipe diameter, D, and bend radius of curvature, r_c (in feet).

4. Orifice Plate: Pipe diameter, D, and diameter of plate opening, d_o (in feet).

5.2.3 *Pressure Drop Calculations*

The procedure shown in Section 5.2.2 to record the pipeline information is also used to calculate the pressure drop developed in the current pipe section. For each step within the DO LOOP structure, computational subroutines corresponding to the type of flow structure are employed and the resultant pressure loss calculated.

Consider the distribution system shown schematically in Figure (5-2). (The geometrical data corresponding to this system are given in Appendix 1.) Examining the path of Pipeline 1, the procedure is as follows. The outer loop is set to i=1 and the inner loop begins with j=1, corresponding to the pipe section (1,1). From memory, the program "knows" this section to be a vertical pipe. Therefore, it calls Subroutine VERN to perform the calculations which correspond to flow through a vertical pipe. (Information about VERN and all other subroutines described in this thesis can be found in Appendix 2.) The subroutine returns values for the particle velocity, voidage coefficient, acceleration length, the total pressure drop, and each of its components, including acceleration effects:

$$\Delta P_T(i,j) = \Delta P_A(i,j) + \Delta P_S(i,j) + \Delta P_{Fg}(i,j) + \Delta P_{Fs}(i,j) \qquad (5\text{-}6)$$

After performing the calculations of step 6 in the flow

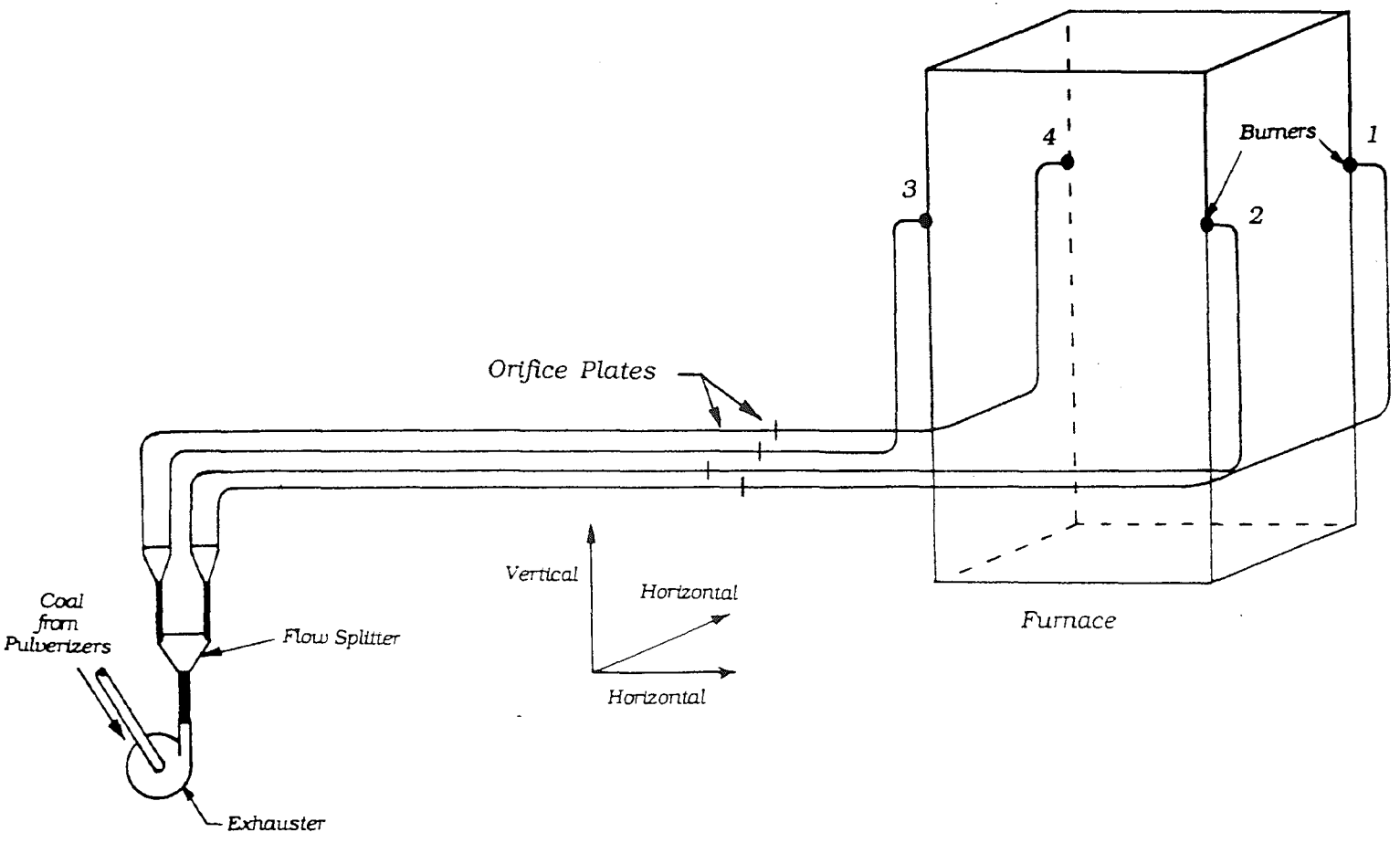

Figure (5-2) Schematic of piping layout used in sample calculations.

chart of Figure (5-1), the total pressure drop found in section (1,1) is added to the total pipeline pressure drop. Since this value is initially zero, after section (1,1) the total pipeline pressure drop is equal to the total pressure drop in the vertical pipe. This summation is represented by step 7 in the flow chart.

The main program then checks to see if $j=j_{max}$, signifying that the pipeline has reached the furnace. Represented as Step 8 in Figure (5-1), this decision is a "No". Thus, the program returns to step 5 to read the next flow section, designated as (1,j=j+1).

Continuing along Pipeline 1 to section (1,2), the corresponding section is a coal riffler. Since the goal of Part I of this program is to determine the flow resistances needed to provide uniformly distributed flow, the coal mass flow entering from section (1,1) is divided into two equal flows exiting to sections (1,2) and (2,2). Similarly, the air flow is also divided into two equal portions. As discussed in Section 4.6, the pressure drop across the riffler is considered negligible.

Still referring to Pipeline 1, the next section, (1,3), is a vertical pipe. As with section (1,1), the subroutine VERN is called to perform the necessary calculations. However, acceleration calculations are not performed since the particles have already been fully accelerated. The total pressure drop calculated for section (1,3) is then added to

the total pressure drop in section (1,1). Thus, a summation is performed within the inner DO LOOP to determine the total pressure drop experienced by the whole pipeline. This procedure is shown in Figure (5-1) as step 7, and can be represented as:

$$\Delta P_{i,T} = \sum_{j=1}^{j=j_{max}} \Delta P_T(i,j) \qquad (5\text{-}7)$$

Another coal riffler is encountered as section (1,4) and, as for section (1,2), the coal and air flows are both equally divided.

Following the vertical pipe of section (1,5), a pipe bend is encountered as section (1,6). The subroutine BENJI is called to perform the calculations necessary to determine the pressure drop which results from the bend. The subroutine returns this value, ΔP_B , to the main program, where it is added to the total pipeline pressure drop.

Section (1,7) is a horizontal pipe and the main program calls the subroutine HOWIE to perform the associated calculations. HOWIE returns to the main program values for the horizontal particle velocity, the voidage coefficient, the total pressure drop, and each of its components. Since the acceleration effects arising from particle collisions with the pipe bend wall in section (1,6) are accounted for by the bend pressure drop correlation, no acceleration pressure drop calculations are performed by HOWIE. Thus, the total pressure

drop for this section can be represented as:

$$\Delta P_T(1,7) = \Delta P_{HZ}(1,7) = \Delta P_{Fg}(1,7) + \Delta P_{Fs}(1,7) \qquad (5\text{-}8)$$

The final section of the pipeline structure which will be discussed is section (1,10). This section corresponds to an orifice plate which has been placed in the pipeline prior to these balancing calculations. Thus, it will be an integral segment of the calculations in Part II of this program when the actual fuel distribution of the current and unaltered pipe system is determined. However, this part of the program (Part I) is concerned with finding the orifice plates necessary to provide ideal coal flow distribution. Thus, the presence of the current orifice plate is neglected in the calculations of Part I.

The process outlined above is repeated for each section of pipeline 1 until it reaches the furnace. This is represented in Figure (5-1) as a "Yes" decision exiting step 8 of the flow chart. Since the procedure must still be performed for pipelines 2, 3, and 4, a "No" decision exits step 9 and the program returns to step 4. There, the outer DO LOOP steps forward to i=2 and the inner DO LOOP again runs from j=1 to $j=j_{max}$, calculating the total pressure drop for pipeline 2. This routine is continued until $j=j_{max}$ when i=N.

This combination elicits "Yes" decisions from both step 8 and step 9 of the flow chart, and the program advances to the orifice calculation routine.

5.2.4 Calculation of Orifice Plate Sizes

When the calculation of the total pressure drop in each of the pipelines has been completed, the N values of are scanned to determine which pipeline experiences the largest pressure loss. This value is designated as ΔP_{max} , and its determination is shown as step 10 in the flow chart of Figure (5-1). Each of the pipelines is compared to ΔP_{max} and their difference is given as:

$$\Delta P_{i,Diff} = \Delta P_{max} - \Delta P_{i,T} \qquad (5\text{-}9)$$

This equation follows along with the procedure presented in Section 4.2.2.

The value of $\Delta P_{i,Res}$ represents the amount of flow resistance which must be added to the pipeline to equalize its pressure drop with the others. Calculation of the orifice plate size which produces this additional pressure drop is performed in the subroutine DRAC. Utilizing the expressions developed in Section 4.3.1, this subroutine determines the value of d_O which yields a pressure drop of $\Delta P_{i,Res}$. In addition, DRAC calculates the number of plates, N_{OP}, which must be added to a pipeline if one plate cannot provide the

pressure drop desired. The subroutine returns this value to the main program along with the corresponding orifice diameters. This procedure is shown as step 11 in the flow chart of Figure (5-1).

The completion of the procedure outlined in step 11 of the flow chart corresponds to the completion of Part I of the burner balancing program. At this point, new orifice plate sizes have been calculated to replace those (if any) currently in the pipeline system. The new plates will provide equalized flow resistances for each of the pipelines so that as the gas-solid flow enters a riffler, it will "see" two identical exit paths. Since the exit pipelines will present equivalent resistances to the incoming flow, the flows will be divided equally. This distribution of equal amounts of coal and air by a single exhauster accomplishes the first objective of this thesis.

5.3 Part II - Actual Fuel Distribution by Current System

The second part of the burner balancing computer code calculates the flow conditions which currently exist in a given pipeline system (including current orifice plates), without the addition of the new orifice plate recommendations from Part I. Outlined in the flow chart of Figure (5-3), the procedure determines the amount of coal a burner actually receives in the current, unaltered system in terms of its mass flow rate. In addition, each burner's subsequent air-to-fuel

ratio is also calculated.

5.3.1 Initial Values for Coal Mass Flow

In step 1 of the flow chart, air mass flow rates are assigned to each pipeline based upon either Method I or Method II, as outlined in Chpater 4. Also, initial guesses are made for the mass fraction of coal in each pipeline. Defined as

$$1 = \sum_{i=1}^{N} y_i \tag{5-10}$$

the mass fraction is used to determine the coal mass flow rate via Eq. (4-16), which is repeated here for convenience:

$$\dot{m}^{u}_{c,i} = y_i \times \dot{M}_{c,T} \tag{4-16}$$

The initial guess is based upon the total pipeline pressure drops calculated in Part I. Since the coal mass flow is inversely related to the pressure drop, the initial guess is derived as:

$$x_i = \frac{\Delta P_{i,T}}{\sum \Delta P_{i,T}} \tag{5-11}$$

$$y_i = \frac{\left(1/x_i\right)}{\sum\left(1/x_i\right)} \tag{5-12}$$

Using these expressions, initial values of the coal mass flow

received by each pipeline are determined.

5.3.2 Pressure Drop due to Imbalanced Flow

In Figure (5-3), steps 2 through 6 are similar to those performed in Part I of the computer program. In steps 2 and 3, DO LOOPS are executed to determine the current pipe section (i,j) and retrieve its corresponding information, which is stored in the program's memory. However, the procedure in step 4 differs from Part I in two ways. First, the effect of a coal riffler is no longer to evenly divide the coal flow, but to divide it according to the mass fractions specified in step 1. For example consider the flow system shown in Figure (5-2). The initial guess calculations provide y_1, y_2, y_3, and y_4, which are then used to work backward and determine how the flow is divided as it encounters each of the rifflers, as shown in Figure (5-4). Thus, when the DO LOOP encounters a coal riffler, it assigns coal mass flows according to these specifications.

The second difference between Part II and Part I is that now the pressure drop due to the presence of an *existing* orifice plate is included in the total pipeline pressure drop. Using the geometry of the orifice plate stored in step 3 of Part I, the subroutine OTTO calculates the resultant pressure loss across it. This value is then added to the total pipeline pressure drop in the same manner put

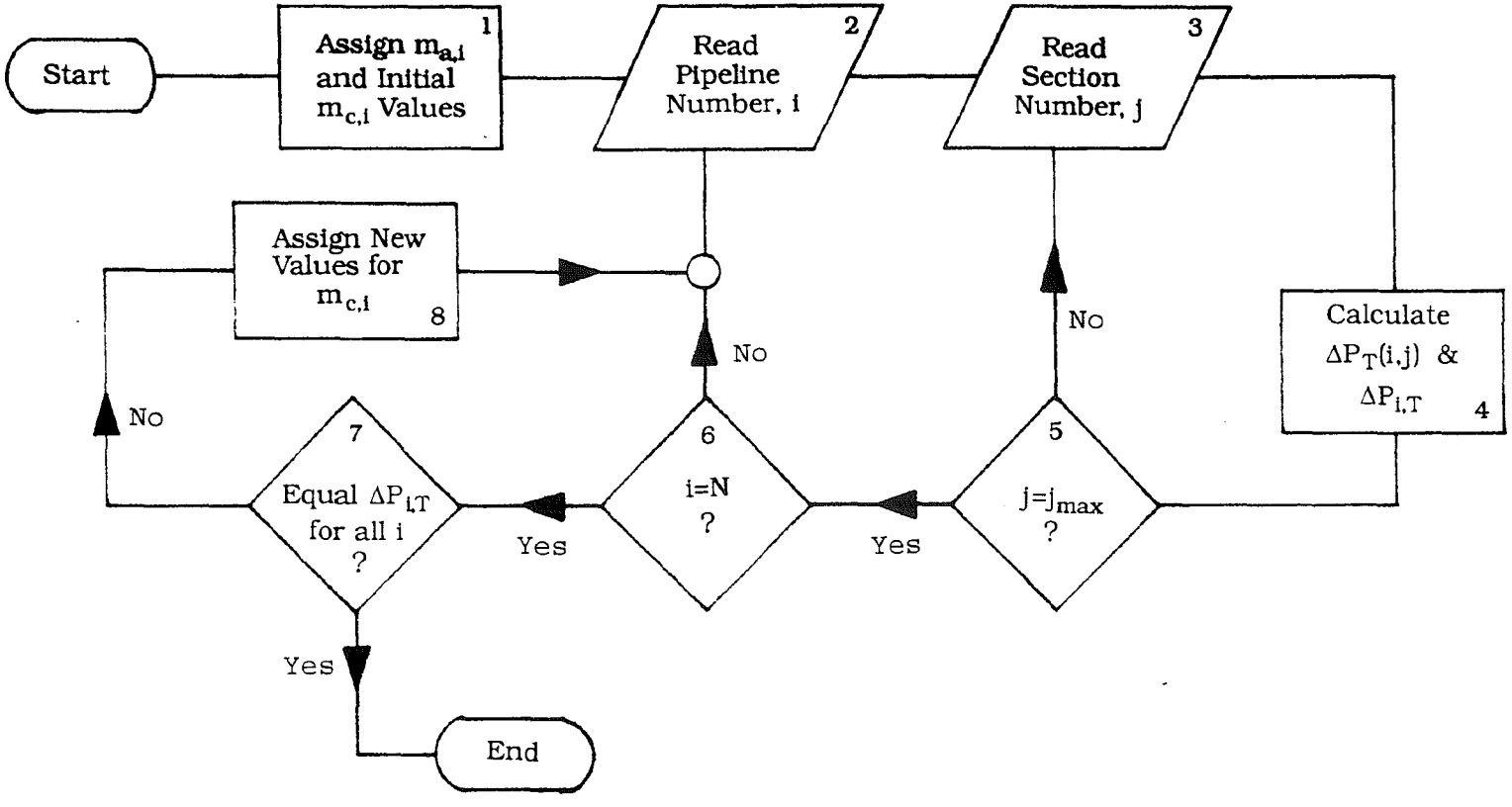

Figure (5-3) Flow chart describing Part II of the computer code.

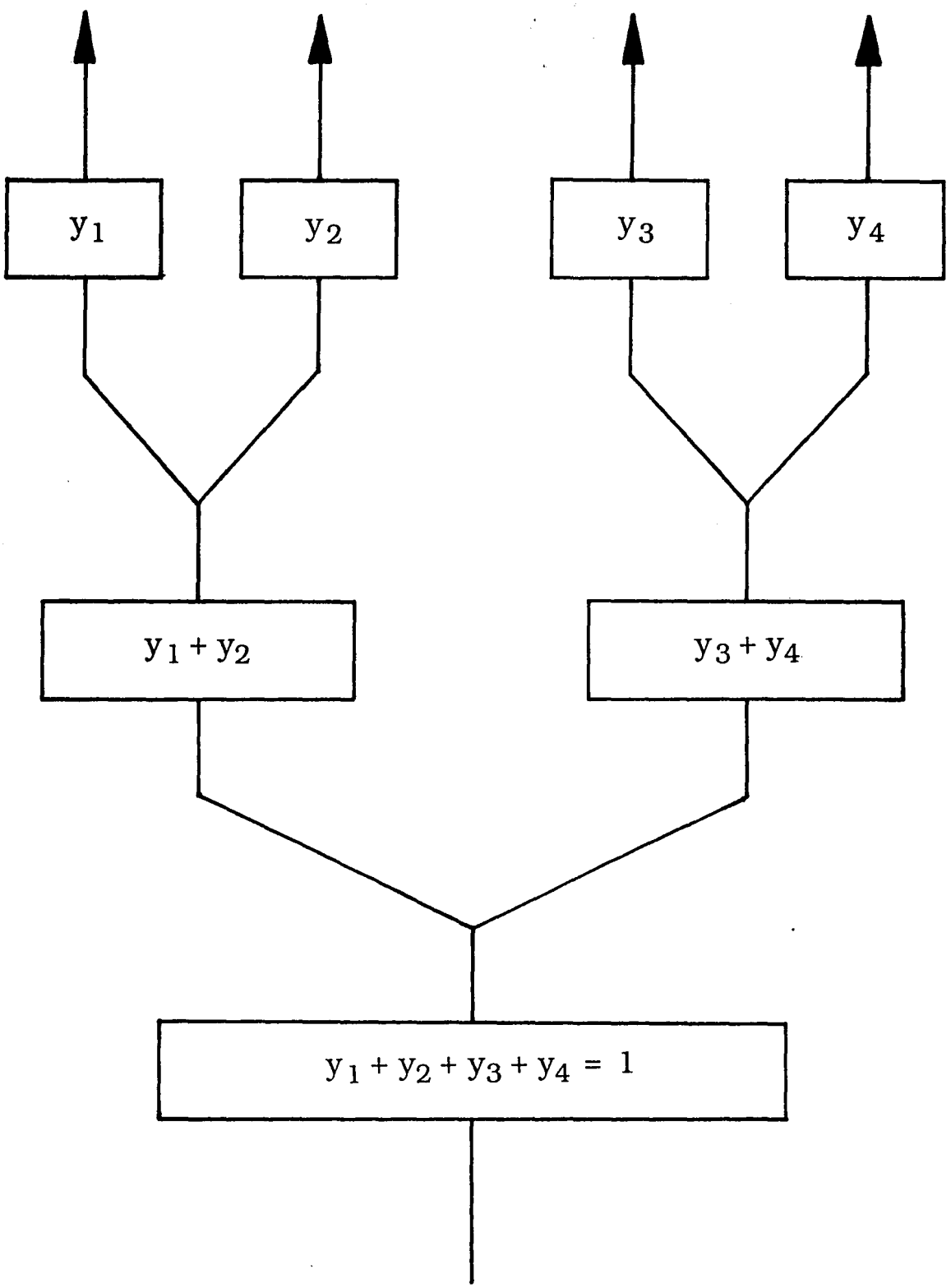

Figure (5-4) Distribution of coal mass fractions.

forth by Eq. (5-7).

Other than these two differences, the total pipeline pressure drops are calculated in the same method as Part I. Furthermore, the decision steps 5 and 6 in Figure (5-3) are identical to those in Figure (5-1). However, step 7 of Figure (5-3) involves a comparison of the pressure drops calculated in Part II. The total pressure drops for each of the pipelines are compared to their mean value to see if they have been equalized. This would satisfy the boundary condition which governs the fuel distribution in actual flow situations. If they differ from the mean beyond a specified error range, then a "No" decision leads to step 8. In this step, coal mass flow values are reassigned based upon the pressure drop values. If the total pressure drop in a pipeline is lower than the mean, then its coal mass fraction is increased. And if the total pressure drop is larger than the mean, then its mass fraction is decreased. After these new mass flows have been assigned, the program repeats the procedure (steps 2 through 6) until a "Yes" value is achieved in step 7. The program ends when the pipeline pressure drops have been equalized and the actual fuel distribution has been determined.

5.3.3 Distribution Information

Along with the amount of coal received by each pipeline, Part II of the program also determines the voidage

coefficient, which allows the air-to-fuel ratios to be calculated:

$$\dot{m}^{u}_{i,air} = \frac{U_o}{\varepsilon_i} \times \frac{\pi D^2}{4} \times \rho_f \qquad (5\text{-}13)$$

$$(A/F)_i = \frac{\dot{m}^{u}_{i,air}}{\dot{m}^{u}_{i,coal}} \qquad (5\text{-}14)$$

where

$$U_o = \frac{EO\left(feet^3/minute\right)}{60\,secs/minute} \times \frac{4}{\pi D^2} \times \frac{1}{N} \qquad (5\text{-}15)$$

Thus, the operating conditions of each burner can be determined and used to analyze the performance of the distribution system. If Method II has been followed, Eq. (5-13) is not performed. Rather, the air mass flow values are assigned based upon clean air flow calculations.

5.4 Sample Application

The computer code discussed in this chapter will now be used to analyze the performance of the distribution system shown in Figure (5-2). Geometrical information pertaining to the pipelines is given in Appendix 1 of this thesis. Operational data and their related parameters are presented in Figure (5-5).

```
-------Operational Data-------

    Conveying air temperature = 165.00 deg. F
        has a humidity level of  50.0000 %
        with density = 0.06348 lbm/ft^3
        and viscosity =  0.13844E-04 lbm/(ft*sec)

    The mill coal feed rate =    720.00 lbm/min.
        with mean particle diameter =  0.26200E-03 feet
        and coal density =  74.8800 lbm/ft^3

    Particle terminal velocity =  0.86926E+00 ft/sec

    The exhauster air output =  24000.00 cfm
        which supplies 4 burners

    The pipeline material is Cast Iron
```

Figure (5-5) Operational data used in sample calculations of Section 5.4.

```
  Section  1 is a Vertical Pipe

     with D= 2.50000 ft. and L=   4.0000 ft.
     Uo=  81.4873 ft/sec     Mc=   12.000000lbm/sec
     Gas friction factor =  0.16147E-01
     Up=  81.48733 ft/sec, with a Voidage of 0.999599E+00
        and YY =  0

     Acceleration dP =  0.112456E+01 inches H2O
     Static Head dP =  0.167708E-01 inches H2O
     Gas Friction dP =  0.221828E+00 inches H2O
     Solids Friction dP =  0.561358E-03 inches H2O
     Total Friction dP =  0.222389E+00 inches H2O
     Total Pressure Drop =  0.136372E+01 inches H2O
```

Figure (5-6) Pressure drop data and flow information for the vertical pipe section (1,1).

MISSING

PAGE

```
Section  6 is a Pipe Bend

   Pipe diameter = 1.25000 ft
   Radius of curvature = 2.00000 ft
   Bend angle =  90.000 degrees
   Uo =  81.4873 ft/sec       Mc =     3.000000 lbm/sec
   Total Bend Pressure Drop =  0.503838E+00 inches H2O
```

a.) Pipe bend data.

```
Section  7 is a Horizontal Pipe

   with D= 1.25000 ft. and L=  50.0000 ft.
   Uo=  81.4873 ft/sec      Mc=     3.000000 lbm/sec
   Gas friction factor=  0.18869E-01
   Up=  81.20340 ft/sec, with a Voidage of  0.999598E+00
      and XX=  2

   Gas Friction dP =  0.380613E+01 inches H2O
   Solids Friction dP =  0.149353E+00 inches H2O
   Total Friction dP =  0.395549E+01 inches H2O
   Total Pressure Drop =  0.395549E+01 inches H2O
```

b.) Horizontal pipe data.

```
Section 10 is a previously existing Orifice Plate

   Plate outer diameter = 1.25000 ft
   Plate inner diameter = 1.23500 ft
   Superficial gas speed =  81.4873 ft/sec
   Pressure Drop =  0.130775E+00 inches H2O
      NOTE: Excluded from Pipeline Total dP
            used for new orifice calculations.
```

c.) Orifice plate data.

Figure (5-7) Pressure drop data and flow information; a.) pipe bend, b.) horizontal pipe, and c.) orifice plate.

```
--Total Pressure Drop for each Pipeline--
     EXCLUDING Orifice Plates

    Pipeline No. 1 has dPt =  0.105038E+02 inches H2O
    Pipeline No. 2 has dPt =  0.845701E+01 inches H2O
    Pipeline No. 3 has dPt =  0.687481E+01 inches H2O
    Pipeline No. 4 has dPt =  0.892164E+01 inches H2O

       *** Pipeline No. 1 has the dominant pressure drop ***
```

Figure (5-8) Total pipeline pressure drop, as calculated by Part I of the computer code.

size. The information pertaining to the required plates is listed in Figure (5-12). In addition, Figure (5-13) provides a graphical representation of the total pressure drop experienced by each pipeline and the orifice plate size needed to balance it. The graph shows that Pipeline 3, which had the smallest pressure drop, receives the plate with the smallest opening. Conversely, Pipeline 1 receives the plate with the largest opening, i.e. no orifice plate is required.

5.4.2 Calculations in Part II, Method I

In the second part of the program (Part II), an iterative procedure is followed until a set of coal mass fraction values produces equalized pressure drops. First, the assumption of evenly distributed air mass flows (Method I) will be employed. Unlike Part I, the calculations in Part II include the presence of any currently existing orifice plates. However, the plate sizes which are determined in Part I are not

-- Percentage contributions of each pressure drop component --

Pipeline Number	Pipe Bends	Flow Accn.	Static Head	Friction -Air-	Friction -Solids-
1	18.814	12.808	0.990	65.253	2.135
2	17.873	15.907	1.230	63.044	1.946
3	21.986	19.568	1.513	55.408	1.525
4	22.150	15.079	1.166	59.761	1.845

-- Percentage contributions of each flow section type --
(EXCLUDING Orifice Plates)

Pipeline Number	Pipe Bends	Horizontal Piping	Vertical Piping
1	18.814	55.733	25.453
2	17.873	50.513	31.614
3	21.986	39.124	38.889
4	22.150	47.883	29.967

Figure (5-9) Percentage contribution to Part I total pipeline pressure drop; a.) by type of loss, b.) by pipe section type.

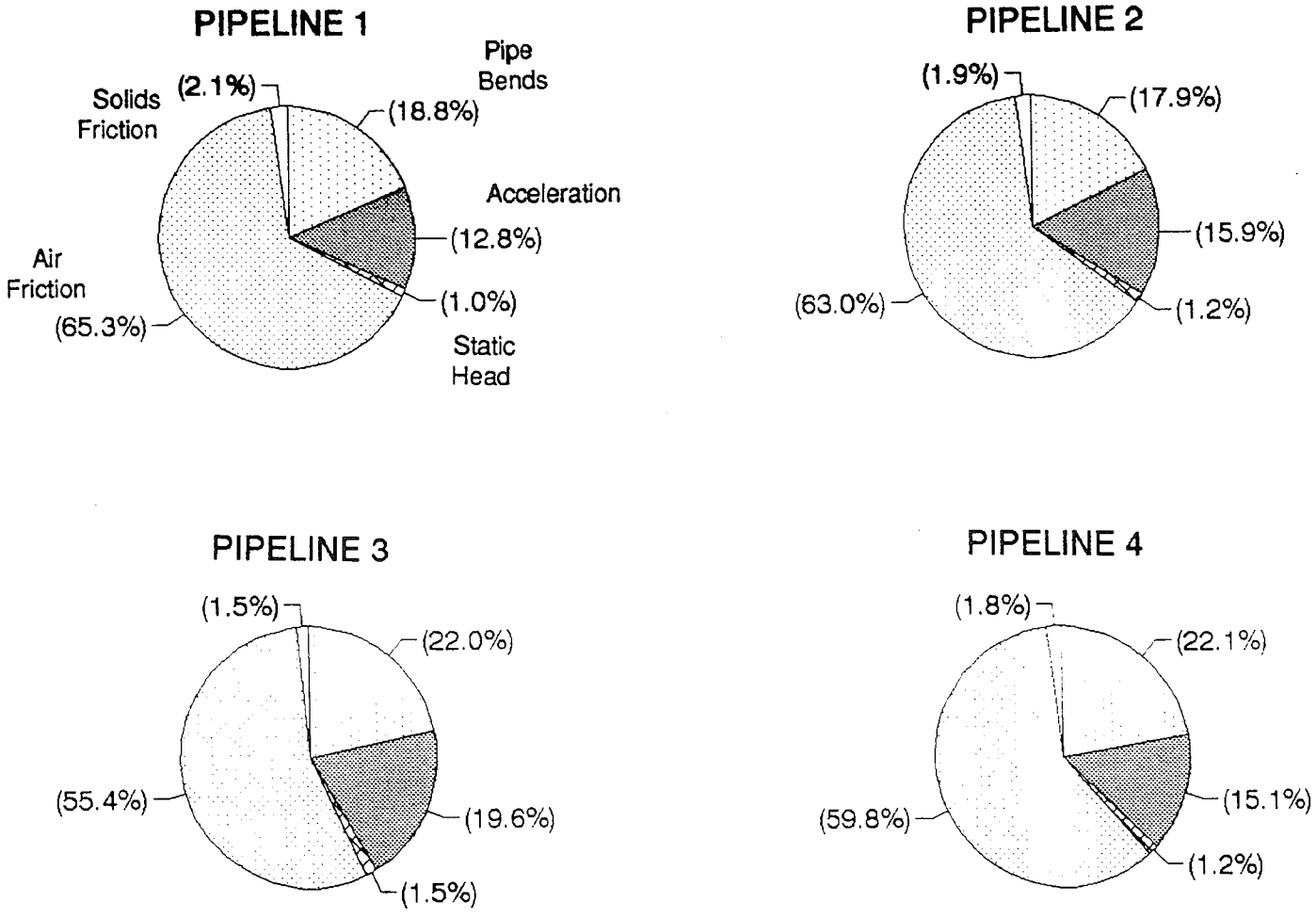

Figure (5-10) Pie chart representation of the percentage contribution to total pressure drop in Part I, by type of loss.

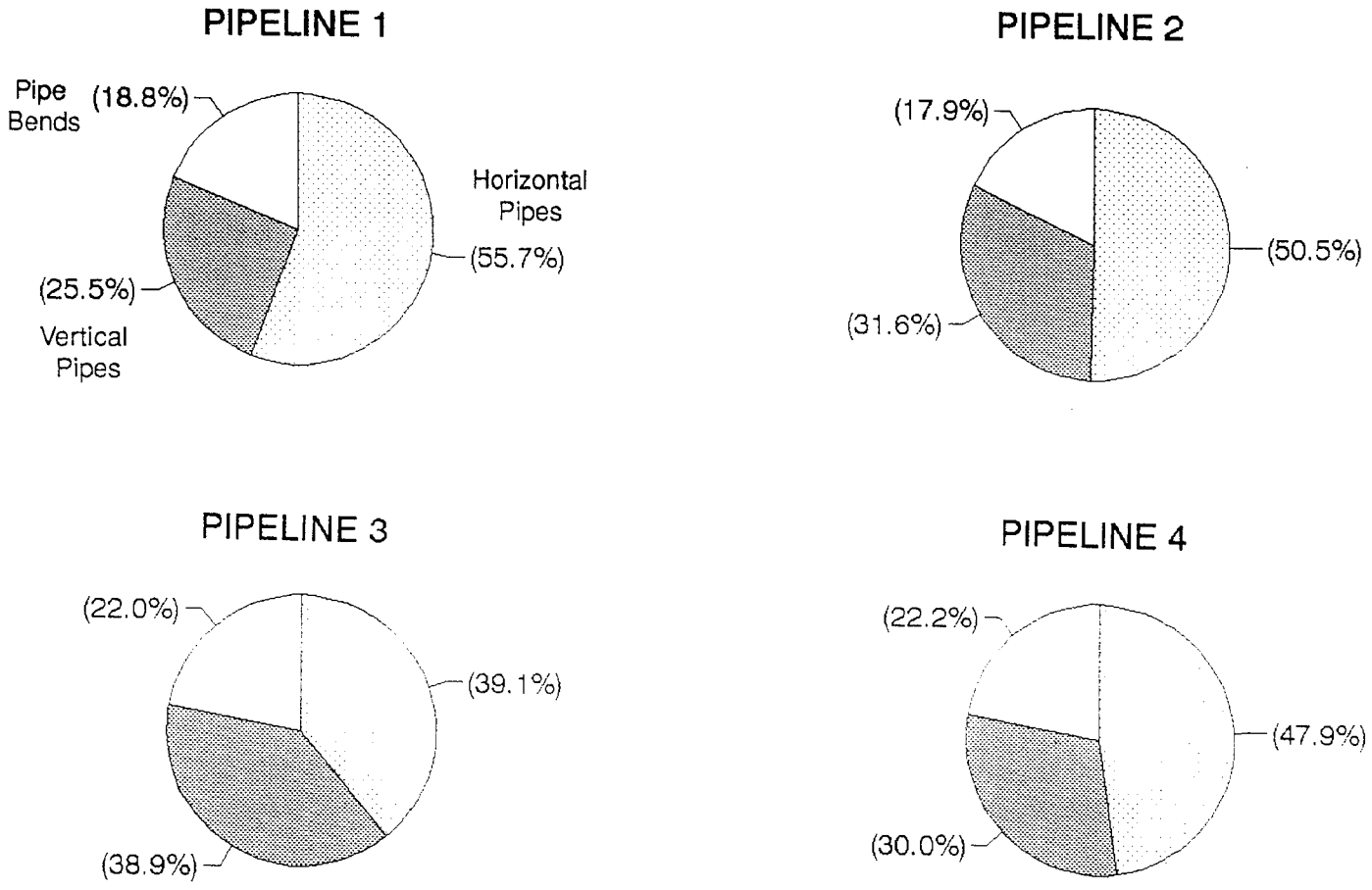

Figure (5-11) Pie chart representation of the percentage contribution to total pressure drop in Part I, by pipe section type.

employed in Part II, since they have not yet been added to the system.

When the iterative process is completed, the information on the percentage contributions of each flow section type to the total pressure drop is presented. These values are tabulated in Figure (5-14).

The effect of improperly sized orifice plates is shown by the data listed in Figure (5-15). Actual coal mass flow rates are plotted in Figure (5-16) and compared to the ideal situation of even fuel distribution. Similarly, the air-to-fuel ratio in each pipeline are shown in Figure (5-17). Due to its high flow resistance, Pipeline 1 receives less than the ideal amount of fuel and consequently its burner fires at a high A/F ratio (fuel lean). The excess oxygen resulting from this type of combustion can lead to increased levels of nitrous oxide formation. Conversely, the low resistance offered by Pipeline 3 allows it to receive a higher than ideal coal flow. This larger flow rate can lead to higher than necessary pipe surface erosion. And the low A/F ratio in Pipeline 3 may result in incomplete combustion of the fuel, lowering the power plant's operating efficiency.

New Orifice Plate Size Recommendations --

Pipeline Number	dP Reqd. inches H2O	Orifice Inner Dia.	No. Plates Reqd.
1	0.000000E+00	15.000000	0
2	0.204683E+01	11.877087	1
3	0.362903E+01	11.064286	1
4	0.158219E+01	12.221051	1

NOTE: Diameter is in inches

Figure (5-12) Orifice plate sizes which will provide balanced flow, as calculated by Part I.

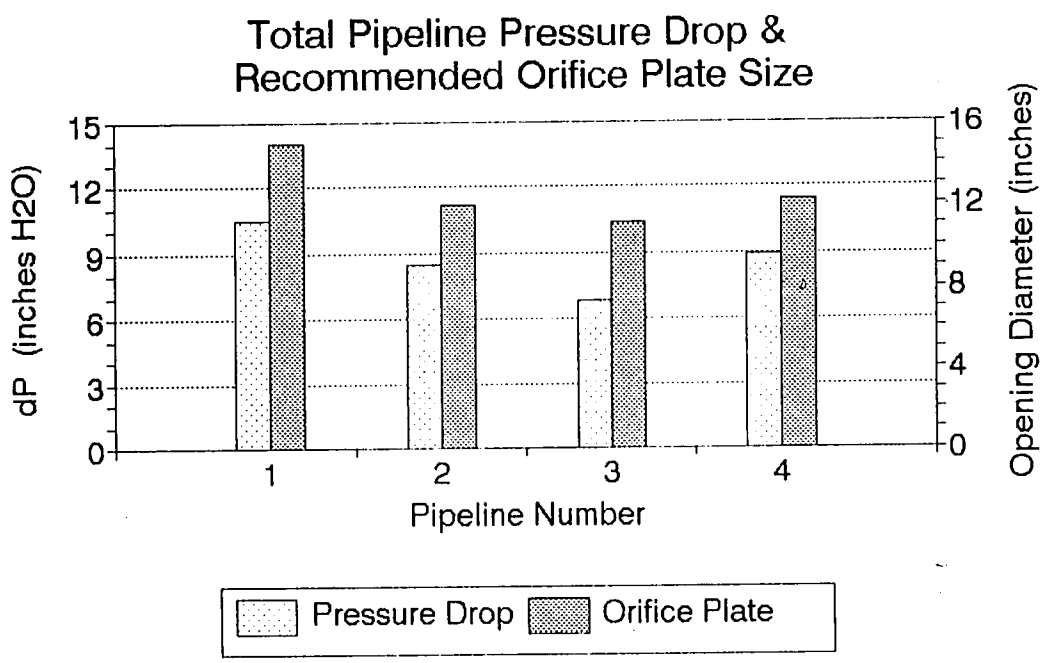

Figure (5-13) Total pressure drop per pipeline (from Part I) and the orifice plate sizes required to equalize them.

--Percentage Contributions to Total Pressure Drop--

Pipeline Number	Pipe Bends	Part. Accn.	Static Head	Friction -Air-	Friction -Solid-	Orifice Plate
1	18.041	12.585	0.895	65.780	1.443	1.256
2	14.498	12.577	1.016	49.710	1.817	20.383
3	14.338	12.568	1.057	34.110	1.633	36.295
4	18.217	12.577	0.926	50.799	1.189	16.293

--Percentage Contributions by Flow Section Type to Total Pressure Drop--

Pipeline Number	Pipe Bends	Horizontal Piping	Vertical Piping	Orifice Plate
1	18.041	55.487	25.216	1.256
2	14.498	40.101	25.018	20.383
3	14.338	24.759	24.608	36.295
4	18.217	40.344	25.146	16.293

Figure (5-14) Percentage contribution to Part II, Method I total pipeline pressure drop; a.) by type of loss, b.) by pipe section type.

--Actual Fuel Distribution for the System--

Pipeline Number	Total dP (inches H2O)	Coal Recvd. (lbm/sec)	Air-Fuel Ratio
1	0.10724E+02	3.15675	2.0119
2	0.10732E+02	3.19750	1.9863
3	0.10740E+02	2.44442	2.5980
4	0.10732E+02	3.20133	1.9839

Pipeline Number	Mass Fraction (%)	Deviation (%)	Air Flow (lbm/sec)
1	26.30629	5.22516	6.35101
2	26.64582	6.58329	6.35101
3	20.37017	-18.51931	6.35101
4	26.67772	6.71088	6.35101

Figure (5-15) Coal flow distribution data as determined by Part II, Method I of the computer code.

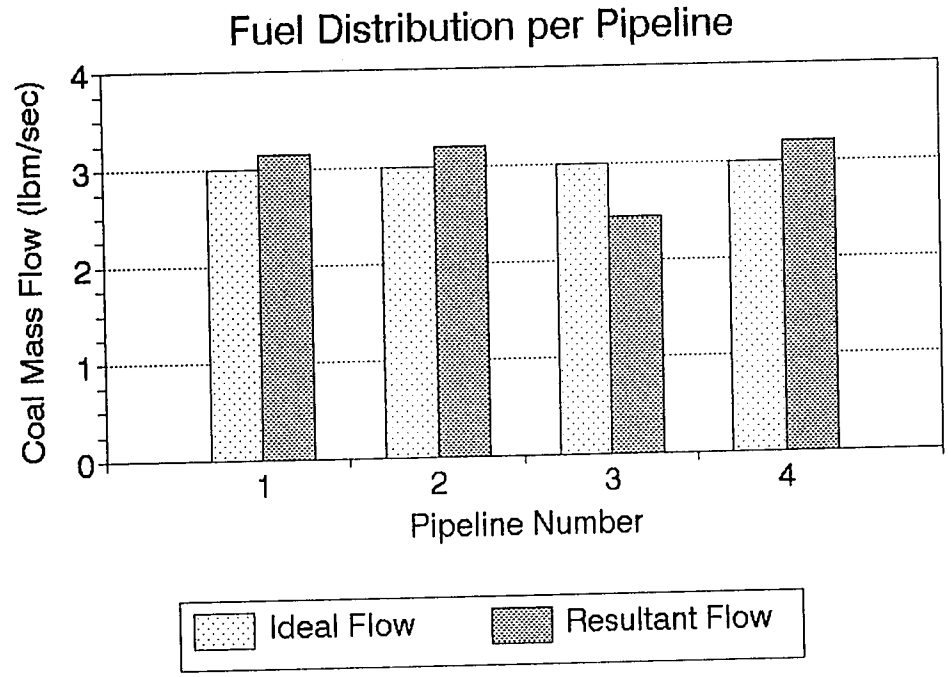

Figure (5-16) Coal mass flow distribution by Method I.

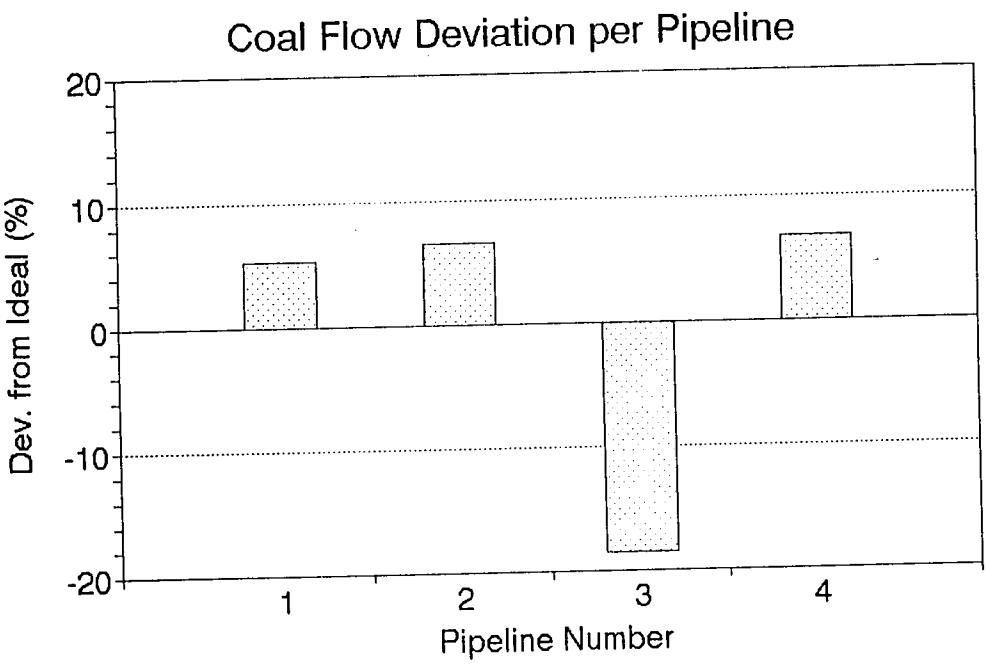

Figure (5-17) Coal flow deviation determined by Method I.

The mass fraction, y_i, was presented earlier in this chapter and is defined as the amount of fuel a pipeline receives divided by the total amount of fuel supplied by the exhauster. In an ideal flow distribution system, each pipeline has the same mass fraction which for this example would be 25%. However, the actual mass fractions are calculated to range from 22.97% to 26.94%.

The amount by which the mass fraction differs from the ideal value is given by the deviation. This parameter is defined as:

$$\text{Deviation} = \frac{y_i - y_{ideal}}{y_{ideal}} \times 100.0 \qquad (5\text{-}16)$$

and is given in terms of percentage. A negative deviation value indicates that the pipeline is receiving less coal than it requires. Likewise, a positive deviation shows that a pipeline is receiving more coal flow than it would in an evenly distributed system. The deviations calculated in the current example are plotted in Figure (5-19).

5.4.3 Calculations in Part II, Method II

The air mass flow rates are now assumed to be distributed according to clean air flow behavior. Thus, step 1 of Figure (5-3) assigns the air flow rate in each pipeline according to these values. After this, the procedure is exactly the same as that used in Section 5.4.1 for Part II, Method I.

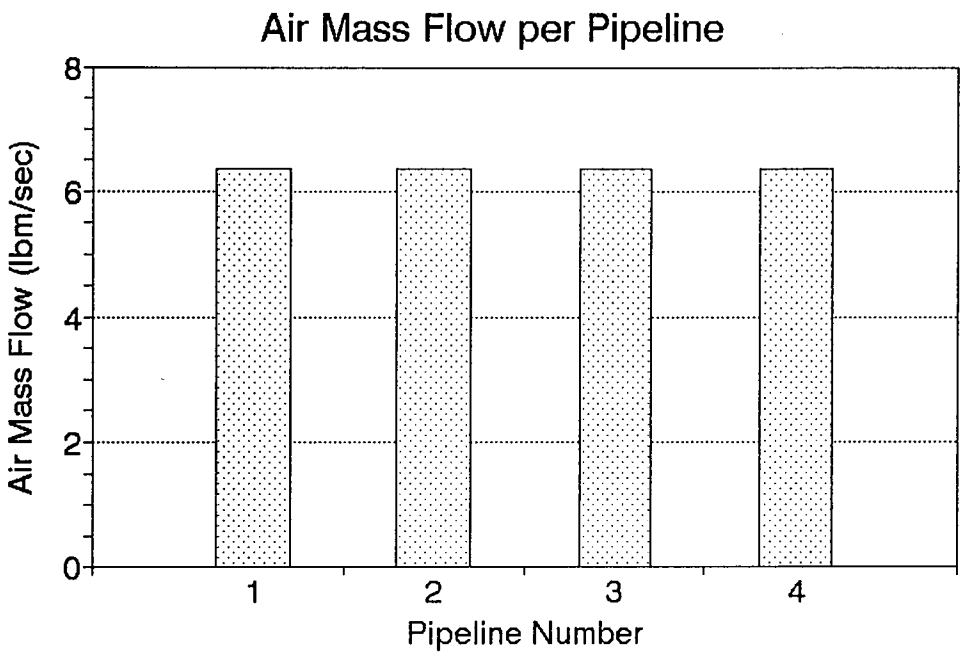

Figure (5-18) Air mass flow distribution by Method I.

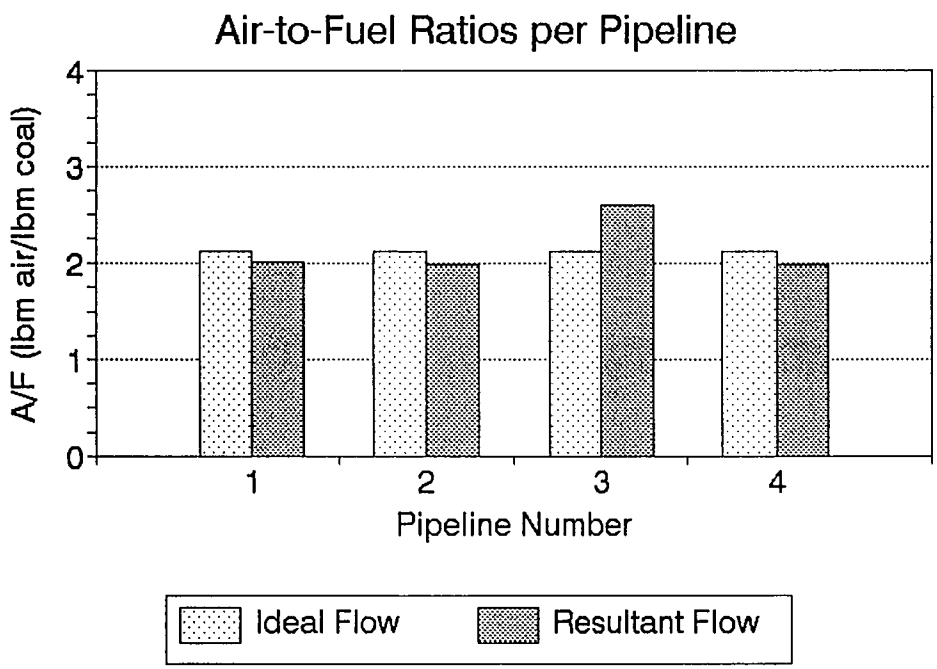

Figure (5-19) Air-to-fuel ratios determined by Method I.

Figure (5-20) shows the contributions of each of the pressure drop components to the overall pipeline pressure drop. Figure (5-21) tabulates the fuel distribution which results from the air flow assumption of Method II. In addition, the assigned air flows are listed along with the coresponding air-to-fuel ratios. The coal and air mass flow rates are plotted in Figure (5-22). Finally, the coal flow deviation is presented in Figure (5-23). As can be seen, the assumption of equally distributed air flows (Method I) yields lower deviations than the assumption based upon clean air flow (Method II).

The determination of the deviation values completes the burner balancing computer program. In Chapter 6, the sensitivity and dependence of this routine on the power plant operational data will be discussed.

--Percentage Contributions to Total Pressure Drop--

Pipeline Number	Pipe Bends	Part. Accn.	Static Head	Friction -Air-	Friction -Solid-	Orifice Plate
1	18.897	12.544	1.022	63.915	2.403	1.219
2	14.546	12.536	1.032	49.684	1.825	20.378
3	12.826	12.526	0.809	35.462	0.575	37.803
4	19.018	12.535	1.014	49.682	1.831	15.920

--Percentage Contributions by Flow Section Type to Total Pressure Drop--

Pipeline Number	Pipe Bends	Horizontal Piping	Vertical Piping	Orifice Plate
1	18.897	54.898	24.986	1.219
2	14.546	40.096	24.980	20.378
3	12.826	24.649	24.723	37.803
4	19.018	40.101	24.961	15.920

Figure (5-20) Percentage contribution to Part II, Method II total pipeline pressure drop; a.) by type of loss, b.) by pipe section type.

--Actual Fuel Distribution for the System--

Pipeline Number	Total dP (inches H2O)	Coal Recvd. (lbm/sec)	Air-Fuel Ratio
1	0.10689E+02	2.75655	2.3336
2	0.10697E+02	3.16674	2.0017
3	0.10705E+02	3.23269	1.9211
4	0.10697E+02	2.84402	2.2546

Pipeline Number	Mass Fraction (%)	Deviation (%)	Air Flow (lbm/sec)
1	22.97123	-8.11508	6.43265
2	26.38954	5.55816	6.33891
3	26.93905	7.75622	6.21023
4	23.70017	-5.19931	6.41201

Figure (5-21) Fuel distribution data determined by PartII, Method II of the computer code.

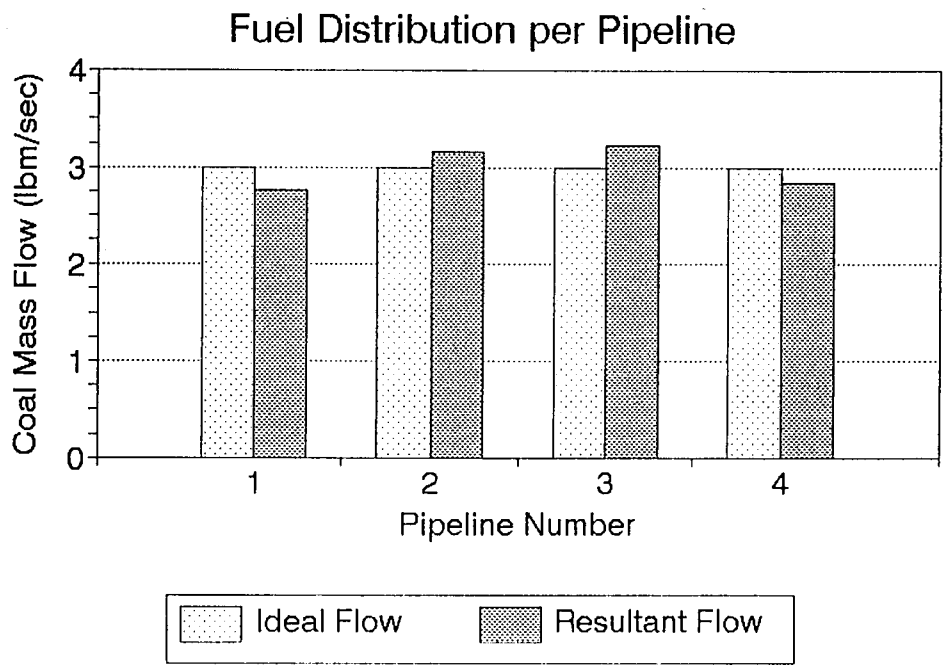

Figure (5-22) Coal flow distribution by Method II.

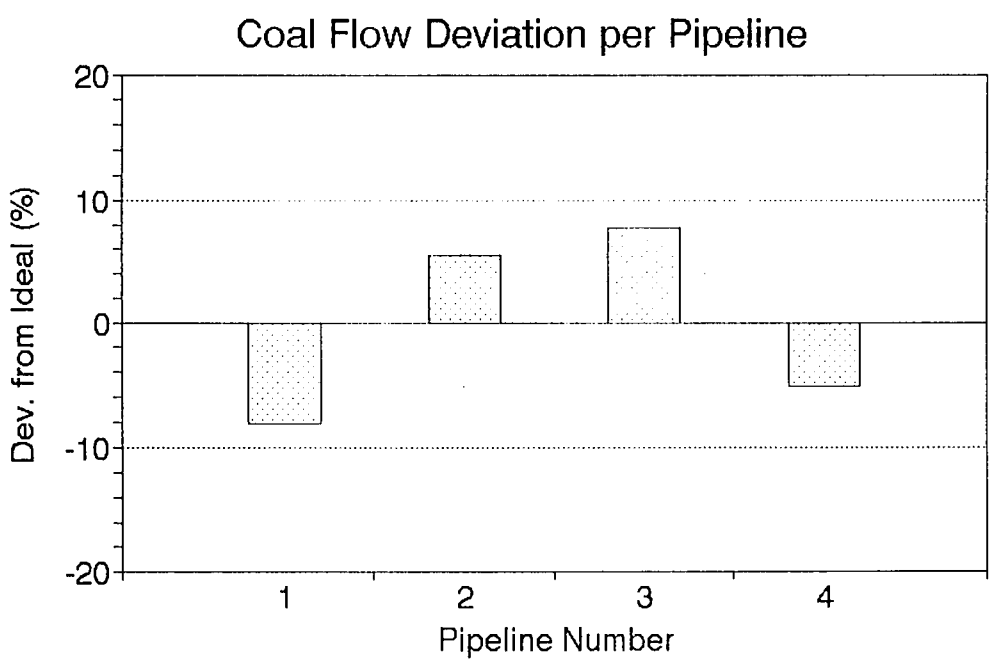

Figure (5-23) Coal flow deviation by Method II.

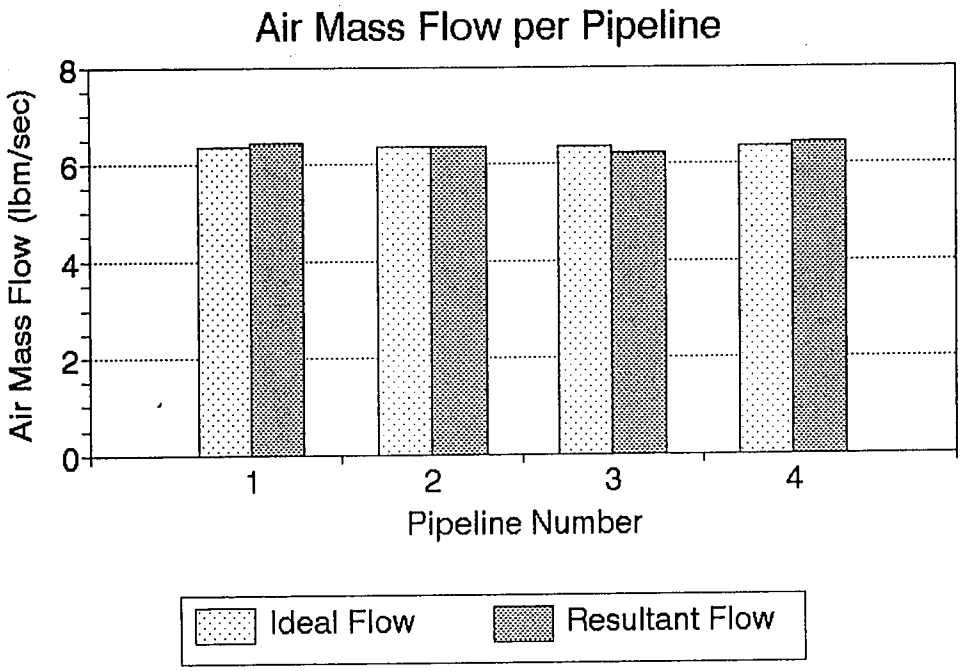

Figure (5-24) Air mass flow distribution by Method II.

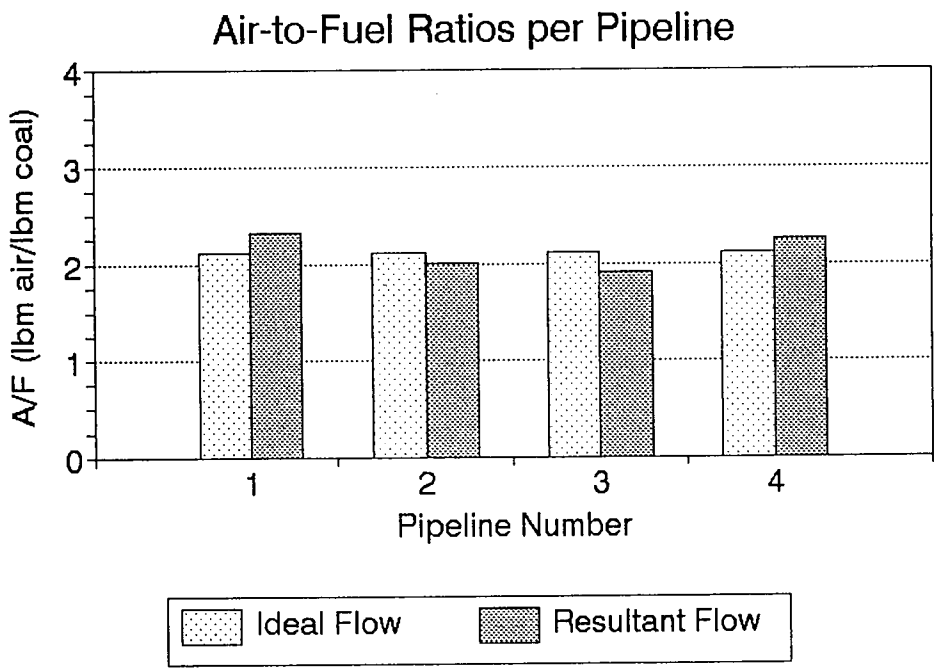

Figure (5-25) Air-to-fuel ratios determined by Method II.

6. SENSITIVITY ANALYSIS

The burner balancing routine presented in this thesis relies upon the input of several parameters. Based upon this information, orifice plate sizes which will provide uniform flow distribution are calculated. However, after these plates have been added to the system, the operating parameters may vary. This chapter examines the effect of such variations upon the fuel distribution.

Limitations of the burner balancing model are also examined in this chapter. For example, the correlations require a uniform particle size. But the pulverized coal transported in electric power plants is composed of a range of particle sizes.

The information generated by the model inherently depends upon the selected correlations. Several bend correlations are substituted into the model to examine the sensitivity of balancing to the choice of equations.

As discussed in Chapter 4, the air flow distribution to each pipeline cannot be determined and assigned values must be assumed. Thus, for each case investigated in this chapter, both Method I and Method II are employed.

Finally, this chapter investigates the use of clean air flow tests to balance the coal flow distribution.

6.1 Variations in Operating Parameters

The computer code input data which vary during power plant operation are the air temperature, exhauster air flow rate, and coal feed rate. Orifice plate sizes which provide balanced flow for one set of these parameters may not produce the same coal flow distribution when one of them is varied. The analysis of this section is based upon the following method. A set of baseline conditions are assumed and the orifice plates needed to balance that flow are calculated. Then, one of the input parameters is changed and the calculations are repeated. Part II of the code's output is examined for any effects upon the previously balanced flow. For each input parameter which is varied, four dependent variables (per pipeline) are presented: coal mass flow rate, air-to-fuel ratio, coal flow deviation, and air mass flow rate. The data for each case is tabulated in Appendix 4.

The baseline operating conditions used in this analysis are identical to those utilized in Section 5.4, which are presented in Figure (5-5). In addition, the piping system outlined in Figure (5-2) and documented in Appendix 1 is employed. The orifice plates which balance these flow conditions (calculated in Section 5.4) and which are used in this section are:

Pipeline Number	Orifice d_o (inches)
1	15.00000
2	11.87709
3	11.06429
4	12.22105

For the calculations performed in this section, these plates replace those given in Appendix 1. The coal and air mass flow rates for the baseline case, in units of (lbm/sec) are:

Pipeline Number	Coal Mass Flow	Air Mass Flow Method I	Air Mass Flow Method II
1	3.00	6.3510	6.3979
2	3.00	6.3510	6.3206
3	3.00	6.3510	6.2985
4	3.00	6.3510	6.3769

6.1.1 Variation of Conveying Air Temperature

The first operating parameter which will be examined is the temperature of the conveying air. In the baseline case, the temperature is 165 degrees Fahrenheit. The values used in this section are: 145, 155, 175, and 185°F. First, the air mass flows were assumed to be equally distributed (Method I). Figure (6-1) shows the coal flow distribution which results from the temperature variation. The amount by which the flows are imbalanced is plotted in Figure (6-2). The most severe deviation values occur when the temperature is at the highest setting. However, the largest deviations do not exceed an imbalance of 5%. Figure (6-3) shows the air mass flow for each case. In accordance with Method I, for each case the

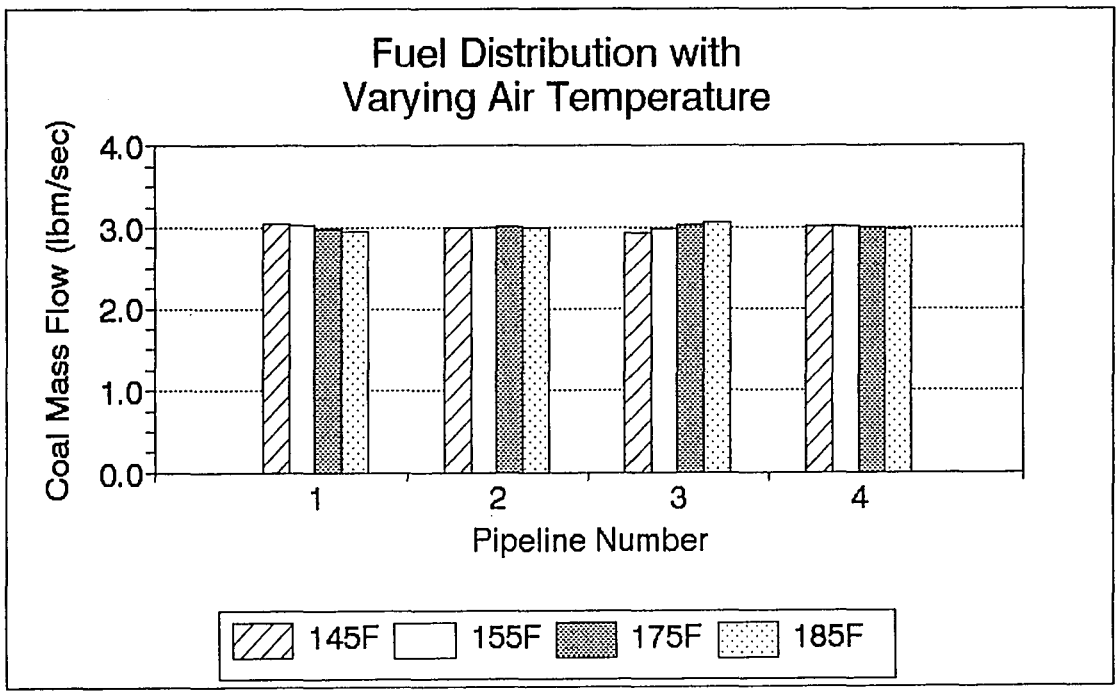

Figure (6-1) The effect of varying air temperature on fuel distribution - Method I.

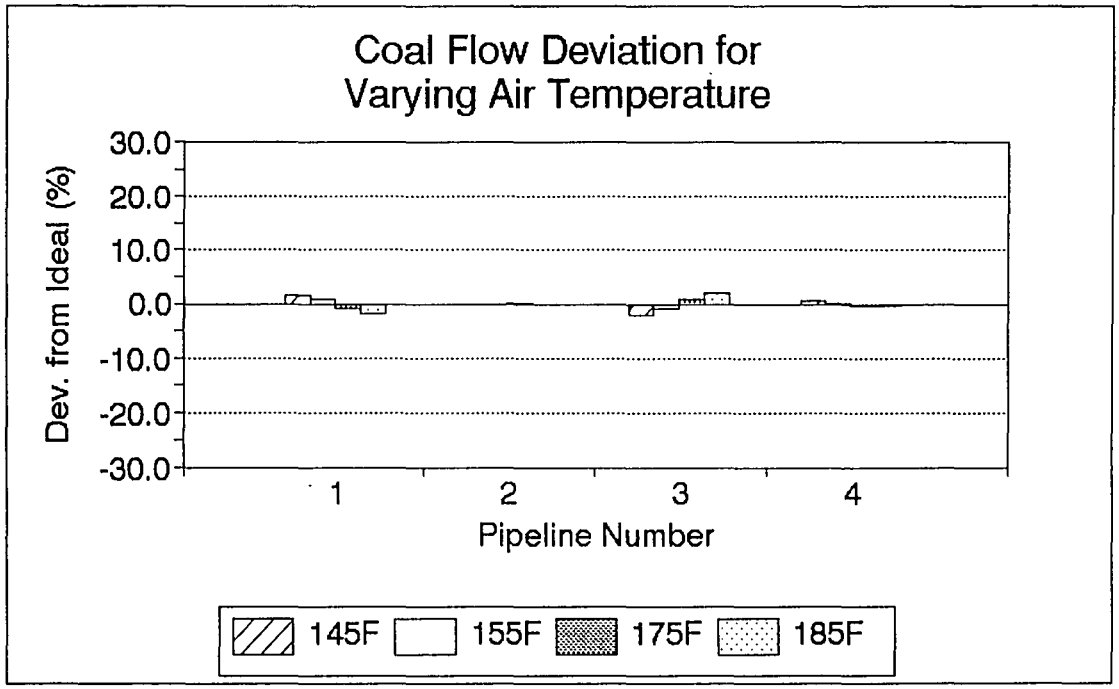

Figure (6-2) The effect of varying air temperature on coal flow deviation - Method I.

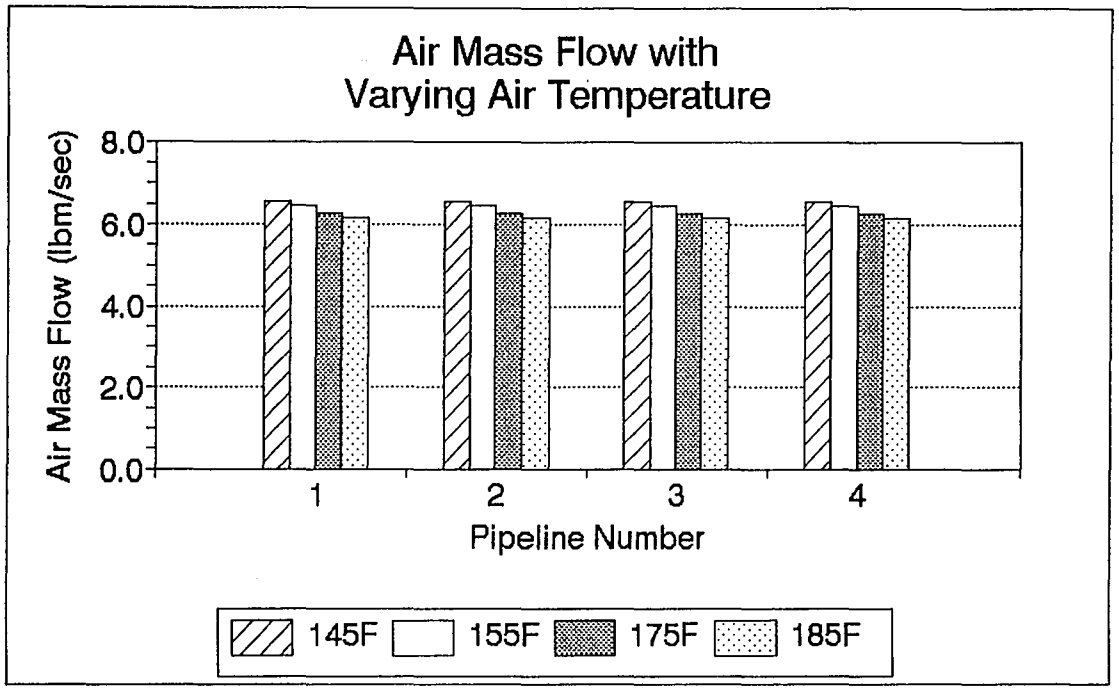

Figure (6-3) The effect of varying air temperature on air mass flow rates - Method I.

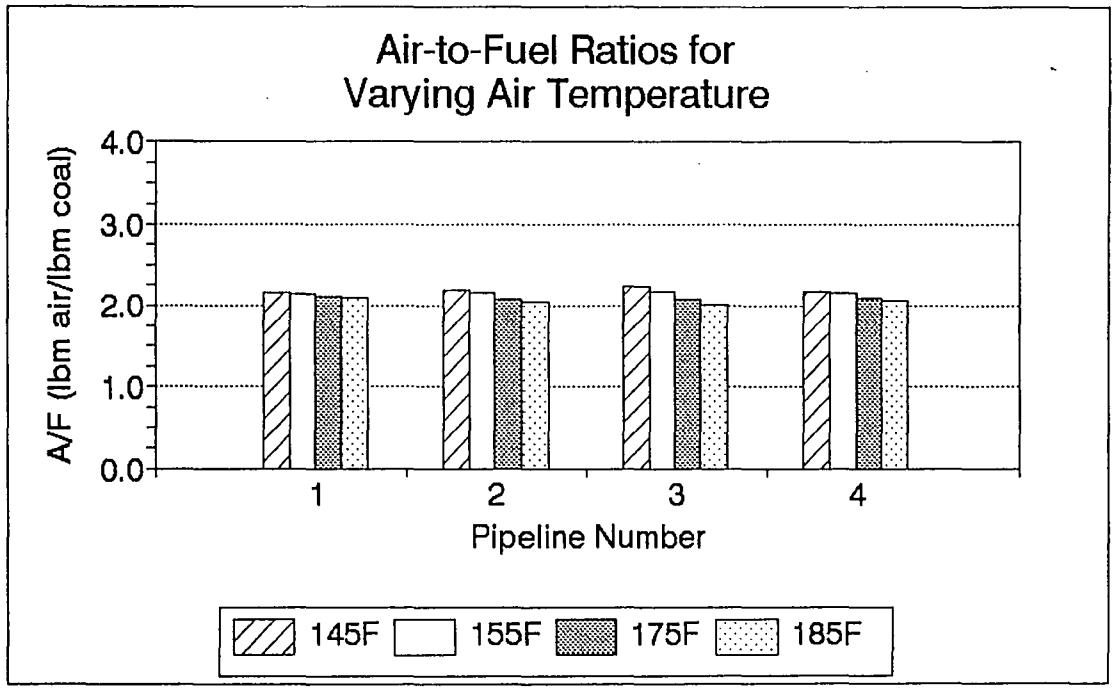

Figure (6-4) The effect of varying air temperature on air/fuel ratios, Method I.

flow is equally distributed to the pipelines. But due to the variation of air density with the change in air temperature, the actual value of the air mass flow rate decreases with increasing temperature.

The air-to-fuel ratios in each pipeline for each of the cases are given in Figure (6-4). Since the air flow is evenly distributed at each temperature value, the variations in A/F are due solely to the imbalance of the coal flow.

In order to provide a gross quantitative figure regarding the effect of temperature variation upon the coal flow, the standard deviation of the coal flow deviation values was determined for each temperature setting. With x_i representing the coal flow deviation, the standard deviation, σ is calculated by

$$\bar{x} = \frac{\sum x_i}{N} \qquad (6\text{-}1)$$

$$\sigma = \sqrt{\frac{\sum \left(x_i - \bar{x}\right)^2}{N}} \qquad (6\text{-}2)$$

In the baseline case, the coal flow deviation per pipeline is zero, and thus the standard deviation is also zero. For this range of temperature values:

Temperature (degrees F)	Standard Deviation of Coal Flow Deviation (%)
145.0	1.37
155.0	0.65
165.0	0.00
175.0	0.62
185.0	1.33

As can be seen, as the temperature either increases or decreases from the base value (165°F), the coal flow deviation increases. The relationship between the temperature value and the imbalance appears to be linear and it does not depend upon whether the temperature is increased or decreased.

The same temperature values were also examined utilizing the air mass flow rates produced by the assumption of Method II. Their values are labeled as the Base Case in Figure (6-7). Figure (6-5) shows the coal flow distribution which results from each of these cases. Although there is an imbalance among fuel received by the pipelines, the effect of temperature variations is small, and the deviation values are plotted in Figure (6-6). Once again, the standard deviation of the coal flow deviation values was calculated:

Temperature (degrees F)	Standard Deviation of Coal Flow Deviation (%)
145.0	6.64
155.0	6.76
165.0	6.81
175.0	6.84
185.0	6.82

Although these values are larger than those produced by

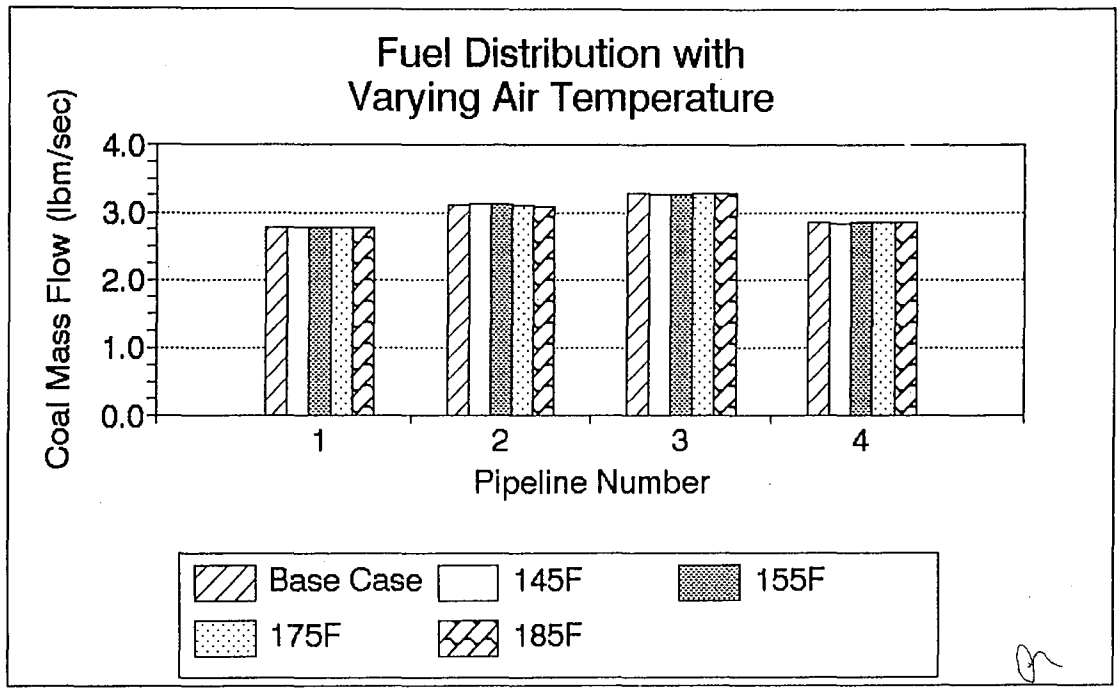

Figure (6-5) The effect of varying air temperature on fuel distribution - Method II.

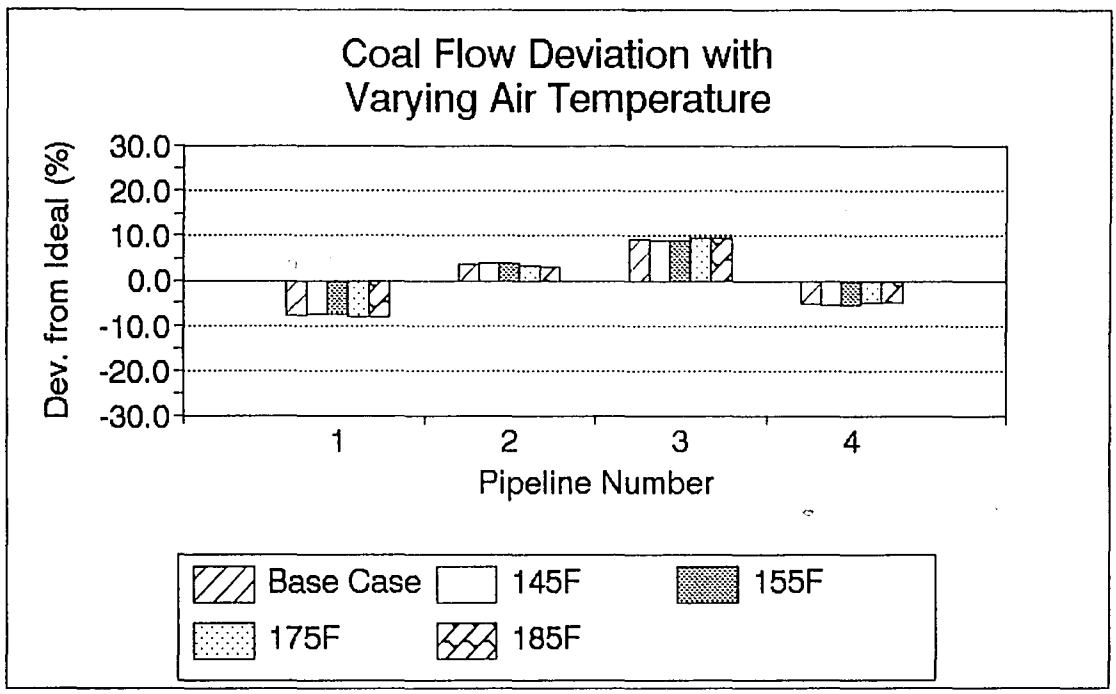

Figure (6-6) The effect of varying air temperature on coal flow deviation - Method II.

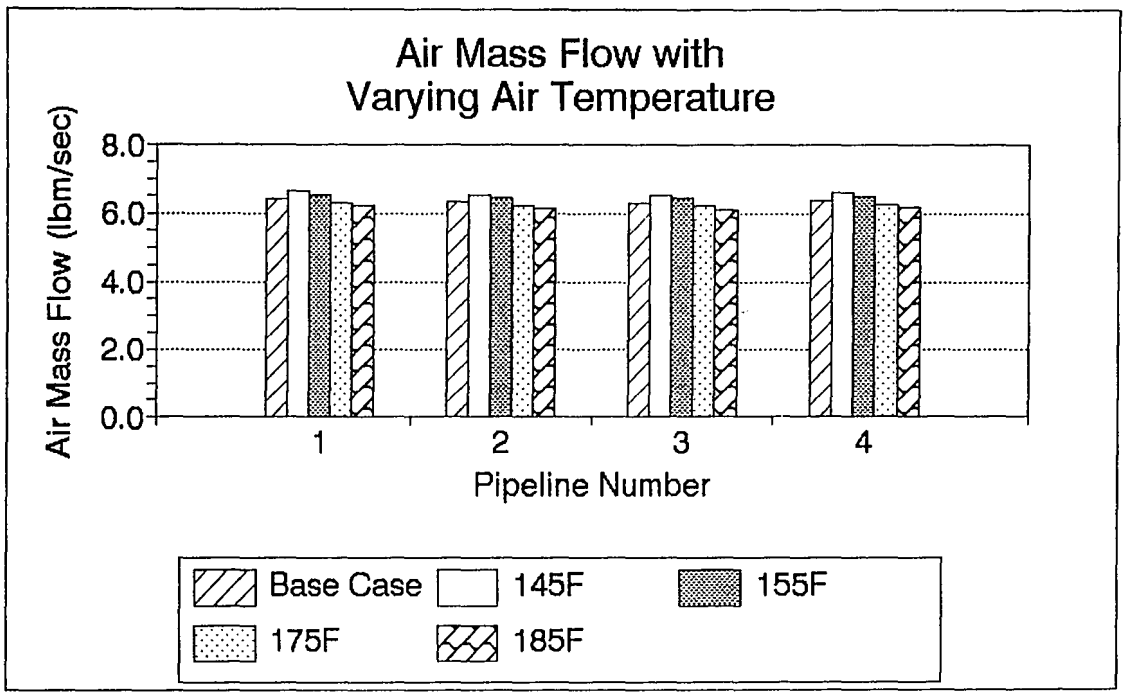

Figure (6-7) The effect of varying air temperature on air mass flow rates - Method II.

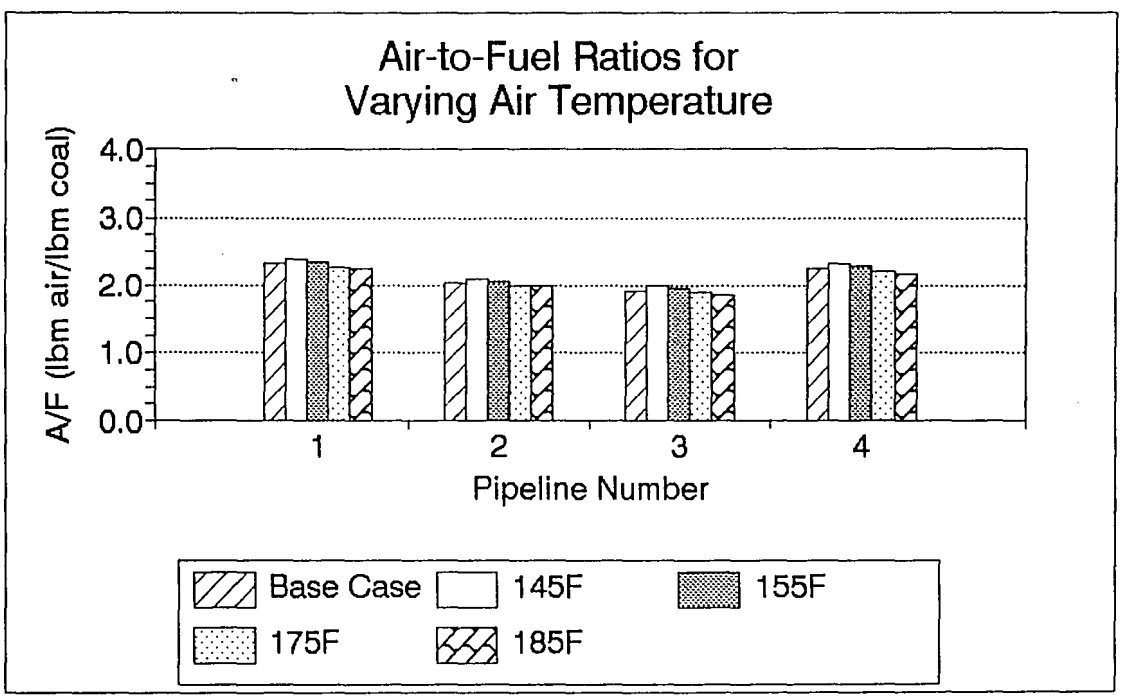

Figure (6-8) The effect of varying air temperature on air/fuel ratios - Method II.

Method I, they must be examined with respect to the deviation at the baseline condition. For Method I, this value is zero, but the assigned air mass flows in Method II yield a coal flow deviation of 6.81%. Compared to this value, it can be seen that the effect of temperature variations upon the baseline conditions is small.

6.1.2 Part-Load Conditions

At times, an electric power plant operates at less than its full generating capacity in response to demand requirements. This is known as operating at part-load. The need for less power allows the plant to decrease the amount of coal fed to the system. In addition, the exhauster air output is reduced to a level which provides for the transport of the coal. The baseline calculations were performed at full load conditions: a total coal feed rate of 720.0 lbm/min and exhauster air output of 24000.0 cfm. In this section, the load is reduced to the following conditions, corresponding to exhauster information from Combustion Engineering:

Loading (%)	Total Coal Flow (lbm/min)	Total Air Flow (cfm)	A/F Ratio
25.0	180.0	16909.1	5.963
50.0	360.0	20727.3	3.655
75.0	540.0	22952.7	2.698
100.0	720.0	24000.0	2.117

The base condition corresponds to full (100%) load.

The information produced by the air flow assumption of Method I is examined first. Figure (6-9) shows the coal

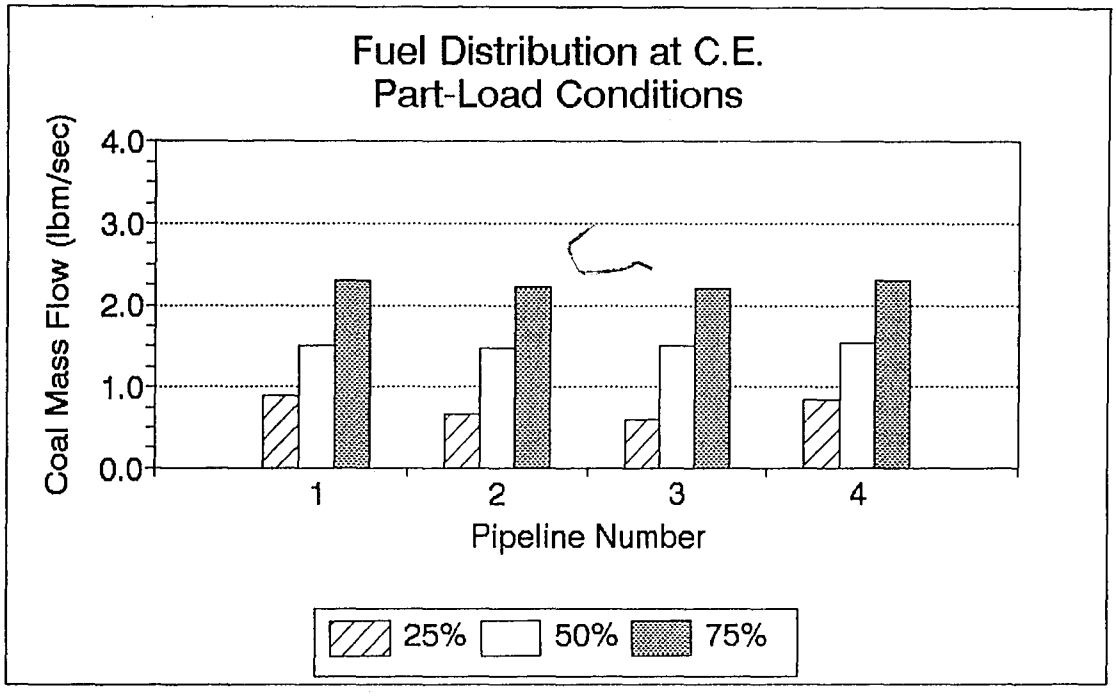

Figure (6-9) The effect of varying load (with C.E. data) on fuel distribution - Method I.

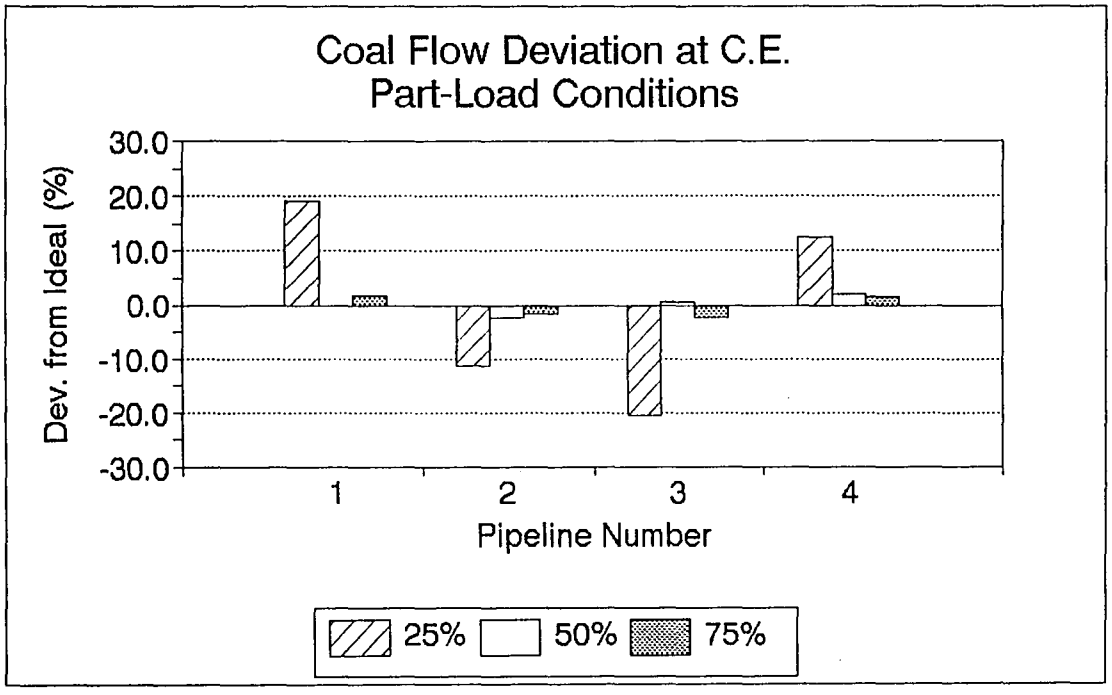

Figure (6-10) The effect of varying load (with C.E. data) on coal flow deviation - Method II.

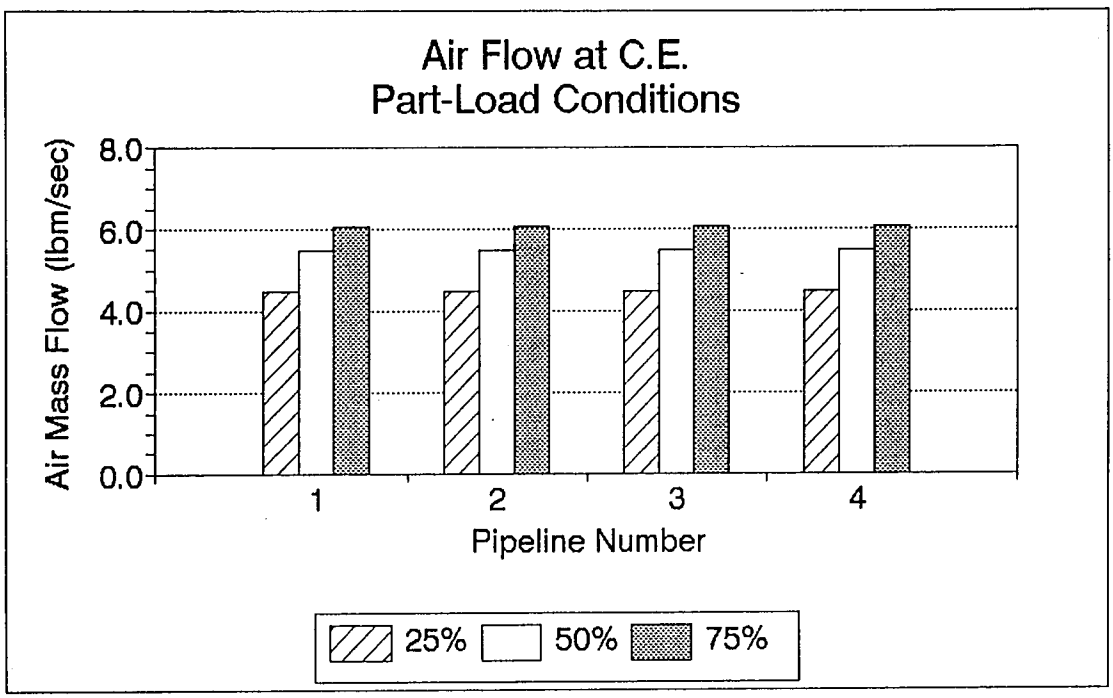

Figure (6-11) The effect of varying load (with C.E. data) on air mass flow rates - Method II.

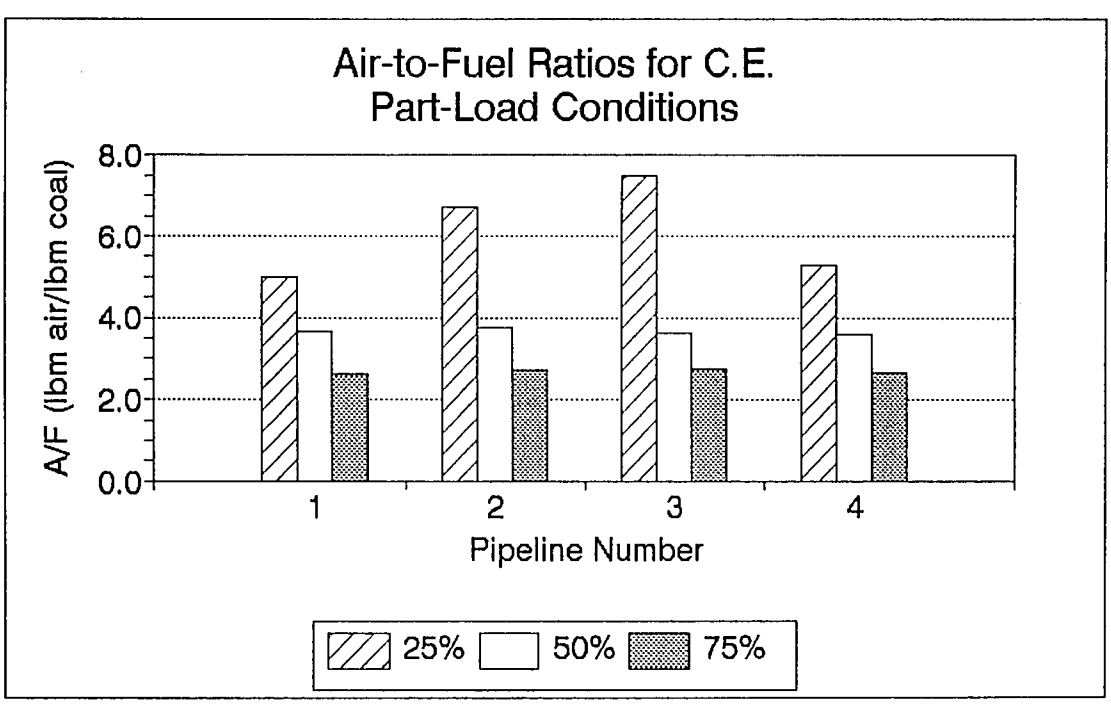

Figure (6-12) The effect of varying load (with C.E. data) on air/fuel ratios - Method I.

flow distribution at each load level. The air mass flow in each pipeline is given in Figure (6-11) and it displays the equalized behavior inherent to Method I. The amount of coal flow imbalance is shown in Figure (6-10), where it can be seen that the most severe deviations occur at the lowest load. The standard deviations of these coal flow deviation values are:

Loading (%)	Standard Deviation of Coal Flow Deviation (%)
25.0	16.41
50.0	1.61
75.0	1.86
100.0	0.00

The severity of the imbalance at the lowest loading level is clear. However, a load level of 50% produces a standard deviation of less than 2%. Thus, it would appear that only drastic reductions in load level have a serious effect upon the baseline balanced flow.

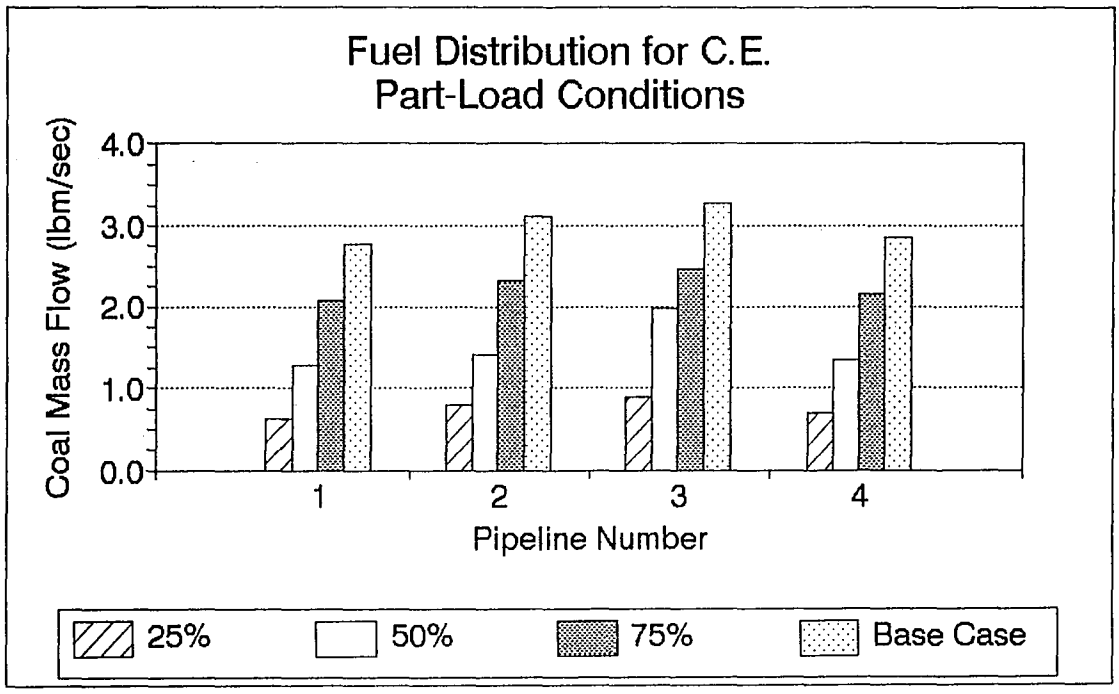

Figure (6-13) The effect of varying load (with C.E. data) on fuel distribution - Method II.

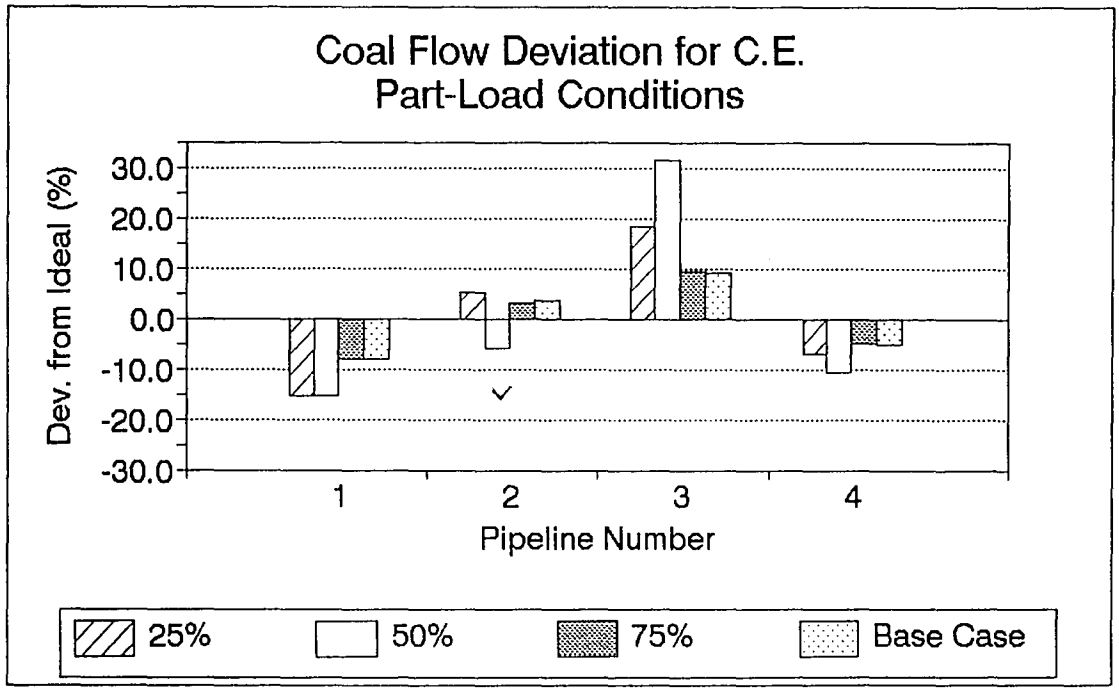

Figure (6-14) The effect of varying load (with C.E. data) on coal flow deviation - Method II.

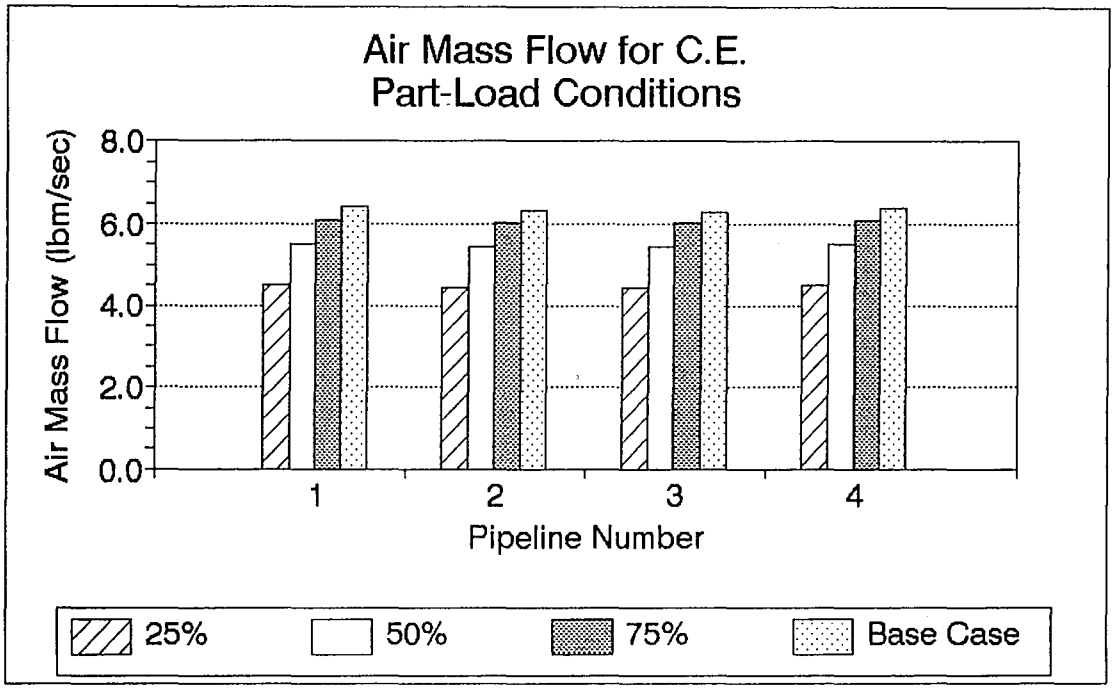

Figure (6-15) The effect of varying load (with C.E. data) on air mass flow rates - Method II.

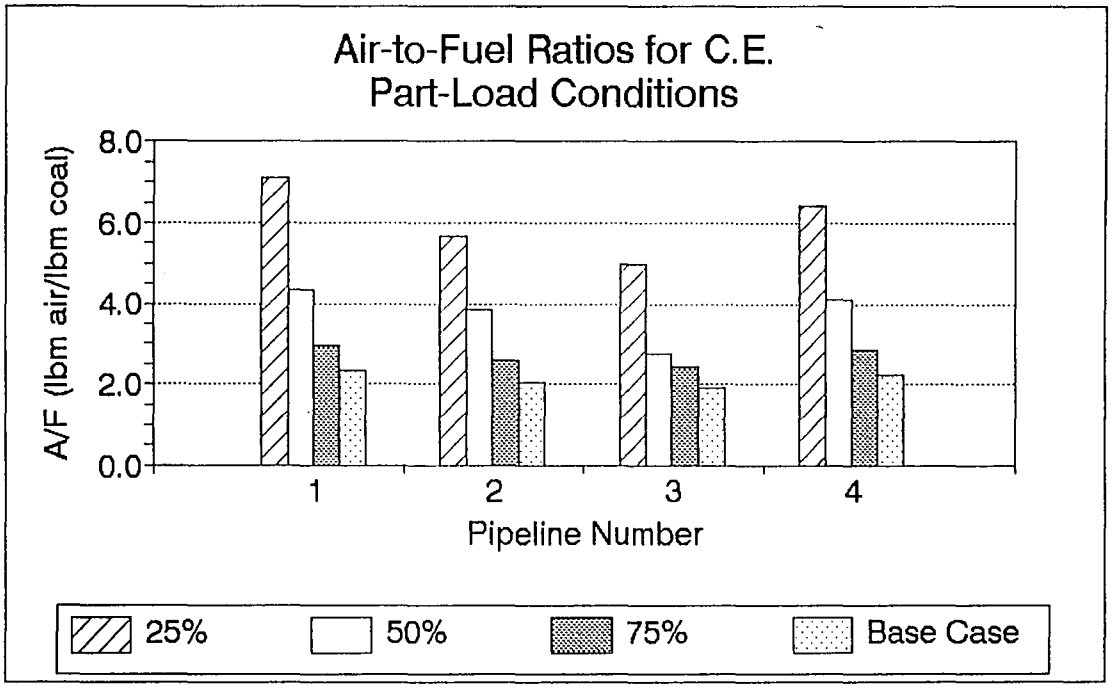

Figure (6-16) The effect of varying load (with C.E. data) on air/fuel ratios - Method II.

When Method II is employed, a different behavior is witnessed. The fuel distribution is plotted in Figure (6-13) and the associated deviation values are given in Figure (6-14), where the largest imbalance now occurs at the load level of 50%. In terms of the standard deviation of the coal flow deviation:

Loading (%)	Standard Deviation of Coal Flow Deviation (%)
25.0	12.74
50.0	18.50
75.0	6.83
100.0	6.81

These values, in comparison to the Method II baseline deviation of 6.81%, show the difference in behavior of the 50% load level for Method I and Method II. For both cases, the level of 75% still provides reasonably balanced flow.

6.1.3 Part-Load Conditions with Constant A/F

This section examines loading levels in which the exhauster air output and coal feed rate are set to a constant air-to-fuel ratio. Using the baseline case, the constant A/F value is 2.117 (lbm air/lbm coal), and thus the data at each load level are:

Loading (%)	Total Coal Flow (lbm/min)	Total Air Flow (cfm)
25.0	180.0	6000.0
50.0	360.0	12000.0
75.0	540.0	18000.0
100.0	720.0	24000.0

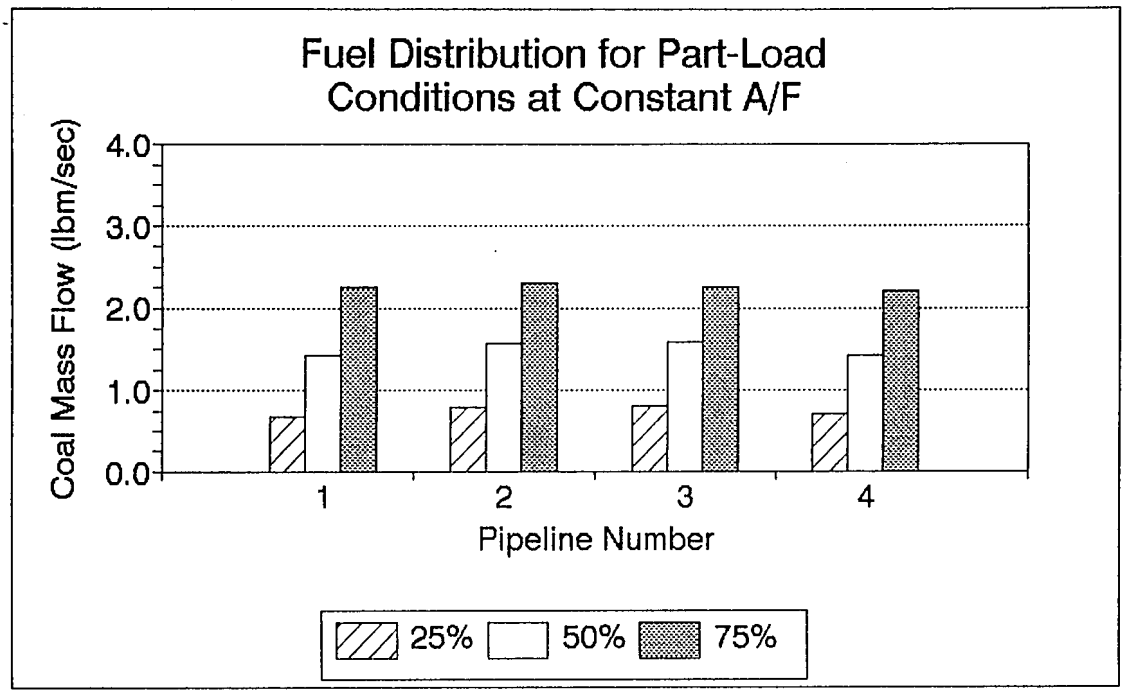

Figure (6-17) The effect of varying load (at constant A/F) on fuel distribution - Method I.

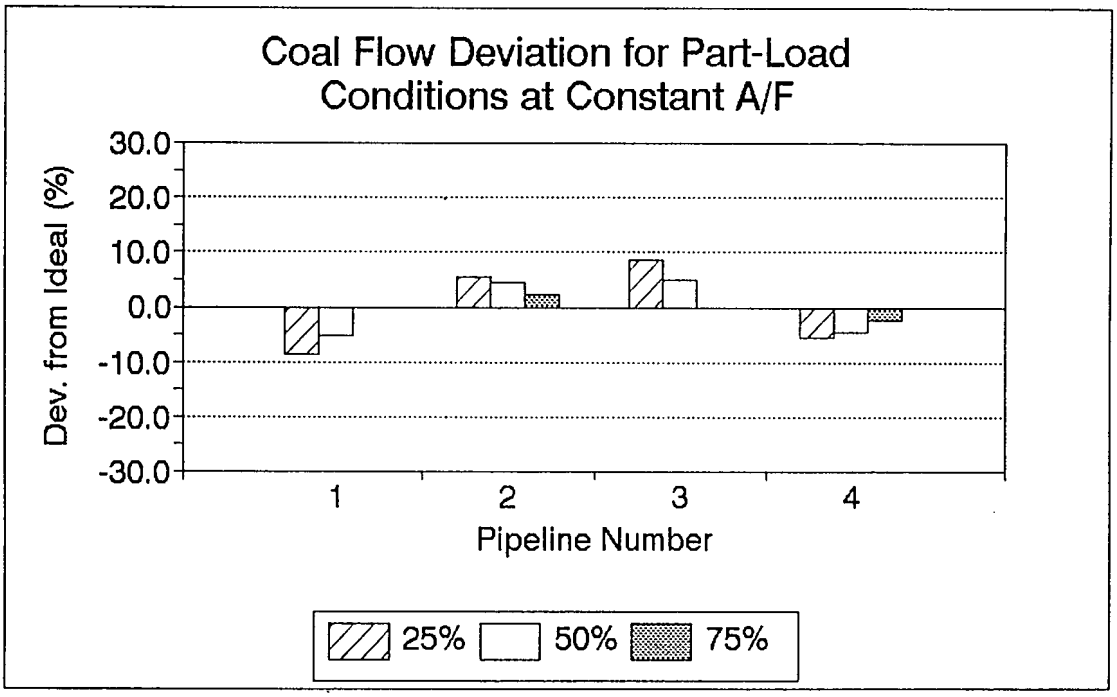

Figure (6-18) The effect of varying load (at constant A/F) on coal flow deviation - Method I.

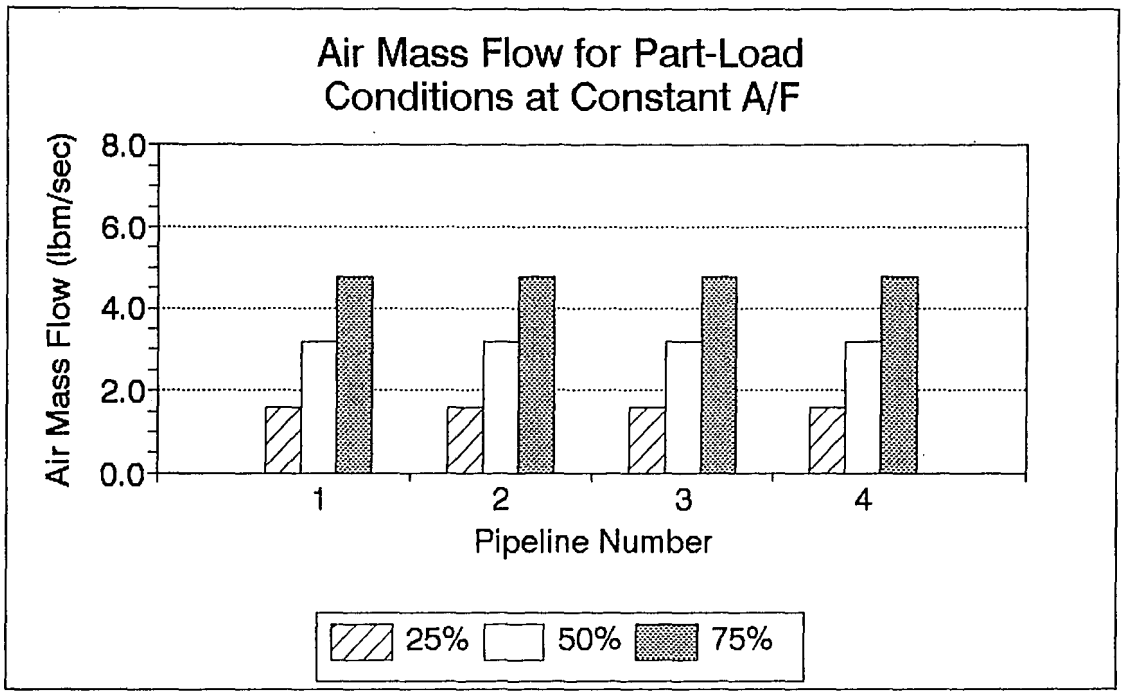

Figure (6-19) The effect of varying load (at constant A/F) on air mass flow rates - Method I.

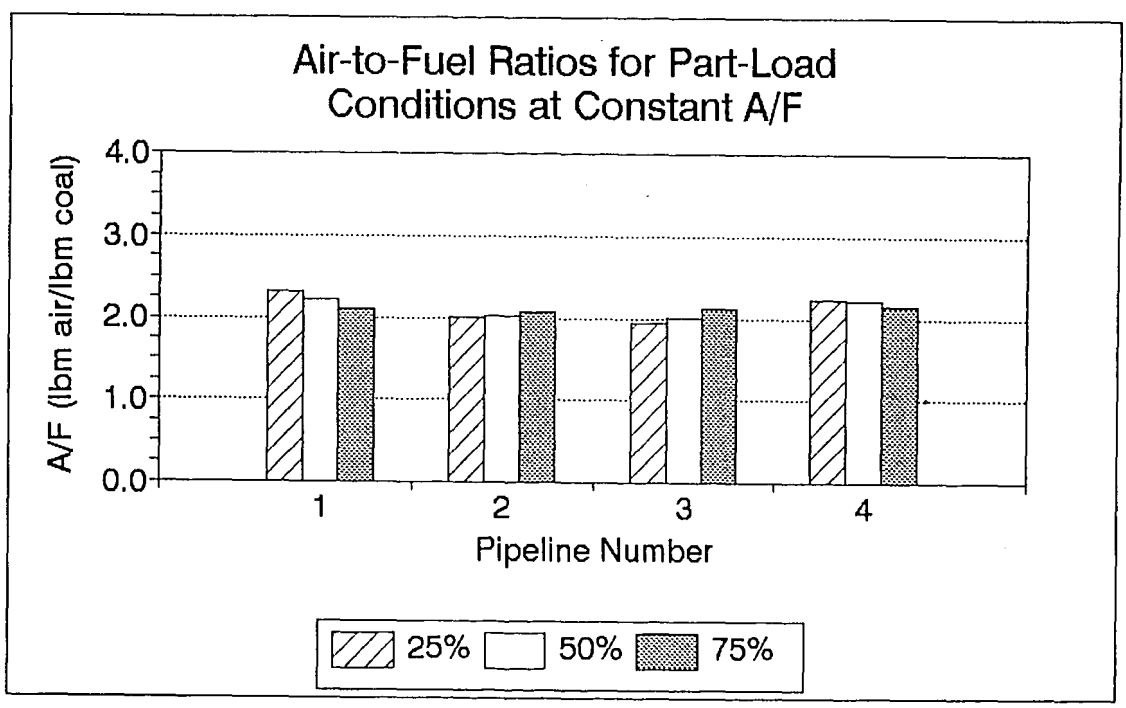

Figure (6-20) The effect of varying load (at constant A/F) on air/fuel ratios - Method I.

The baseline case corresponds to full (100%) load.

Figure (6-17) shows the fuel distribution at each of these loading levels. This information was obtained using the air flow assumption of Method I. In accordance with this method, the air flow is equally divided among the pipelines, as shown in Figure (6-19). However, the variation in coal flow rates produce different A/F ratios in each pipeline (though the *overall* A/F remains constant), as given in Figure (6-20). The coal flow deviation per pipeline, plotted in Figure (6-18), does not exceed 10% for any of the pipelines. For each load level, the standard deviation of the coal flow deviations has been calculated:

Loading (%)	Standard Deviation of Coal Flow Deviation (%)
25.0	7.20
50.0	4.75
75.0	1.57
100.0	0.00

As in the case where Combustion Engineering data were used to perform part-load calculations with Method I, the largest deviation occurs for the 25% load level and the deviation decreases with increasing load level.

When Method II is employed, a different behavior is observed. Using the same load level values for the coal and air flows, the fuel distribution is as shown in Figure (6-21), with the base case representing full (100%) load. The flow deviation values are plotted in Figure (6-22) and should be

examined in conjunction with the base case deviation values. Standard deviation values for these loading levels are:

Loading (%)	Standard Deviation of Coal Flow Deviation (%)
25.0	10.34
50.0	10.42
75.0	9.31
100.0	6.81

The base case of full load yields a standard deviation of 6.81%. Thus, lowering load level increases the coal flow deviation. However, there is virtually no difference between the load of 50% and the load of 25%. This behavior was not displayed by any of the previous part-load conditions examined in this chapter.

Air mass flow rates which were assigned according to the clean air flow technique of Method II are plotted in Figure (6-23). Although the discrepancy among these values is small, the coal flow deviations yield air-to-fuel ratios which differ for each pipeline, but are relatively unaffected by load variations.

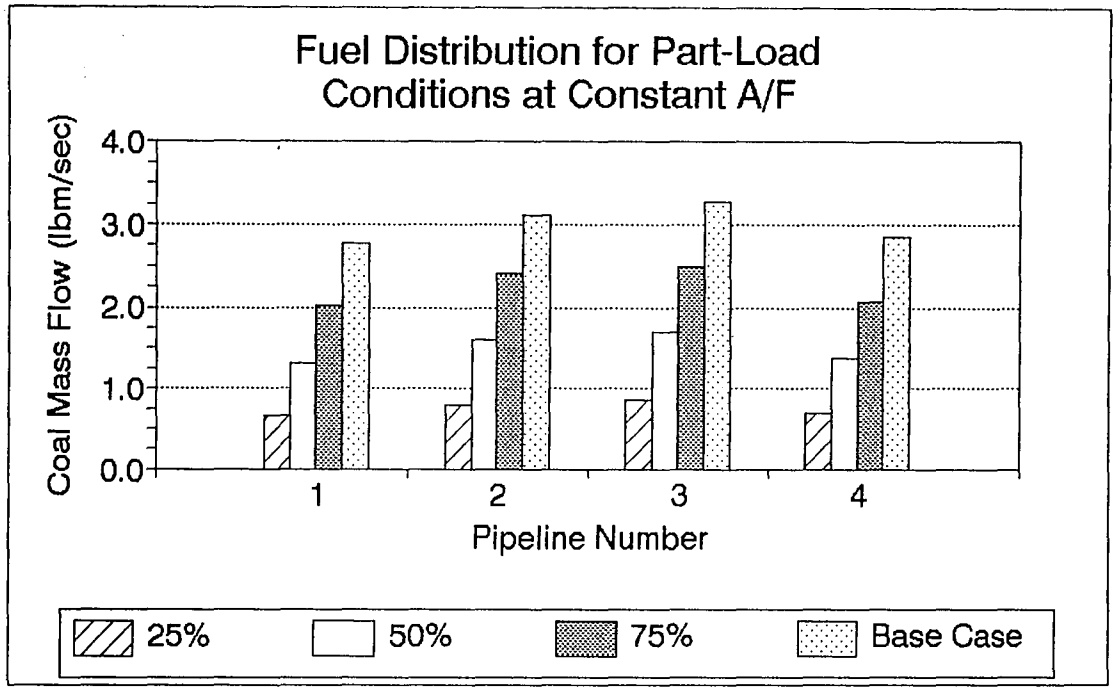

Figure (6-21) The effect of varying load (at constant A/F) on fuel distribution - Method II.

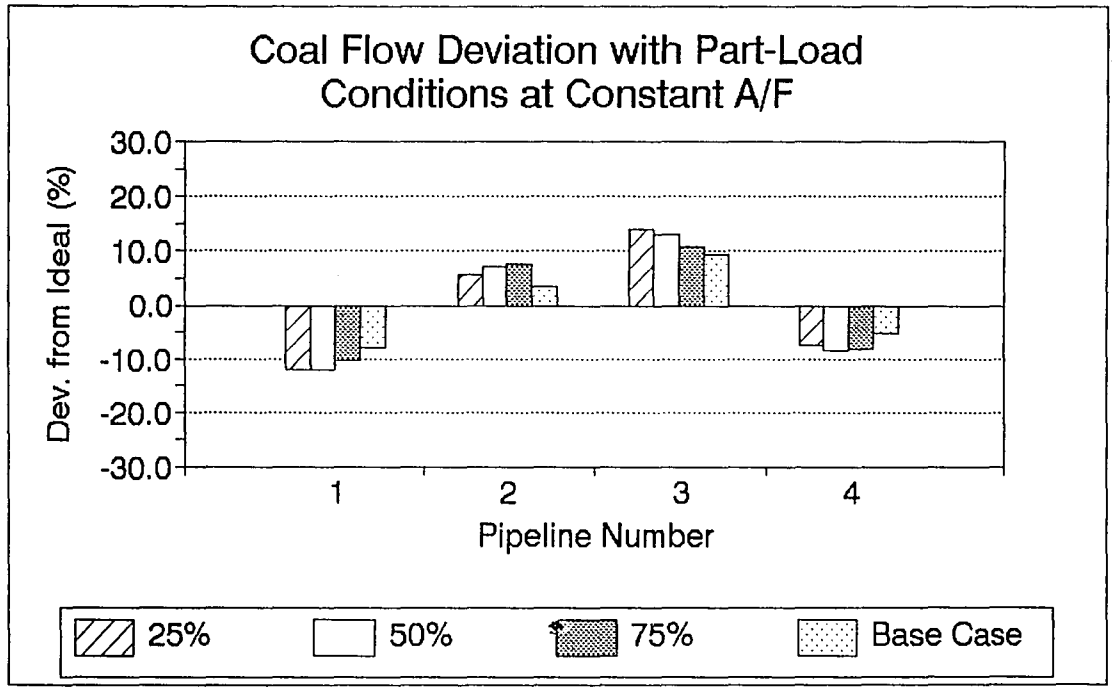

Figure (6-22) The effect of varying load (at constant A/F) on coal flow deviation - Method II.

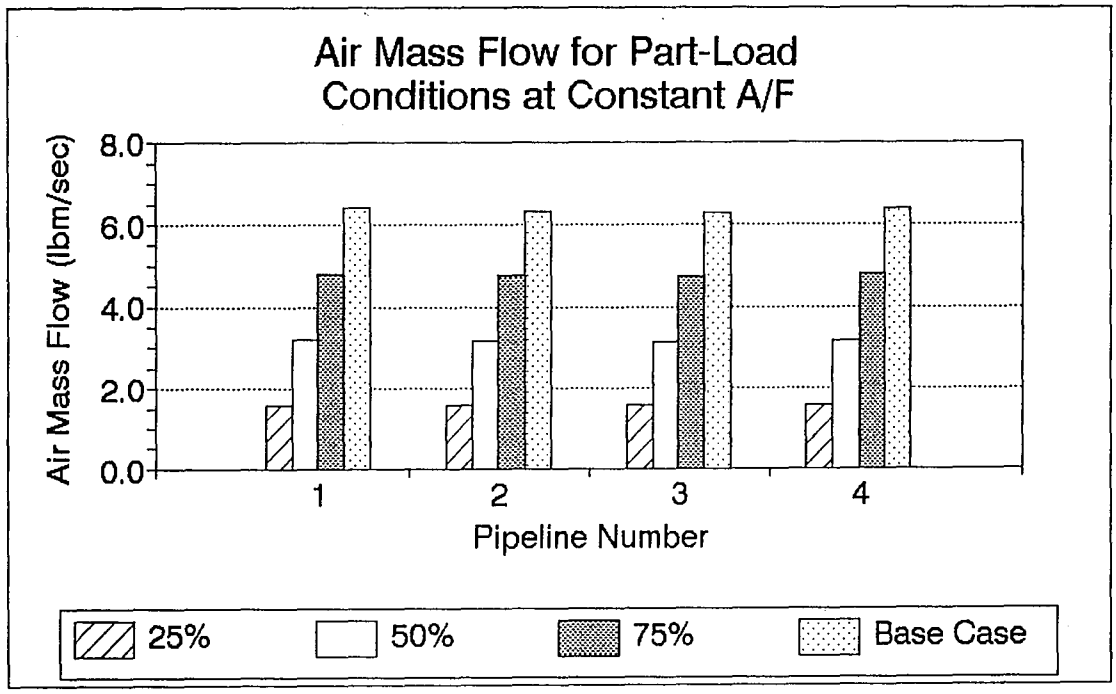

Figure (6-23) The effect of varying load (at constant A/F) on air mass flow rates - Method II.

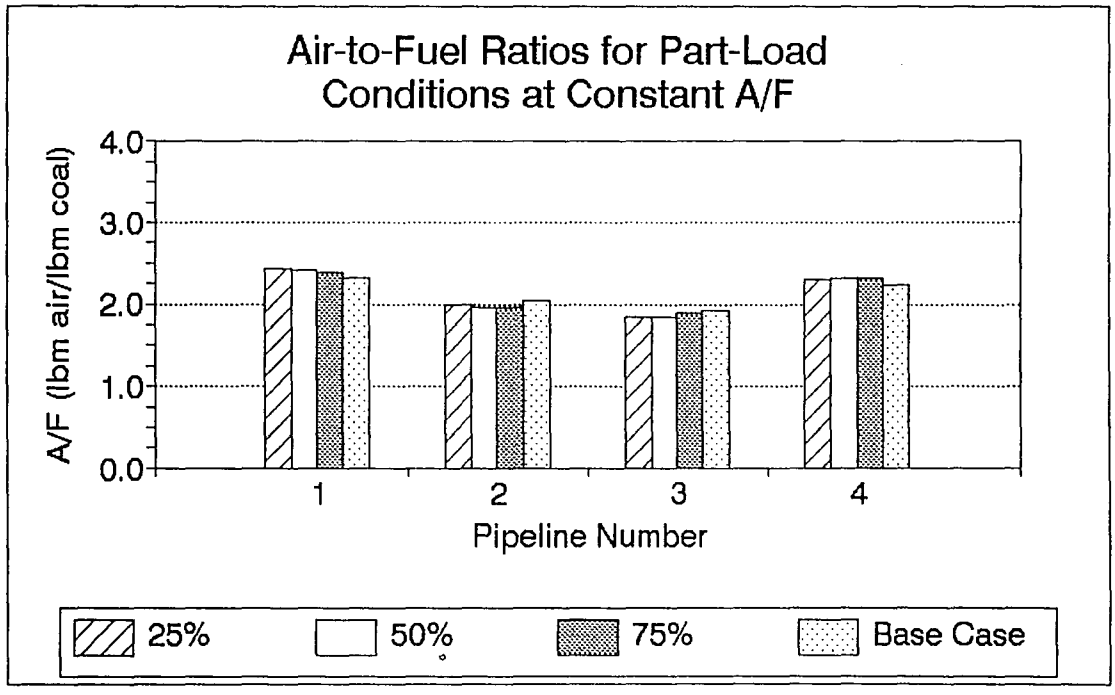

Figure (6-24) The effect of varying load (at constant A/F) on air/fuel ratios - Method II.

6.2 Variation of Model Assumptions

6.2.1 Variation of Particle Size

The burner balancing routine presented in this thesis relies upon the use of a single parameter to represent the size of the conveyed particles. However, the pulverized coal used in electric power plants is composed of a range of particle sizes. The assumption of a uniform particle size is needed to calculate the orifice plate sizes, but the actual range of particle sizes may produce a different set of pipeline pressure drops. This section examines the effect of particle size on the performance of the orifice plates recommended by the baseline case. The baseline conditions, are identical to those given in Section 6.1.

The following particle diameter sizes are examined in this section: 50, 65, and 100 microns. Using the air distribution of Method I, the resultant fuel distribution is shown in Figure (6-25). Although a coal flow imbalance exists, its variation (per pipeline) with particle size is small. The flow deviation values are plotted in Figure (6-26), which shows that the deviation per pipeline is almost constant. Standard deviation values for each of the particle sizes are:

Particle Size (microns)	Standard Deviation of Coal Flow Deviation (%)
50.0	3.56
65.0	3.85
85.0	0.00
100.0	3.41

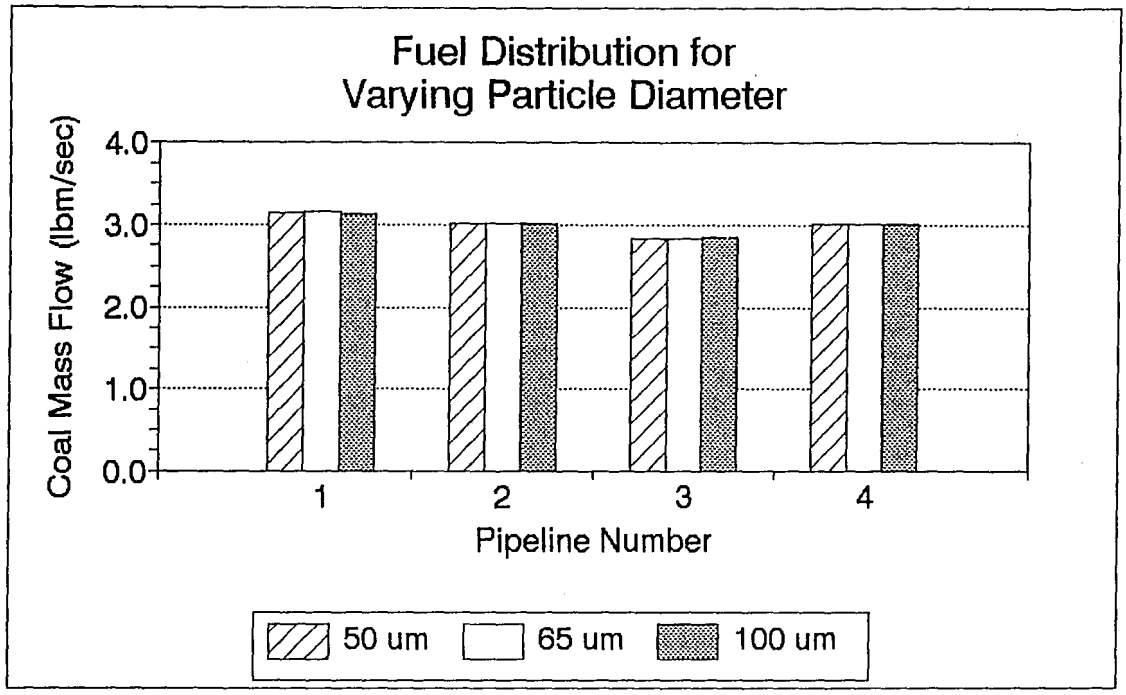

Figure (6-25) The effect of varying particle size on fuel distribution - Method I.

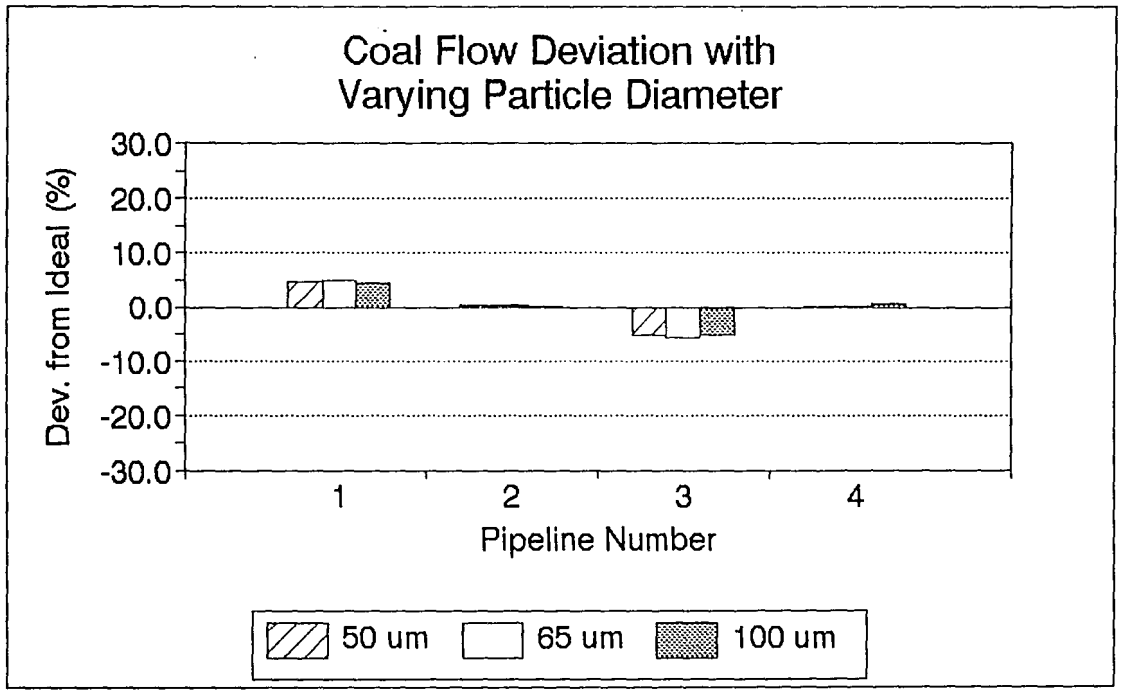

Figure (6-26) The effect of varying particle size on coal flow deviation - Method I.

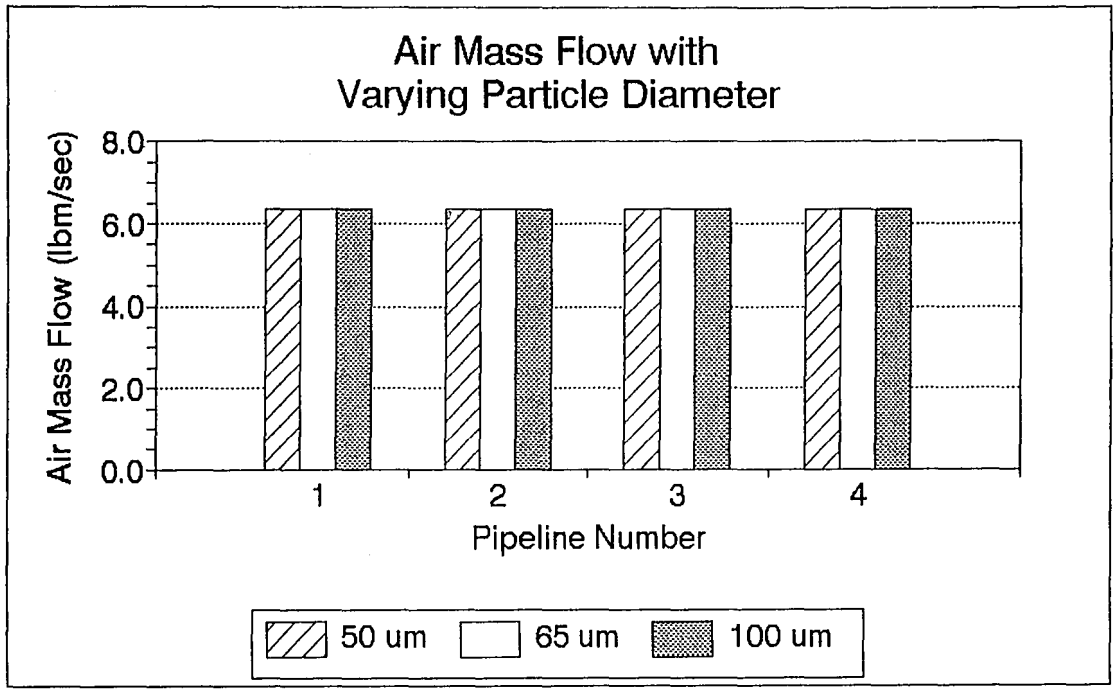

Figure (6-27) The effect of varying particle size on air mass flow rates - Method I.

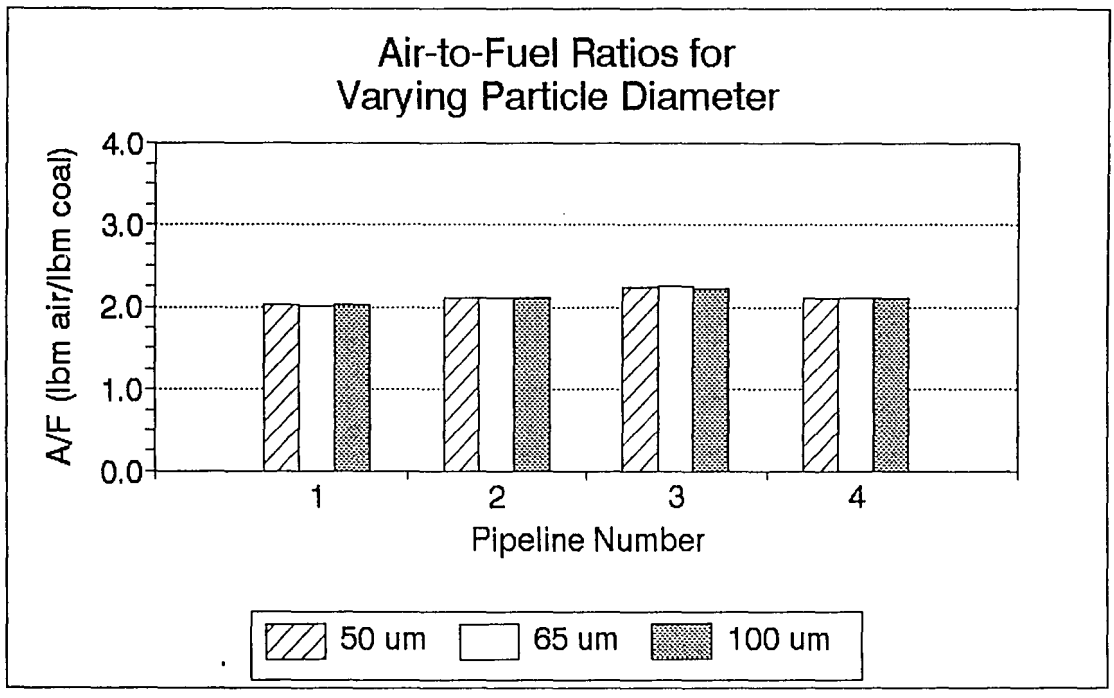

Figure (6-28) The effect of varying particle size on air/fuel ratios - Method I.

with the standard deviation (and coal flow deviations) of the base case being 0.00%. Thus, this range of particle sizes creates a coal flow imbalance which is nearly constant (per pipeline).

In accordance with the assumption of Method I, the air mass flow is equally divided among the pipelines (see Figure (6-27). The variation in air-to-fuel ratios in each of the pipelines, shown in Figure (6-28), is therefore directly due to the coal flow imbalance.

When Method II is used to assign air flow rates, the overall imbalance behavior is similar to that produced by Method I. However, a comparison of the Method II fuel distribution (see Figure (6-29)) with the Method I distribution (see Figure (6-25)) shows that Pipeline 3 changes from fuel-lean in Method I to fuel-rich in Method II. Pipeline 1 displays the opposite behavior. However, with respect to the base case of Method II, only a particle size of 50 microns produces measurable variations from the other cases. As shown in Figure (6-30), the coal flow deviations per pipeline are nearly constant for the 65, 100, and 80 (base case) micron values. But the 50 micron value varies from the others. The standard deviation of the coal flow deviation for each particle size is presented below.

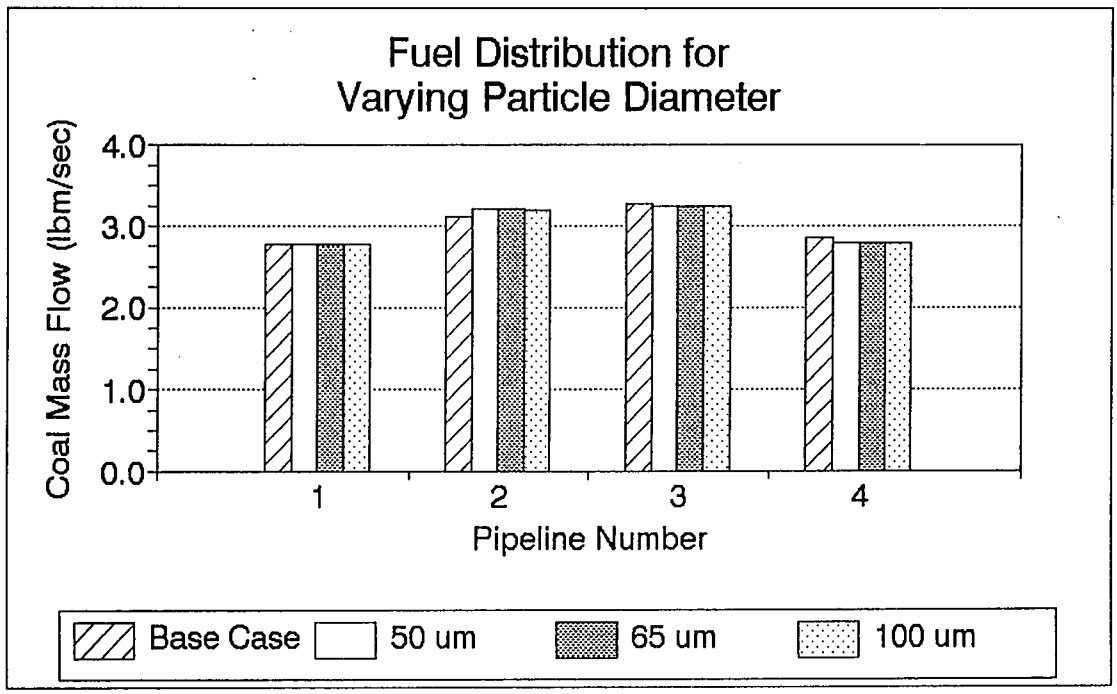

Figure (6-29) The effect of varying particle size on fuel distribution - Method II.

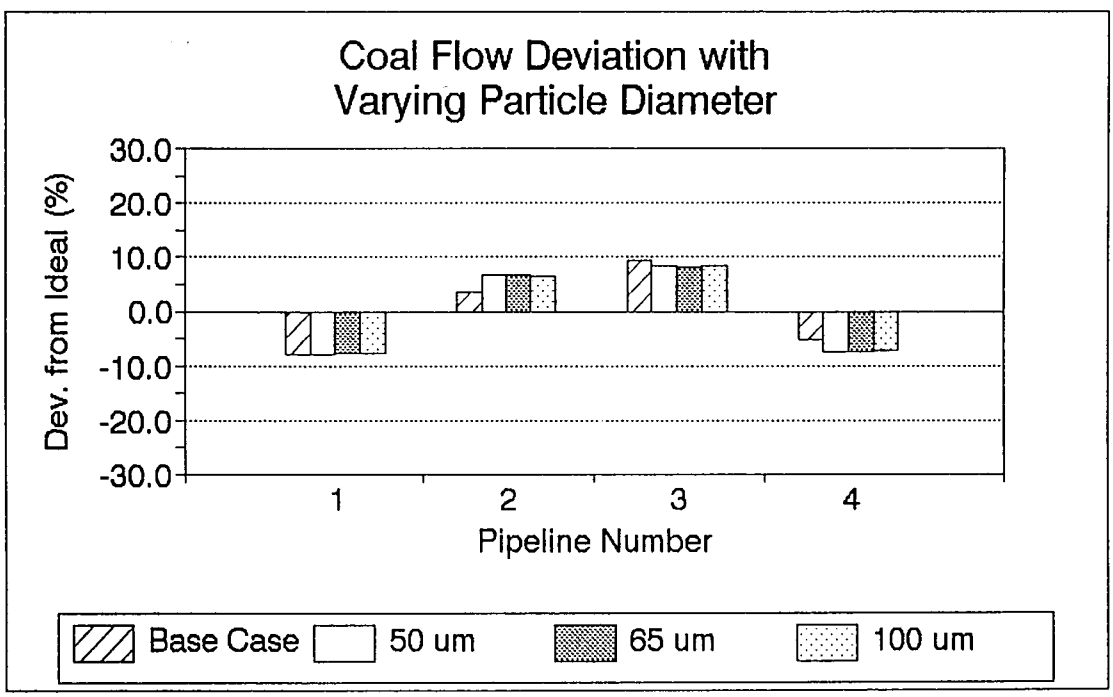

Figure (6-30) The effect of varying particle size on coal flow deviation - Method II.

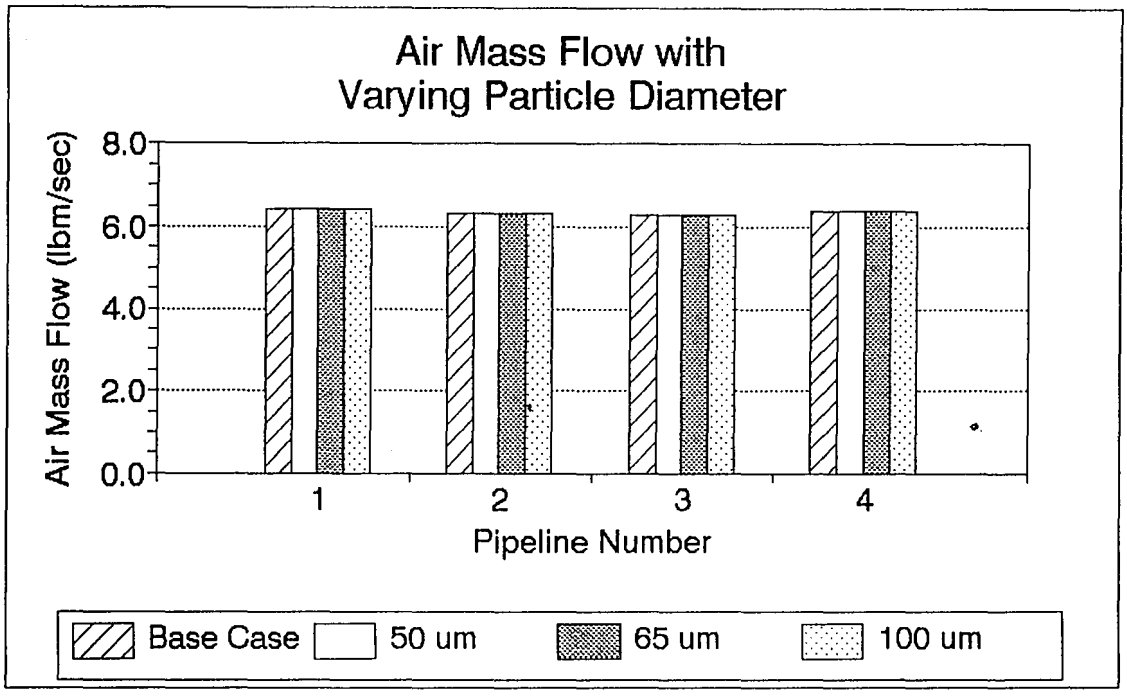

Figure (6-31) The effect of varying particle size on air mass flow rates - Method II.

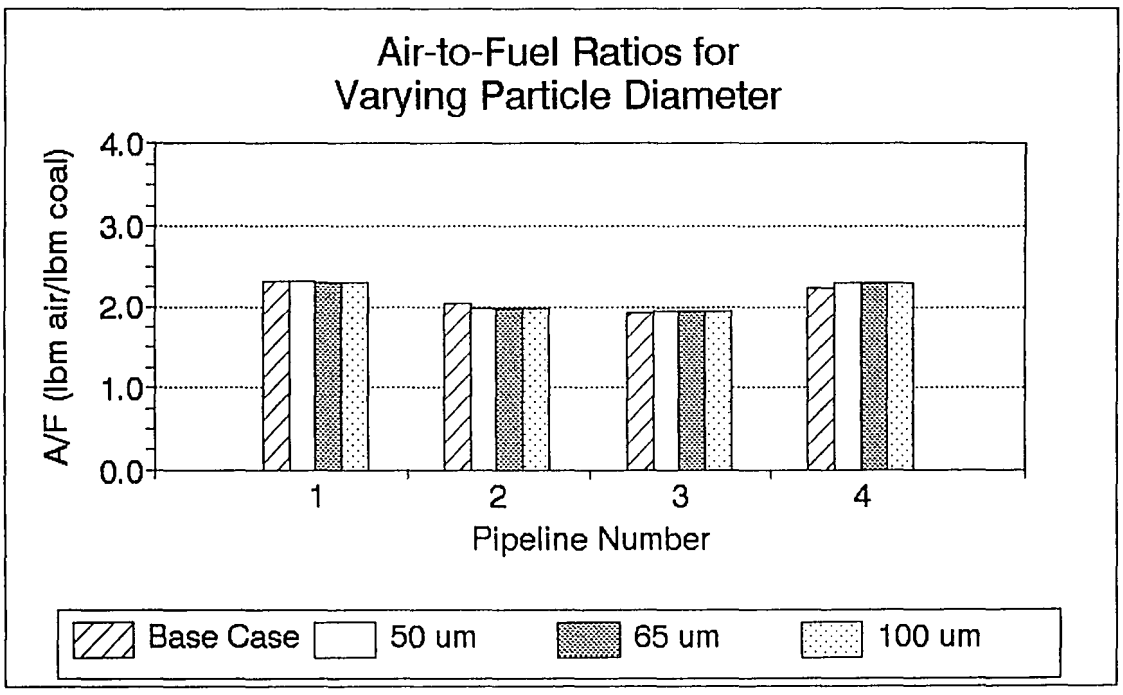

Figure (6-32) The effect of varying particle size on air/fuel ratios - Method II.

Particle Size (microns)	Standard Deviation of Coal Flow Deviation (%)
50.0	7.55
65.0	7.51
85.0	6.81
100.0	7.42

Thus, although the 50 micron particle diameter does not behave like the other settings on a per pipeline basis, its overall behavior is the same. In reference to these standard deviation values, the base case (80 microns) yields a standard deviation of 6.81%.

The air flow rate values, which are plotted in Figure (6-31), are unaffected by variation in particle size since their values are assigned via Method II. Therefore, the variation of the air-to-fuel ratio in each pipeline with particle size, shown in Figure (6-32), is due to the coal flow imbalance.

6.2.2 Variation of Pipe Wall Roughness

The pressure drop equations used by the burner balancing routine utilize a gas friction factor which is a function of the flow Reynolds number and the pipeline material. Although the pipeline material will not vary from the base case during power plant operation, the surface condition of the material will change with time due to the flow of the air and solid particles. The resultant erosion does not occur smoothly, but instead causes "pitting" in the pipe walls, yielding a surface which is rougher than the original. Thus, the friction

coefficient calculated for the base case, which is based upon the pipes being in "new' condition, will become incorrect as the pipe ages. In this section, the effect of variation in surface roughness is examined.

The following pipe relative roughness values are investigated: 0.00015/D, 0.0005/D, and 0.0004/D. These values are compared to the base case value of 0.00085/D. Appendix 3 details the significance of each of these values. Employing Method I, varying surface roughness produced the fuel distribution shown in Figure (6-33). Pipelines 2 and 4 behave similarly and show little variance due to the change in roughness. But Pipelines 1 and 3 show a strong dependence upon the roughness value. Figure (6-34) plots the coal flow deviation values for each of the pipelines. The value of 0.00015/D, which is the roughness value which most differs from the base case, produces the largest deviations. For each roughness value, the following standard deviation values were calculated:

Relative Roughness	Standard Deviation of Coal Flow Deviation (%)
0.00015/D	17.16
0.0004/D	9.46
0.0005/D	7.11
0.00085/D	0.00

Obviously, changes in pipe surface roughness have a serious effect upon coal flow distribution. However, due to the use of Method I, the air flow rates per pipeline do not change with variations in surface roughness. (See Figure (6-35)).

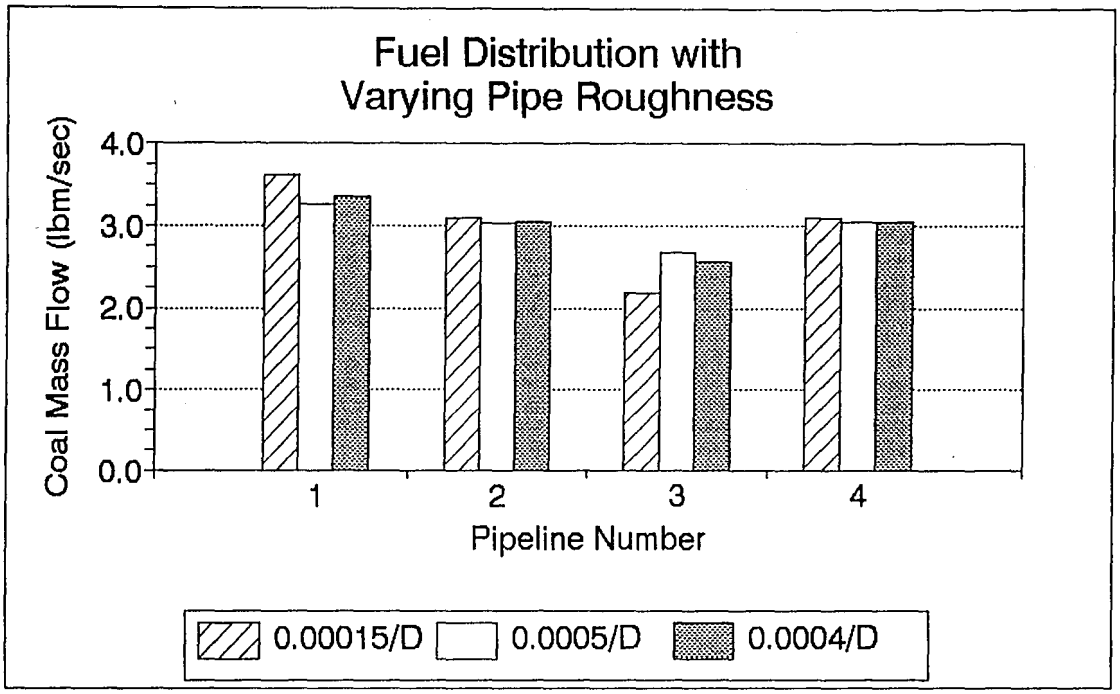

Figure (6-33) The effect of varying pipe wall roughness on fuel distribution - Method I.

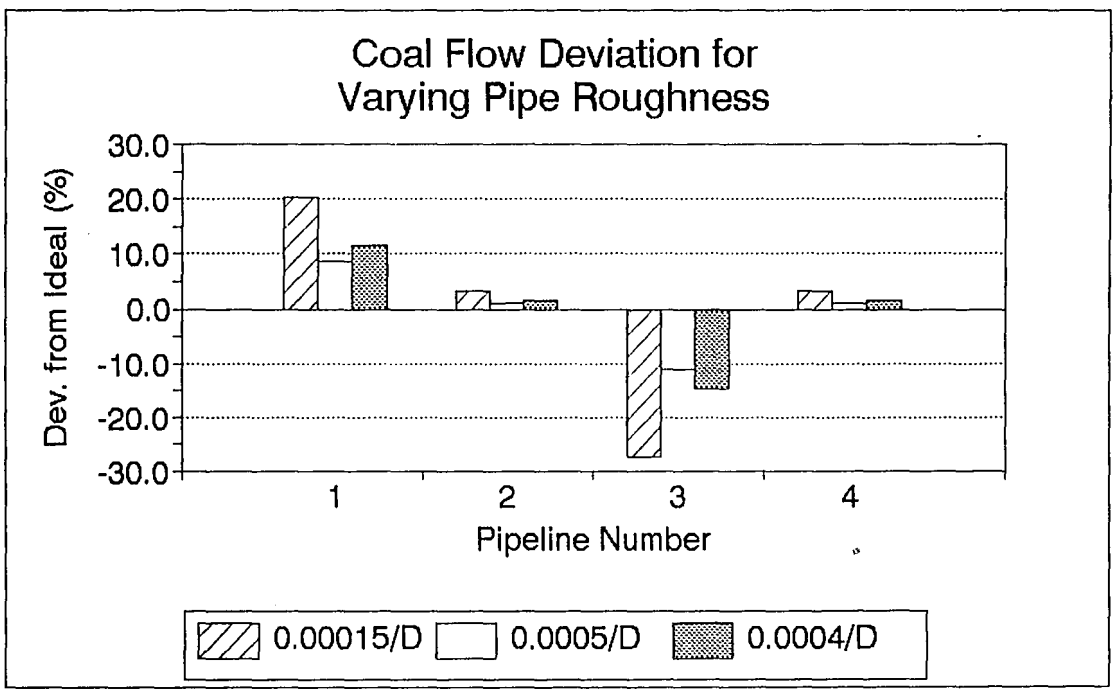

Figure (6-34) The effect of varying pipe wall roughness on coal flow deviation - Method I.

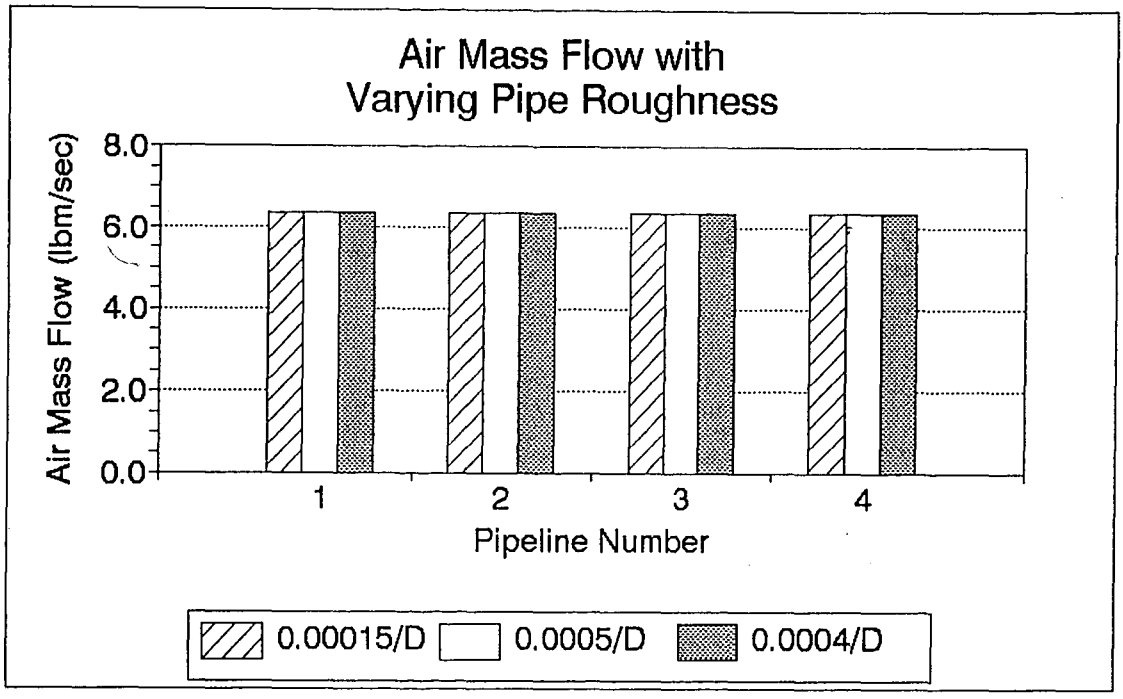

Figure (6-35) The effect of varying pipe wall roughness on air mass flow rates - Method I.

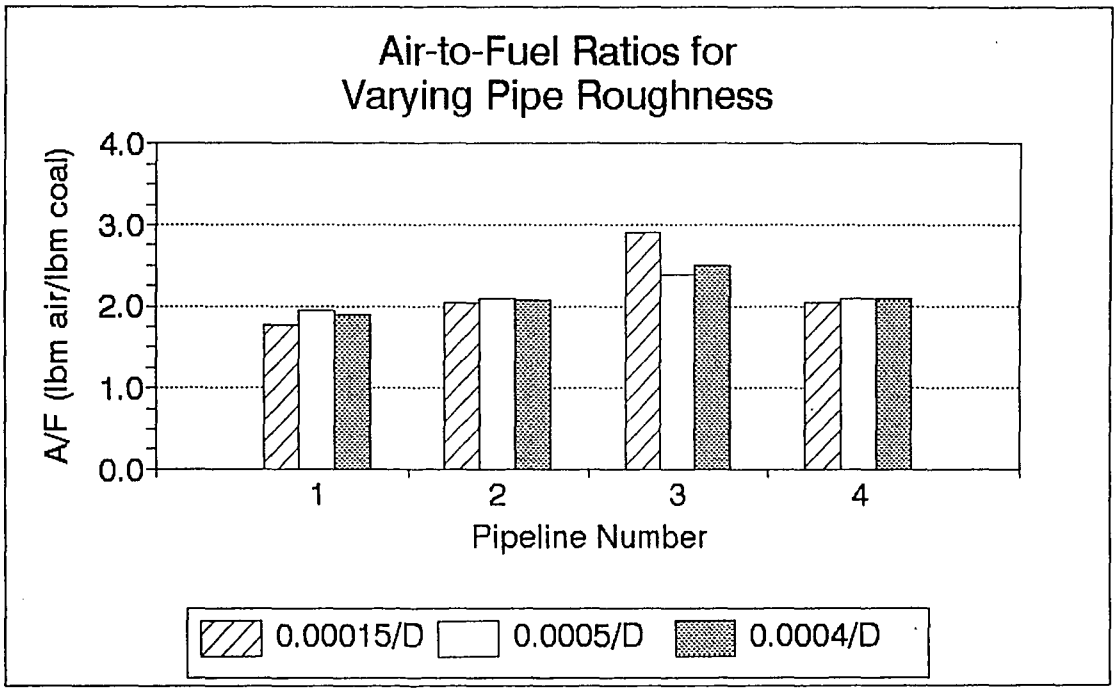

Figure (6-36) The effect of varying pipe wall roughness on air/fuel ratios - Method I.

The variation in air-to-fuel ratios shown in Figure (6-36) are therefore due solely to the coal flow imbalances.

The effect of surface roughness was also investigated using the air flow distribution of Method II. Figure (6-37) shows the resultant fuel distribution. In the base case, Pipeline 1 receives the least, and Pipeline 3 receives the largest, amount of coal. But when the roughness is changed to 0.00015/D, the flow pattern is reversed. As the roughness is varied, the flow distribution changes and progresses towards the base case behavior. Figure (6-38) shows that the highest individual coal flow deviations occur for Pipelines 1 and 3. The standard deviation values for each roughness value are:

Relative Roughness	Standard Deviation of Coal Flow Deviation (%)
0.00015/D	12.28
0.0004/D	4.83
0.0005/D	3.18
0.00085/D	6.81

In comparison with the base case deviation of 6.81%, the variation in relative roughness values has a strong effect upon the fuel distribution.

In accordance with the assumption of Method II, the air distribution for each of these roughness values was determined under clean-air flow conditions. As shown in Figure (6-39), the variation of surface roughness has no measurable effect upon the clean air flow distribution for the pipeline system analyzed in this chapter (see Figure (5-2)). Thus, the

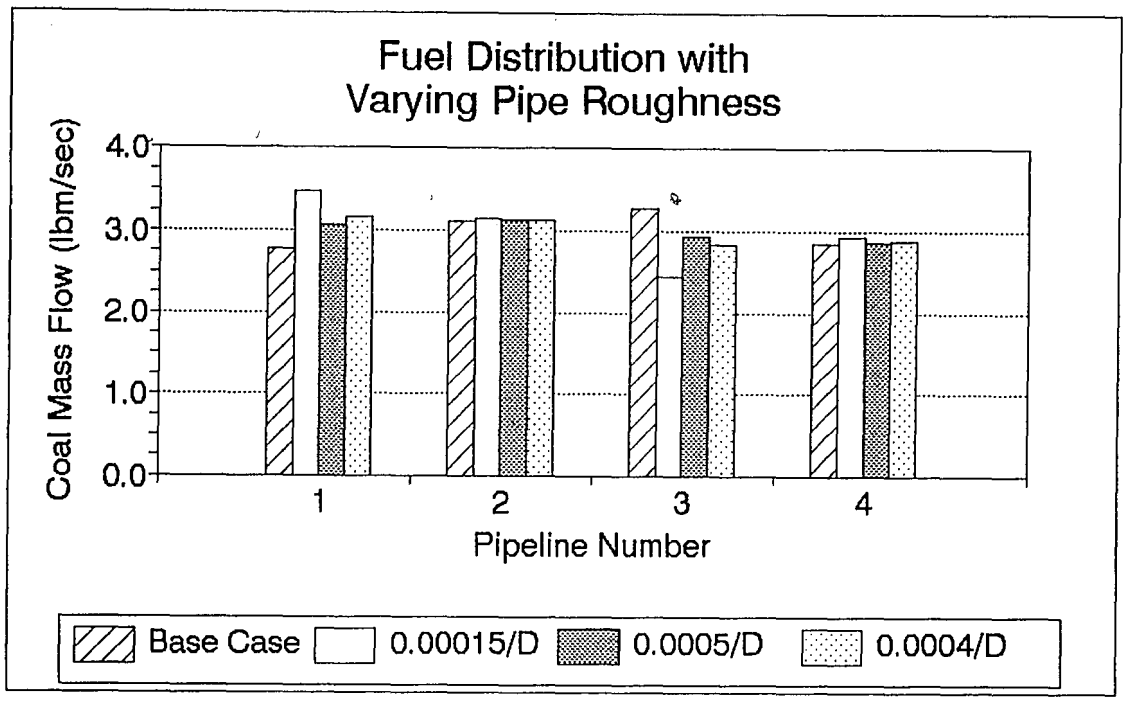

Figure (6-37) The effect of varying pipe wall roughness on fuel distribution - Method II.

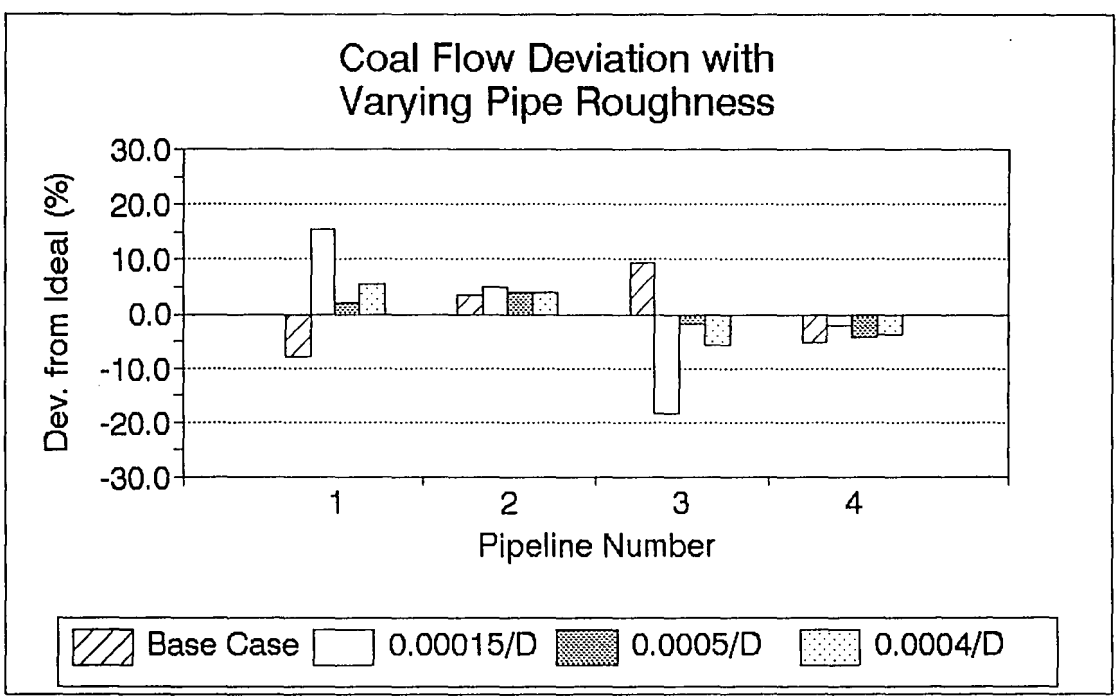

Figure (6-38) The effect of varying pipe wall roughness on coal flow deviation - Method II.

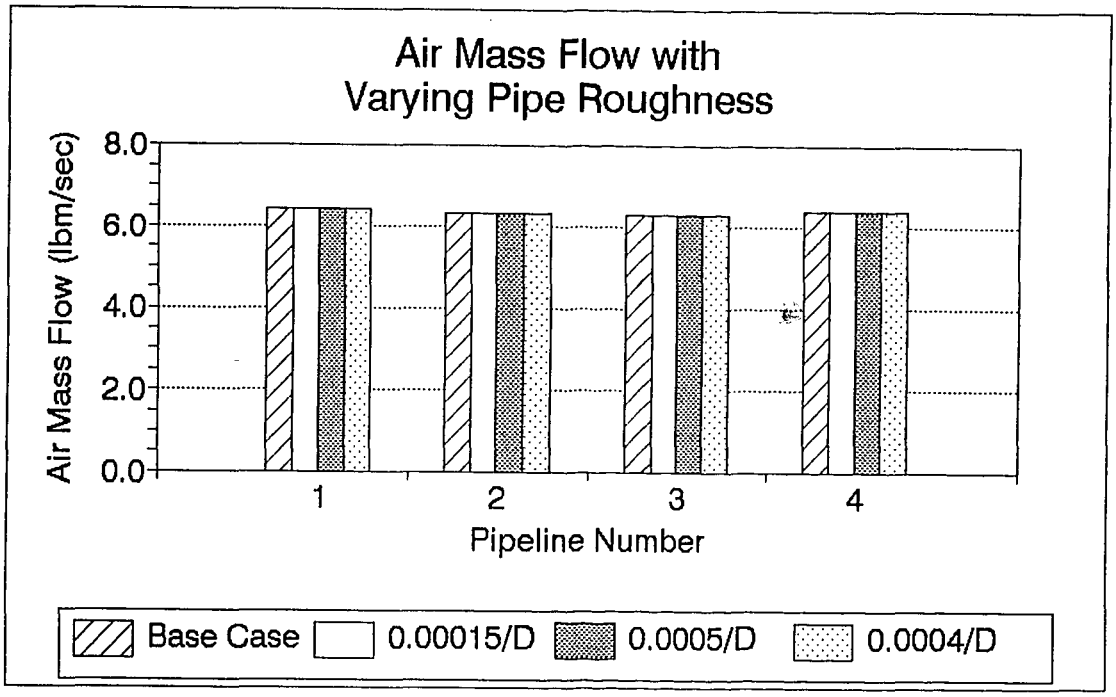

Figure (6-39) The effect of varying pipe wall roughness on air mass flow rates - Method II.

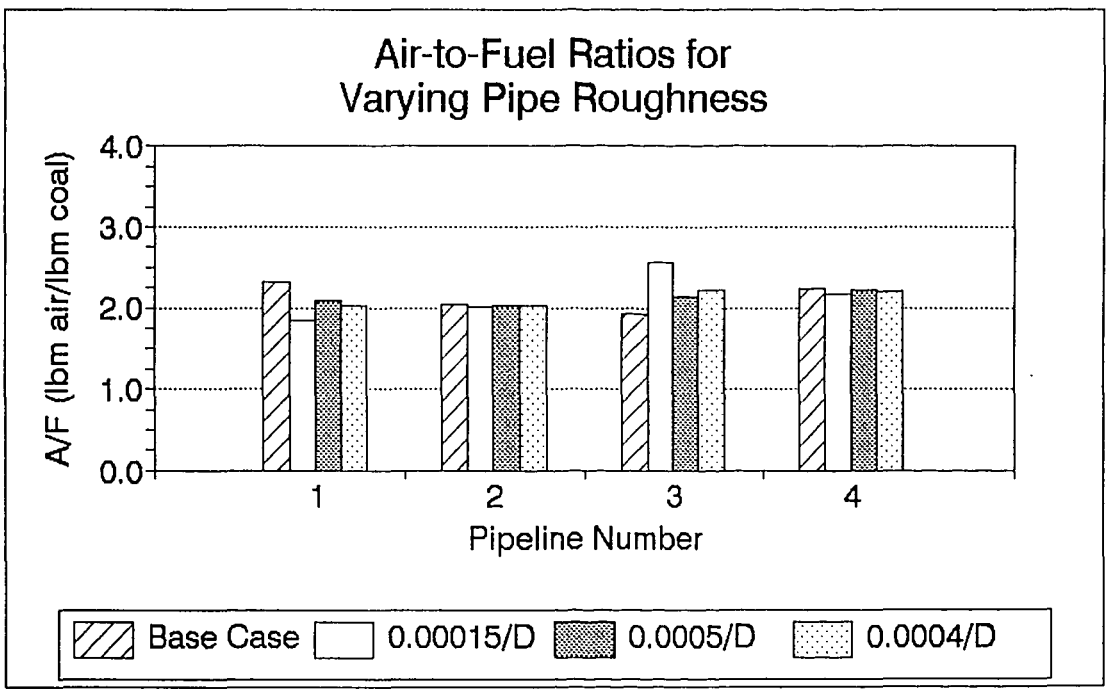

Figure (6-40) The effect of varying pipe wall roughness on air/fuel ratios - Method II.

variation among the air-to-fuel ratios plotted in Figure (6-40) is directly due to the coal flow.

6.3 Variation of Bend Pressure Drop Correlation

The burner balancing routine inherently depends upon the pressure drop correlations which it employs. This section investigates the effect of substituting several other researcher's expressions for the model's "base case" use of the bend pressure drop equation of Michaelides [20]. Specifically, the equations of Michaelides will be replaced by two different correlations: the expressions developed by Schuchart [22] and Mason & Smith [23] (see Chapter 2). The balancing routine uses each of these correlations to calculate the orifice plate sizes needed to provide balanced flow for the baseline operating conditions put forth in Section 6.1. The following orifice plates were calculated:

Pipeline Number	d_o by Schuchart (inches)	d_o by Mason & Smith (inches)
1	15.00000	15.00000
2	12.18769	11.44754
3	11.24556	10.78966
4	12.22105	12.22150

The Michaelides' equations were then placed back into the balancing routine (restoring the original routine) and the code then analyzed the performance of the plates recommended by the other two bend pressure drop correlations.

Using the equalized air distribution of Method I, the resultant fuel distribution is shown in Figure (6-41) in

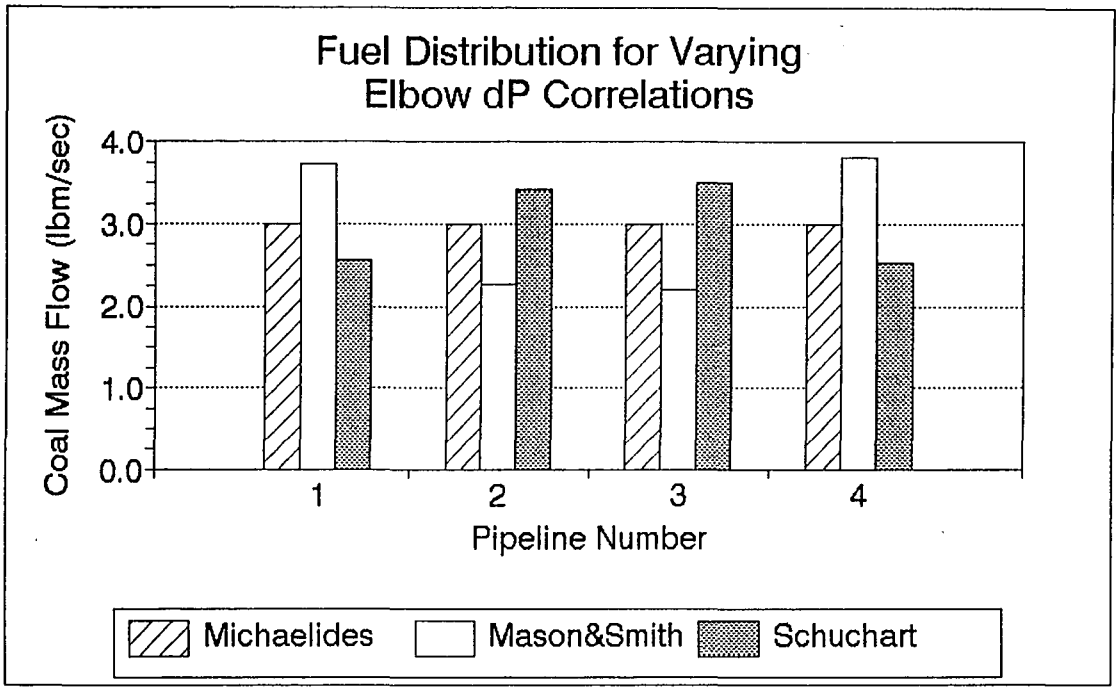

Figure (6-41) The effect of varying elbow pressure drop correlations on fuel distribution - Method I.

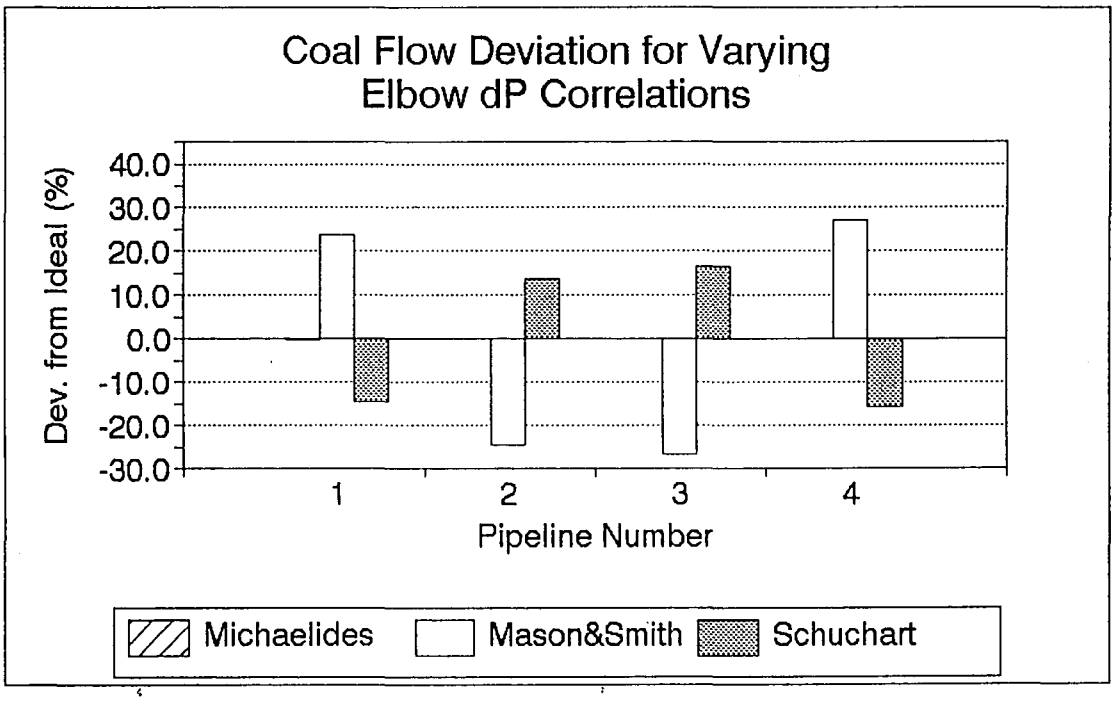

Figure (6-42) The effect of varying elbow pressure drop correlation on coal flow deviation - Method I.

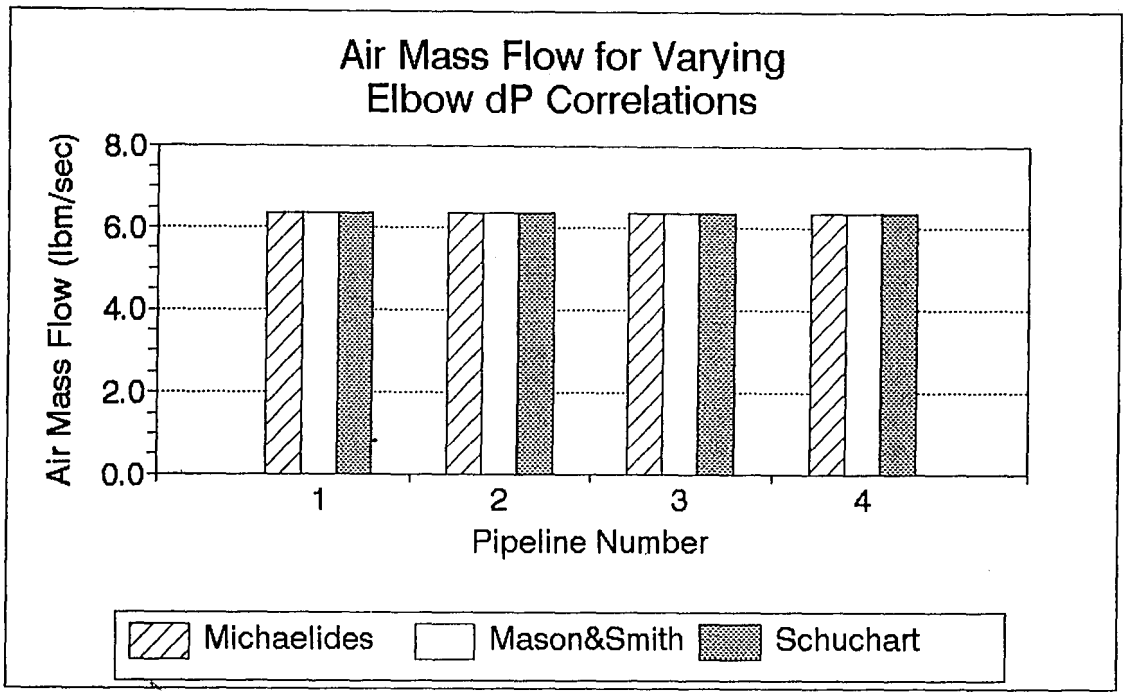

Figure (6-43) The effect of varying elbow pressure drop correlations on air mass flow rates - Method I.

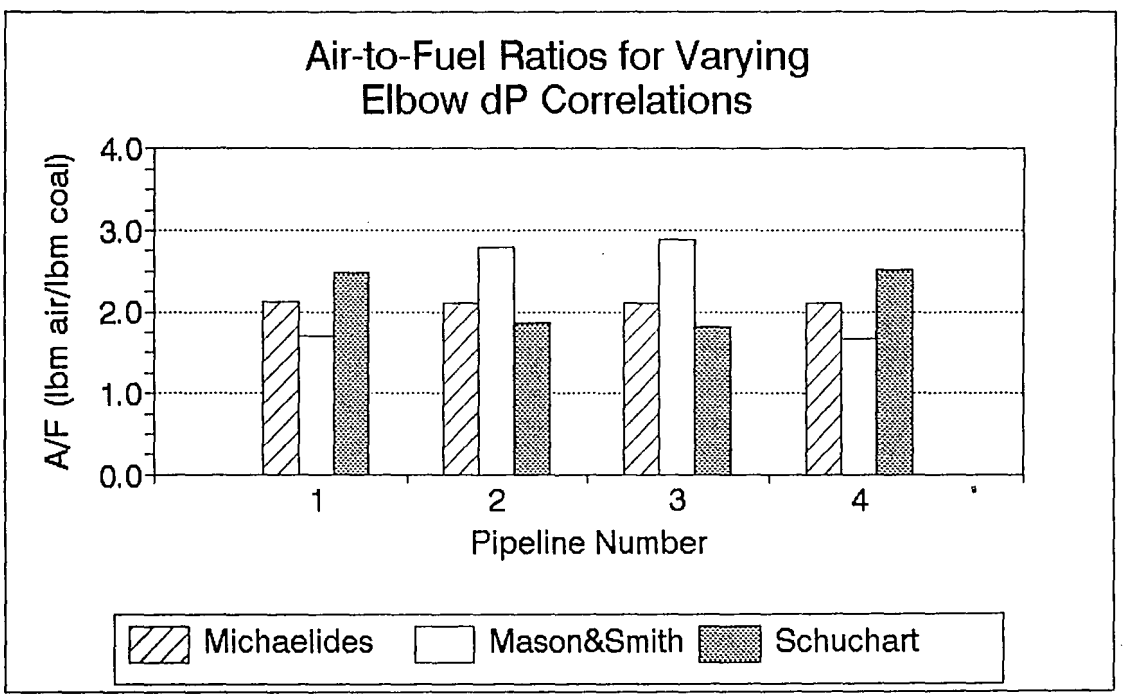

Figure (6-44) The effect of varying elbow pressure drop correlations on air/fuel ratios - Method I.

comparison to the reference base case (Michaelides). The plates calculated by the Schuchart and Mason & Smith expressions clearly do not produce balanced flow. Figure (6-42) shows the coal flow deviation values produced by the use of the plates recommended by the Schuchart and Mason & Smith equations. The Mason & Smith correlation caused the largest deviations, with imbalances approaching 30%. The standard deviation values for the coal flow imbalances are:

Bend Correlation	Standard Deviation of Coal Flow Deviation (%)
Mason & Smith	25.52
Schuchart	15.16

The choice of which bend correlation to use in the burner balancing routine clearly effects the fuel distribution.

The air flow distribution is given in Figure (6-43), which shows the equalized assumption of Method I. Figure (6-44) plots the air-to-fuel ratios per pipeline, whose variations depend solely upon the coal flow imbalance.

When the clean-air flow assumption of Method II is employed, the flow deviations increase beyond those calculated by Method I. Substituting each of the bend correlations into the code, the clean-air distribution produced by the corresponding orifice plates for each was determined. Then the Michaelides' expressions were placed back into the code,

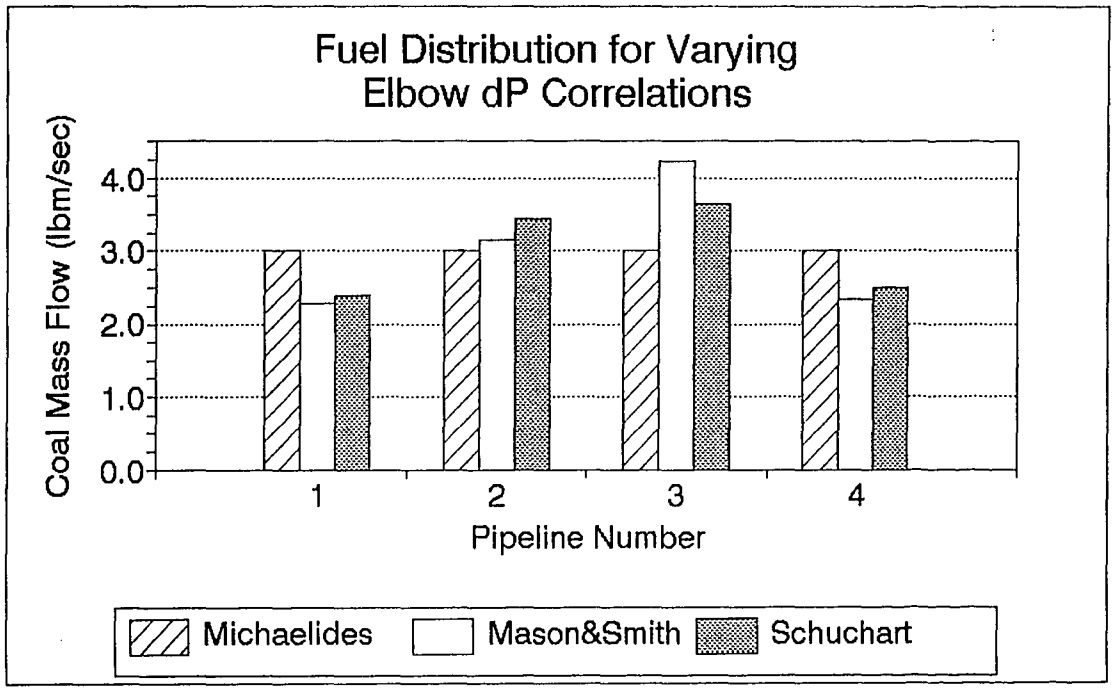

Figure (6-45) The effect of varying elbow pressure drop correlations on fuel distribution - Method II.

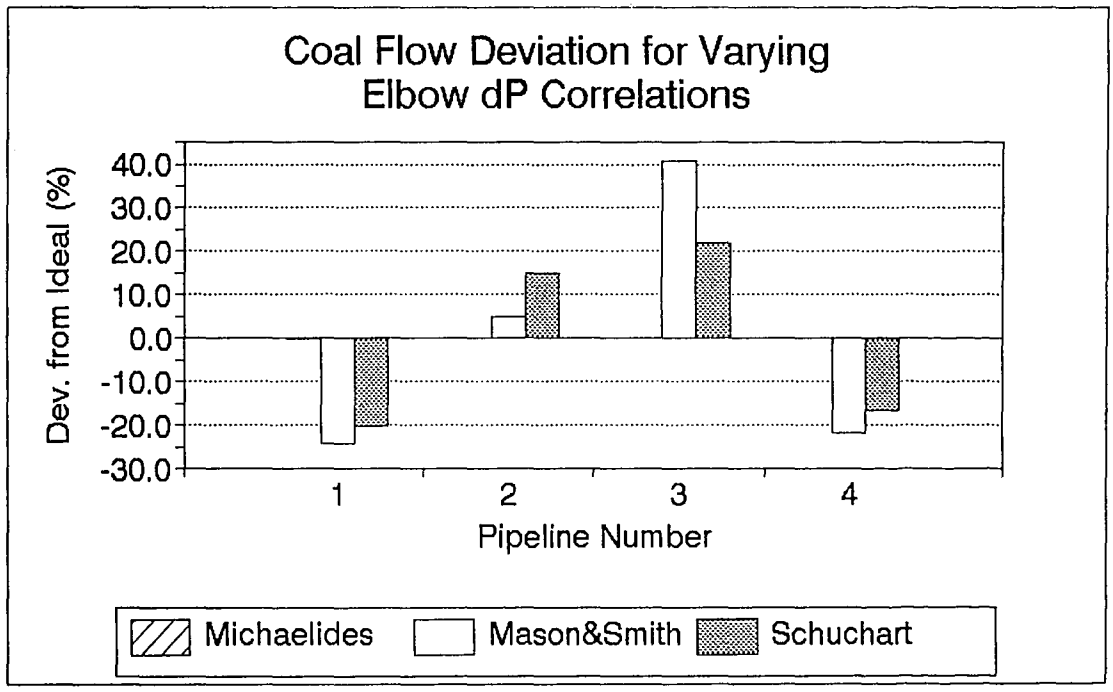

Figure (6-46) The effect of varying elbow pressure drop correlations on coal flow deviation - Method II.

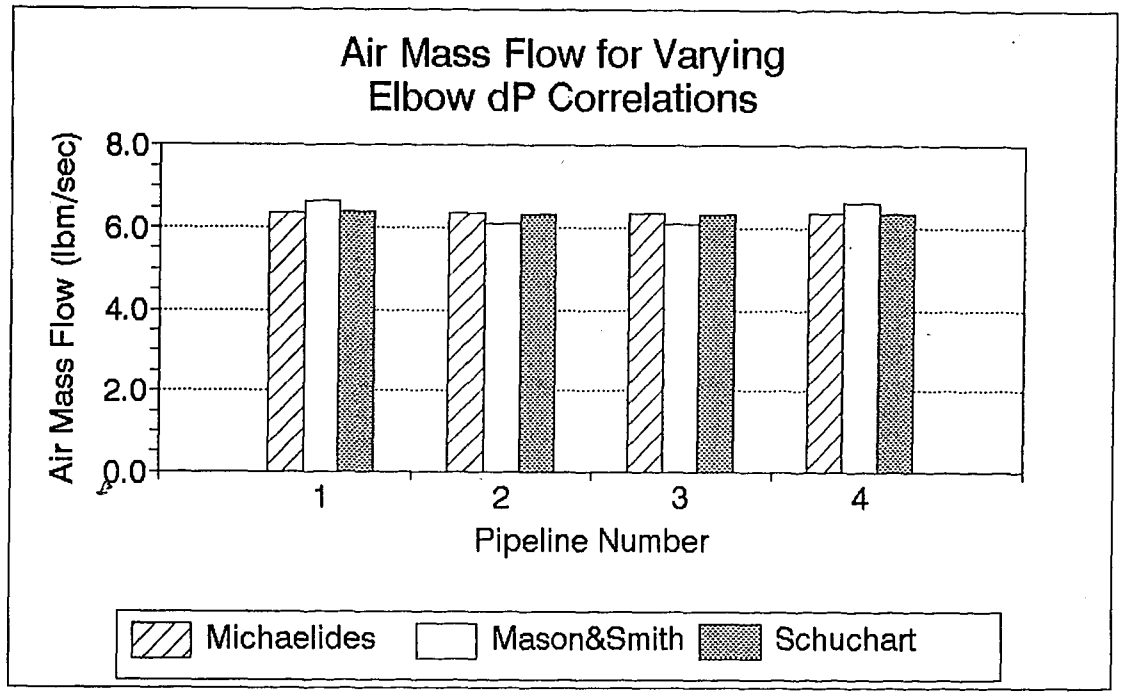

Figure (6-47) The effect of varying elbow pressure drop correlations on air flow rates - Method II.

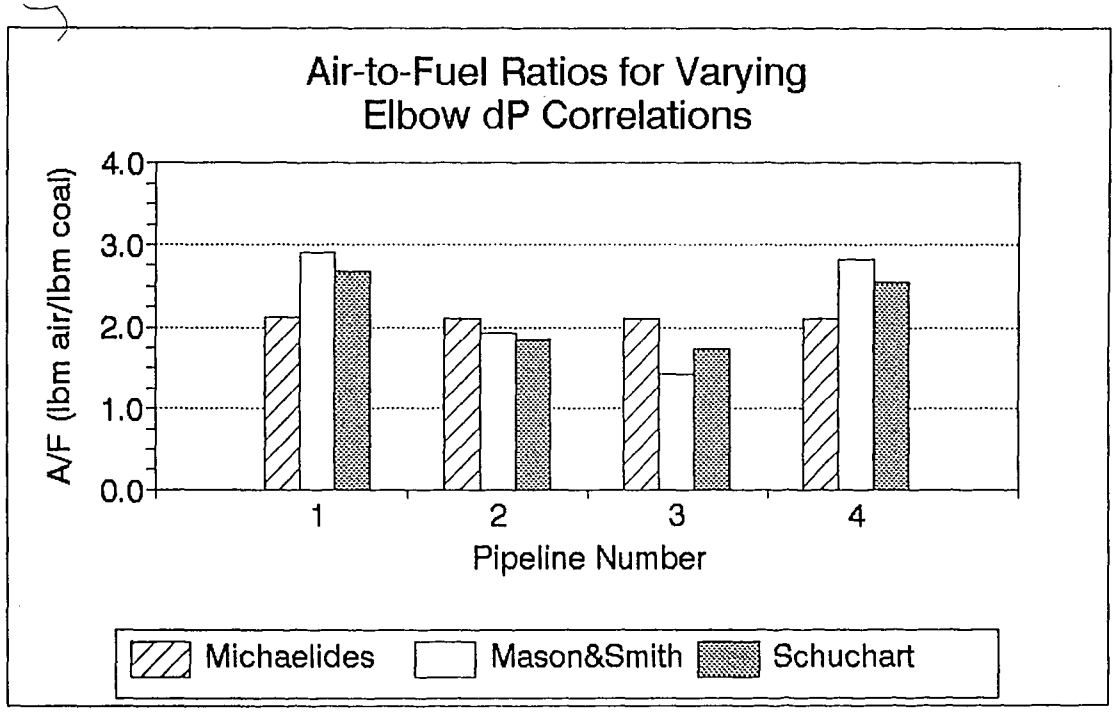

Figure (6-48) The effect of varying elbow pressure drop correlations on air/fuel ratios - Method II.

and the resultant fuel distributions were calculated for each case. As shown in Figure (6-45), the individual pipelines experience similar imbalances for the two cases, which differs from the distributions in Method I. The amounts of the flow imbalances are given in Figure (6-46). Pipeline 3 experiences an imbalance of more than 40% when the Mason and Smith expression is used to calculate the orifice plate sizes and air flow distribution. Overall, the standard deviation for each correlation is:

Bend Correlation	Standard Deviation of Coal Flow Deviation (%)
Mason & Smith	26.28
Schuchart	18.64

As for Method I, the choice of correlation used to calculate orifice plate sizes has a pronounced effect upon the subsequent coal flow distribution.

The air flow distributions, as determined by Method II, are plotted in Figure (6-47). Although the air flow deviations caused by the orifice plate recommendations of Michaelides and Schuchart are small, the plates recommended by Mason & Smith produce a measurable clean-air flow imbalance. The air-to-fuel ratio, shown in Figure (6-48), varies among the pipelines due to the combined coal and air flow imbalances.

6.4 Use of Clean Air Flow Balancing

Clean air testing is a common technique used by electric power plant engineers to balance coal flow distribution. With no coal in the air stream, pitot tube measurements are made in each of the pipelines at a location downstream of the final riffler. Based upon the measured pressure data, flow restrictions (usually orifice plates) are then added to each pipe on a trial and error basis until the pitot tube measures equalized pressure losses. These flow resistances, which provide balanced clean air flow, are assumed to also provide balanced coal flow distribution.

The burner balancing routine developed in this thesis was used to examine the effect of using a balanced clean air flow assumption. Using the baseline operating conditions presented in Section 5.4 and the pipeline system of Figure (5-2), Part I of the burner balancing routine calculated the orifice plate sizes needed to balance the *clean* air flow. Then, with the coal feed rate set to the baseline value, the routine calculated the performance of these "clean-air" plates under dirty air flow conditions.

Figure (6-49) shows the resultant fuel distribution in comparison to the baseline case (balanced flow). The orifice plates which balanced the clean air distribution do not have the same effect upon the dirty air flow. Coal flow deviation values, plotted in Figure (6-50), are on the order of 10%. The standard deviation of the coal flow deviation values is

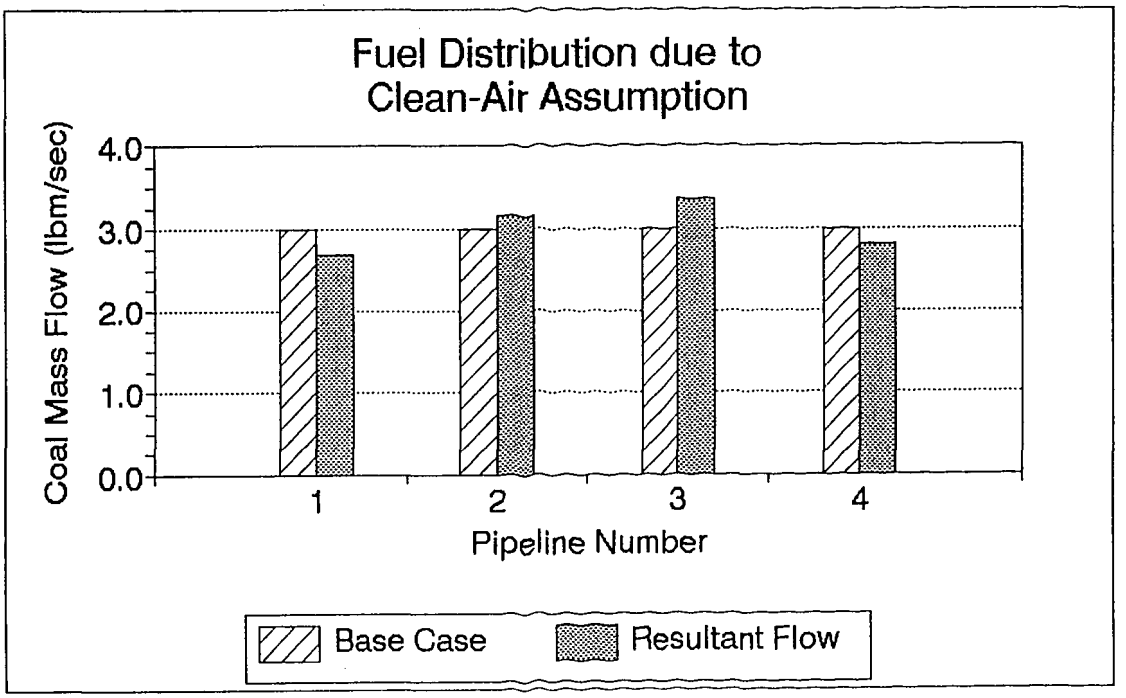

Figure (6-49) The fuel distribution which results from the clean air balancing technique.

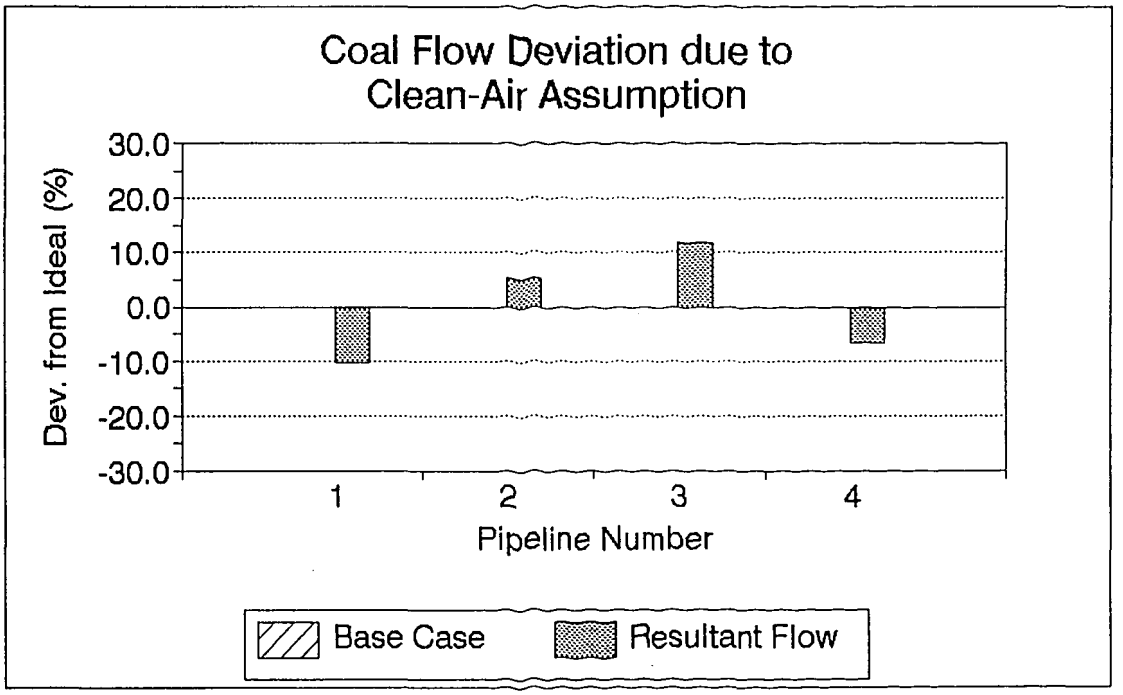

Figure (6-50) The resultant coal flow deviation for the clean air balancing technique.

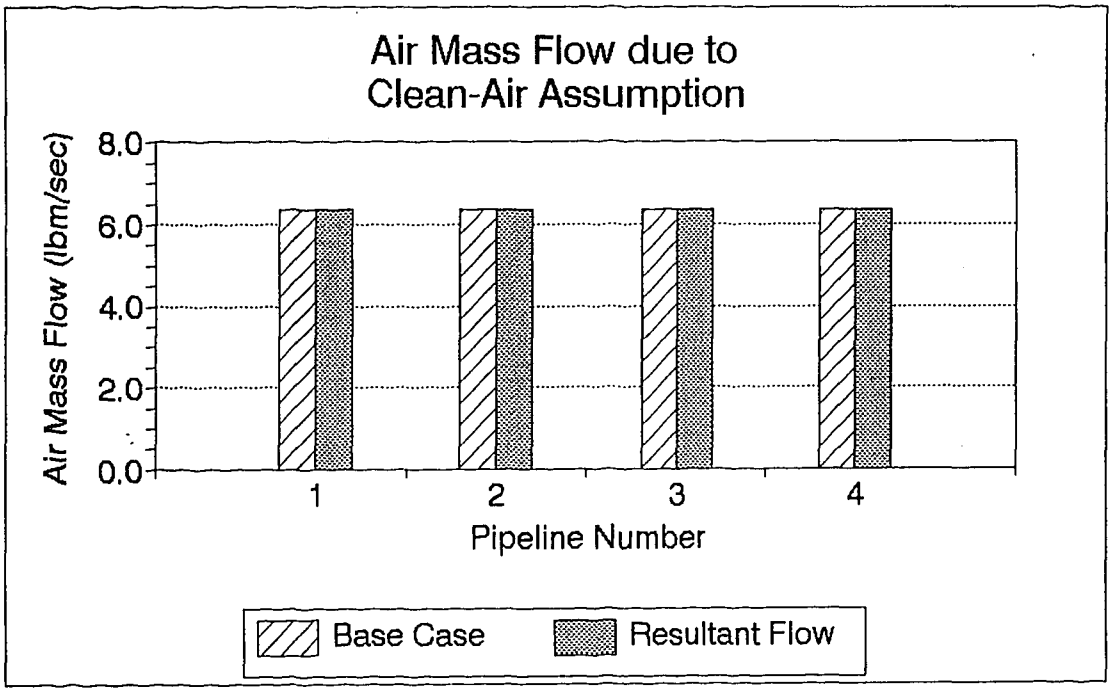

Figure (6-51) The air mass flow rates which result from the clean air balancing technique.

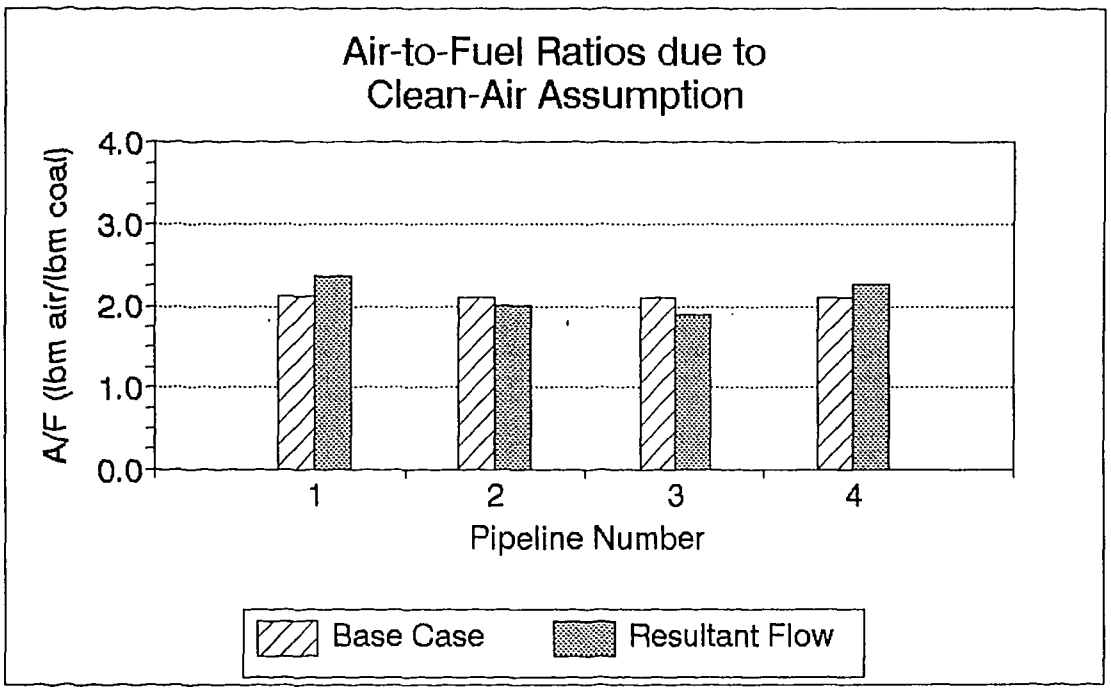

Figure (6-52) The air/fuel ratios which result from the clean air balancing technique.

8.9%, which represents a significant imbalance.

The air mass flow distribution is given in Figure (6-51). Since the orifice plates were originally calculated for clean air flow, the air flow assumptions of Method I and Method II are identical. The resulting air-to-fuel ratios are imbalanced due to the coal flow deviations. Thus, the use of clean air flow information by the balancing routine of this thesis does not provide balanced coal flow.

7. CONCLUSIONS & RECOMMENDATIONS

7.1 The Burner Balancing Model

A computational method for balancing the fuel distribution in electric power plants, based upon pipeline pressure loss, has been developed in this thesis. After reviewing a variety of research publications regarding gas-solids transport, the pressure drop correlations developed by Yang [5] and Michaelides [20] were chosen to perform the calculations. The model has been extended into a FORTRAN computer code which calculates pressure losses in each section of a pipeline system. Based upon these calculations, the flow restrictions which must be added to the system to provide balanced flow are determined. In addition, the performance of the current, unaltered system is calculated.

7.2 Limitations of the Model

As detailed in Chapter 6, the burner balancing method relies upon several assumptions which do not accurately represent actual pulverized coal flow. Variation of the particle diameter and pipe surface roughness were shown to produce coal flow deviations up to 7% and 15%, respectively. In addition, the air flow distribution used in Part II of the computer code relies upon the assumption of either equally divided flow (Method I) or clean air flow behavior (Method II). The actual air flow in each pipeline cannot be

determined, as explained in Chapter 4. Although each of the cases examined in Chapter 6 displayed differing behavior for the two methods, the error due to the assumptions cannot be determined.

The model is further limited by its use of a single phase (gas flow) expression for the pressure drop across an orifice plate. Although this assumption is based upon the concept that the vast majority of the particles do not "notice" the plate, it will actually cause some of the particles to fall out of the flow and form a dune on one side of the plate. In a horizontal plate, this would create a partial converging-diverging nozzle along the bottom of the pipe, with the potential of creating a Venturi/orifice plate hybrid. For vertical pipes, the downstream side of the plate will act as a shelf for the particles which fall out of the flow, and the plate may act as a diverging nozzle. However, the author could not find a gas-solids correlation for orifice plates in the literature. The extent of the error due to the single-phase assumption is thus unresolved.

As shown in Chapter 3, the pressure drop correlations are accurate only to within a range of 30%. Thus, their ability to precisely balance coal flow distribution, even with exact data for the operating parameters, is questionable. It should be mentioned again that the pressure drop correlations selected for the burner balancing model are judged to be the most accurate available. Therefore, the model is judged to be

as accurate as this calculational method allows.

7.3 Recommendations

The computational method presented in this thesis relies upon empirical correlations and assumed flow behavior. But the experimental conditions under which the correlations were developed do not accurately represent those encountered in the flow of pulverized coal in electric power plants, and they may be beyond their range of applicability. This model would be better served by the use of correlations derived from actual pulverized coal transport data. A parameter should be developed to account for the range of particle sizes and shapes.

An examination of the sensitivity analysis performed in Chapter 6 shows small deviations for temperature variations and part-load values of 75%. Thus, the practice of permanently installing an orifice plate to provide balanced flow at the conditions which a plant most frequently operates appears to be adequate for such operating variations. However, frequent load changes could have a more severe effect upon the coal distribution, as evidenced by the high deviations at low load which were calculated in Chapter 6.

The degree of burner balancing required for the efficient operation of coal-fired power plants has not been determined. Field studies should be conducted to investigate the effect of coal flow deviation on unit performance. This information

could also be used to examine the validity of the burner balancing model presented in this thesis.

REFERENCES

[1] Zenz, F.A. and Othmer, D.F., Fluidization and Fluid-Particle Systems. New York: Reinhold Publishing Corporation, 1960.

[2] Wen, C.Y. and Simons, H.P., *AIChE Journal*, **5**, p. 263, (1959).

[3] Klinzing, G.E., Gas-Solid Transport. McGraw-Hill Book Company, 1981.

[4] Vetter, A.A. and Vetter, R.S., "Balancing Pulverized Coal Flows in Parallel Piping," *Journal of Engineering for Gas Turbines and Power*, **107**, pp. 679-684, (1985).

[5] Yang, W.C., "A Unified Theory on Dilute Phase Pneumatic Transport," *Journal of Powder & Bulk Solids Technology*, **1**, pp. 89-95, (1977).

[6] Vetter, A.A., "Fundamentals of Two-Phase Flow for Pneumatically Conveyed Pulverized Coal." From the Instrument Society of America POWID '89 Symposium, Paper VA-1, May 1989.

[7] Michaelides, E.E., "Motion of Particles in Gases: Average Velocity and Pressure Loss," *Transactions of the ASME: Journal of Fluids Engineering*, **109**, pp. 172-178, (1987).

[8] Vogt, E.G. and White, R.R., "Friction in the Flow of Suspensions," *Industrial and Engineering Chemistry*, **40**, pp. 1731-1738, (1948).

[9] Hairu, O.H. and Molstad, M.C., "Pressure Drop in Vertical Tubes in Transport of Solids by Gases," *Industrial and Engineering Chemistry*, **41**, pp. 1148-1160, (1949).

[10] Barth, W., "Flow Problems with Mixtures of Gases and Entrained Solid Particles," *Engineer's Digest*, **23**, pp. 81-85, (1962).

[11] Jones, J.H., Braun, W.G., Daubert, T.E., and Allendorf, H.D, "Estimation of Pressure Drop for Vertical Transport of Solids," *AIChE Journal*, **13**, pp. 608-611, (1967).

[12] Konno, H. and Saito, S., "Pneumatic Conveying of Solids Through Straight Pipes," *Journal of Chemical Engineering of Japan*, **2**, pp. 211-217, (1969).

[13] Rose, H.E. and Duckworth, R.A., "Transport of Solid Particles in Liquids and Gases," *The Engineer*, March, pp. 392-396, 430-433, 478-483, (1969).

[14] Capes, C.E. and Nakamura, K., "Vertical Pneumatic Conveying: An Experimental Study with Particles in the Intermediate and Turbulent Flow Regimes," *Canadian Journal of Chemical Engineering*, **51**, pp. 31-38, (1973).

[15] Khan, J.I. and Pei, D.C., "Pressure Drop in Vertical Solid-Gas Suspension Flow," *Industrial and Engineering Chemical Processing, Design, and Development*, **12**, pp. 428-431, (1973).

[16] Yang, W.C., "Estimating the Solid Particle Velocity in Vertical Pneumatic Conveying Lines," *Industrial and Engineering Chemistry Fundamentals*, **12**, pp. 349-352, (1973).

[17] Yang, W.C., "Estimating the Solid Particle Velocity in Horizontal Pneumatic Conveying Lines," *Canadian Journal of Chemical Engineering*, **51**, pp. 779-781, (1973).

[18] Yang, W.C., "Correlations for Solid Friction Factors in Vertical and Horizontal Pneumatic Conveying," *AIChE Journal*, **20**, pp. 605-607, (1974).

[19] Yang, W.C., "A Correlation for Solid Friction Factor in Vertical Pneumatic Conveying Lines," *AIChE Journal*, **24**, pp. 548-551, (1978).

[20] Michaelides, E.E., Westman, M.A., and Thomson, F.M., "Pressure Losses Due to Bends in Pneumatic Conveying," *Journal of Pipelines*, **7**, pp. 15-20, (1987).

[21] Michaelides, E.E. and Roy, I., "Evaluation of Several Correlations Used for the Prediction of Pressure Drop in Particulate Flows," *International Journal of Multiphase Flow*, **13**, pp. 433-442, (1987).

[22] Schuchart, P., *Chem. Eng. Tech.*, **41**, p.1251, (1969).

[23] Mason, J.S. and Smith, B.U. "Pressure Drop and Flow Behavior for the Pneumatic Transport of Fine Particles Around 90° Bends," From BHRA Pneumotransport 2, Paper A2, 1973.

[24] Klinzing, G.E., "A Comparison of Pressure Losses in Bends Between Recent Data and Models for Gas-Solid Flow," *Canadian Journal of Chemical Engineering*,

58, pp. 670-672, (1980).

[25] Hinkle, B.L., "Acceleration of Particles and Pressure Drops Encountered in Horizontal Pneumatic Conveying." PhD Dissertation, Georgia Institute of Technology, Atlanta, GA, (1959).

[26] Handbook of Multiphase Systems, edited by G. Hetsroni. Hemisphere Publishing Company, 1982.

[27] Dogin, M.E. and Lebedev, V.P., *Ind. Chem. Eng. (USSR)*, **2**, pp. 64-67, (1962).

[28] Fox, R.W. and McDonald, A.T., Introduction to Fluid Mechanics. John Wiley & Sons, 3rd ed., 1985.

[29] Morikawa, Y., Tsuji, Y., Matsui, K., and Jittani, Y., "Pressure Drops Due to Pipe Bends in Air-Solids Two-Phase Flows: Circular and Eliptical Bends," *Journal of Multiphase Flow*, **4**, pp. 575-583, (1978).

[30] Mason, J.S. and Smith, B.U., *Powder Technology*, **6**, p.323, (1972).

[31] Benedict, R.P., Fundamentals of Temperature, Pressure and Flow Measurements. John Wiley & Sons, 2nd ed., 1977.

[32] Fluid Meters: Their Theory and Application. A Report of ASME Research Committee on Fluid Meters. New York, 6th ed., 1971.

[33] Carlson, H.M., Frazier, P.M., and R.B. Engdahl, "Meter for Flowing Mixtures of Air and Pulverized Coal," *Transactions of the ASME*, **70**, pp. 65-79, (1948).

[34] Idelchik, I.E., Handbook of Hydraulic Resistance. Hemisphere Publishing Corporation, 2nd ed., 1986.

[35] Yang, W.C. Personal Communication. August, 1991.

[36] Press, W.H., Flannery, B.P., Teukolsky, S.A., and Vetterling, W.T., Numerical Recipes: The Art of Scientific Computing. Cambridge University Press, 1990.

[37] Moody, L.F., "Friction Factors for Pipe Flow," *Transactions of the ASME*, **66**, pp. 671-684, (1944).

[38] Steam: Its Generation and Use. Babcock & Wilcox, 39th ed., 1978.

[39] Combustion: Fossil Power Systems. J.G. Singer, editor. Combustion Engineering, Inc. 3rd ed., 1981.

APPENDIX 1 - Pipeline Data Used in Chapter 5 & Chapter 6

Pipeline 1

SECTION, j	DESCRIPTION	DIMENSIONS
1	Vertical Pipe	D=2.5 , L=4.0
2	Coal Riffler	A_{in}=4.91 , A_{out}=3.14
3	Vertical Pipe	D=2.0 , L=3.0
4	Coal Riffler	A_{in}=3.14 , A_{out}=1.23
5	Vertical Pipe	D=1.25 , L=3.0
6	Pipe Bend	D=1.25 , r_c=2.0
7	Horizontal Pipe	D=1.25 , L=50.0
8	Pipe Bend	D=1.25 , r_c=3.0
9	Horizontal Pipe	D=1.25 , L=20.0
10	Orifice Plate	D=1.25 , d_O=1.235
11	Pipe Bend	D=1.25 , r_c=2.0
12	Vertical Pipe	D=2.0 , L=12.0
13	Pipe Bend	D=1.25 , r_c=2.0
14	Horizontal Pipe	D=1.25 , L=4.0

NOTE: A_{in} and A_{out} are in units of ft^2.
D, L, r_c, and d_O are in units of ft.

Pipeline 2

SECTION, j	DESCRIPTION	DIMENSIONS
1	Vertical Pipe	D=2.5 , L=4.0
2	Coal Riffler	A_{in}=4.91 , A_{out}=3.14
3	Vertical Pipe	D=2.0 , L=3.0
4	Coal Riffler	A_{in}=3.14 , A_{out}=1.23
5	Vertical Pipe	D=1.25 , L=4.0

SECTION, j	DESCRIPTION	DIMENSIONS
6	Pipe Bend	D=1.25 , r_c=2.0
7	Horizontal Pipe	D=1.25 , L=50.0
8	Orifice Plate	D=1.25 , d_O=0.9822
9	Pipe Bend	D=1.25 , r_c=2.0
10	Vertical Pipe	D=1.25 , L=11.0
11	Pipe Bend	D=1.25 , r_c=2.0
12	Horizontal Pipe	D=1.25 , L=4.0

NOTE: A_{in} and A_{out} are in units of ft^2.
D, L, r_c, and d_O are in units of ft.

Pipeline 3

SECTION, j	DESCRIPTION	DIMENSIONS
1	Vertical Pipe	D=2.5 , L=4.0
2	Coal Riffler	A_{in}=4.91 , A_{out}=3.14
3	Vertical Pipe	D=2.0 , L=3.0
4	Coal Riffler	A_{in}=3.14 , A_{out}=1.23
5	Vertical Pipe	D=1.25 , L=5.0
6	Pipe Bend	D=1.25 , r_c=2.0
7	Horizontal Pipe	D=1.25 , L=30.0
8	Orifice Plate	D=1.25 , d_O=0.9082
9	Pipe Bend	D=1.25 , r_c=2.0
10	Vertical Pipe	D=1.25 , L=10.0
11	Pipe Bend	D=1.25 , r_c=2.0
12	Horizontal Pipe	D=1.25 , L=4.0

NOTE: A_{in} and A_{out} are in units of ft^2.
D, L, r_c, and d_O are in units of ft.

Pipeline 4

SECTION, j	DESCRIPTION	DIMENSIONS
1	Vertical Pipe	D=2.5 , L=4.0
2	Coal Riffler	A_{in}=4.91 , A_{out}=3.14
3	Vertical Pipe	D=2.0 , L=3.0
4	Coal Riffler	A_{in}=3.14 , A_{out}=1.23
5	Vertical Pipe	D=1.25 , L=6.0
6	Pipe Bend	D=1.25 , r_c=2.0
7	Horizontal Pipe	D=1.25 , L=30.0
8	Pipe Bend	D=1.25 , r_c=3.0
9	Horizontal Pipe	D=1.25 , L=20.0
10	Orifice Plate	D=1.25 , d_O=1.01
11	Pipe Bend	D=1.25 , r_c=2.0
12	Vertical Pipe	D=1.25 , L=9.0
13	Pipe Bend	D=1.25 , r_c=2.0
14	Horizontal Pipe	D=1.25 , L=4.0

NOTE: A_{in} and A_{out} are in units of ft^2.
D, L, r_c, and d_O are in units of ft.

APPENDIX 2 - Computer Code Subroutines

The burner balancing calculation procedure presented in this thesis has been developed into a FORTRAN computer code. A main program, MOWGLI, coordinates the general process through a series of DO LOOPS and control mechanisms as shown in the flow charts of Figures (5-1) and (5-3). However, the majority of the detailed, gas-solid flow calculations are performed in subroutines which are written specifically for a pipe section type (vertical pipe, bend, etc.). In addition, the root-finding and numerical integration routines needed to solve the expressions in Chapter 3 are also performed in subroutines. This Appendix provides a summary of the subroutines and functions used in MOWGLI.

A2.1 Subroutine VERN

The subroutine VERN is used to calculate the pressure drop experienced by the gas-solid flow in a vertical pipe. As input, it requires:

1.) The constant flow parameters:
   - air density
   - air viscosity
   - solid particle density
   - particle terminal velocity, U_t
   - mean particle diameter

2.) The relative roughness of the pipe wall. (For its derivation, see Appendix 3)

3.) An indicator which signals the need to perform acceleration calculations, based upon the location of the section in the

pipeline.

4.) The "section-specific" flow information:
- coal mass flow rate
- pipe diameter
- pipe length
- superficial air speed, U_o

This information is used in conjunction with the equations presented in Chapter 3 in the following manner. The group of expressions which describe the fully-accelerated particle velocity in vertical flow, Eqs. (3-2), (3-8), (3-11), and (3-14), are used to solve for the particle velocity. Since these 4 equations are interdependent, a root-solving technique is needed. The subroutine ZBRAK is called to determine which regions of the range from U_t to U_o contain a zero-crossing of the implicit particle velocity function. The actual root (i.e. $U_{p,v}$) within the region specified by ZBRAK is then determined by the function ZBRENT in conjunction with the function KONG, which is simply the 4 interrelated particle velocity equations and their resultant implicit function.

The air friction factor is calculated via the expressions developed in Appendix 3.

The acceleration length, if needed, is determined via the numerical integration scheme in the subroutine MIDPNT. MIDPNT uses the operational information and combines it with Eq. (3-17), presented in the function MAKO, to perform the integration. The lower integration limit is derived from Eq. (3-2) with the voidage coefficient set to a value of 0.65, indicating a dense-phase flow. The upper limit is equal to

95% of the fully-accelerated particle velocity, $U_{p,v}$. Since the integrating equation experiences a singularity as it approaches the actual particle velocity, the upper limit is set to 95% of the fully-accelerated particle velocity, $U_{p,v}$ [35].

If acceleration effects are present, then the effective length is calculated, as given by Eq. (3-19)

$$L_e = L - L_A \tag{3-19}$$

When the acceleration length is greater than the actual pipe length, the effective length is set equal to zero. And in situations where the flow has been fully-accelerated before it enters the current flow section, the effective length equals the actual pipe length.

Finally, the pressure drop calculations are performed. Eq. (3-24) is utilized for the acceleration pressure drop (if required). Due to the absence of information regarding $U_{p,v}$ as a function of the pipe length within the acceleration region, l, the integration of Eqs. (3-25) - (3-28) assumes the constant, fully-accelerated values for the variables in the integrated functions [35]. Thus, these integrals reduce to simple algebraic expressions. Then, using the effective length, the other components of the pressure drop are calculated from Eqs. (3-20), (3-22), and (3-23).

VERN returns the following information to the main

program MOWGLI:

1.) Fully-accelerated vertical particle velocity, $U_{p,v}$.

2.) Air friction coefficient, f_g.

3.) Voidage coefficient.

4.) Pressure drop components:
- acceleration
- static head
- air friction
- solids friction
- combined friction
- total

A2.2 Subroutine HOWIE

This subroutine performs the calculations pertaining to horizontal pipe sections and is very similar to subroutine VERN. The same information input to VERN is also supplied to HOWIE. Subroutine ZBRAK and the function ZBRENT are used to calculate the particle velocity, $U_{p,h}$, from the combination of Eqs. (3-2), (3-8), (3-12), and (3-15).

If acceleration effects are present, the same procedure followed by VERN is used in HOWIE, with Eq. (3-18) substituting for Eq. (3-17). And the total horizontal pressure drop is calculated in the same manner as VERN, with the exclusion of the static head contribution.

Finally, the parameters returned by HOWIE to MOWGLI are the same as those returned by VERN.

A2.3 Subroutine BENJI

This subroutine calculates the pressure drop in a pipe bend. As input, it receives the following information:

1.) The constant flow parameters:
    - air density
    - air viscosity
    - solid particle density
    - particle terminal velocity, U_t
    - mean particle diameter

2.) The "section-specific" data:
    - pipe diameter
    - bend radius of curvature
    - coal mass flow rate
    - superficial air velocity

Using this information, the routine calculates the pressure loss in the bend from the expressions presented in Chapter 3: Eqs. (3-30), (3-31), and (3-32). BENJI then returns this total bend pressure drop value to MOWGLI.

A2.4 Subroutine DRAC

This subroutine performs the calculations which are the crux of Part I of MOWGLI: determining the orifice plate sizes needed to provide balanced flow. As input, DRAC receives the following information:

1.) The pipe diameter

2.) The superficial air velocity

3.) The desired pressure drop

Using the method presented in Chapter 4, Eqs. (4-7) to (4-15) are solved to determine which size plate opening will produce the desired pressure drop. Since this process involves working backwards through this series of equations, a root-

finding technique is employed which requires the use of subroutine ZBRAK and function ZBRENT. To simplify this procedure, Eqs. (4-7) to (4-15) are listed and performed in the function VLAD.

When the orifice opening has been determined, DRAC returns this value to MOWGLI. In addition, if one plate cannot provide the desired pressure drop in the range of (d_o=D/2 to d_o=D), then this routine determines how many plates are required to achieve the necessary pressure loss. This value is also returned to MOWGLI.

A2.5 Function JAWS

The horizontal acceleration length equations are listed and executed in this function. Called by HOWIE and driven by the subroutine MIDPNT, this function performs the numerical integration of Eq. (3-18).

A2.6 Function KONG

The vertical, fully-accelerated particle speed equations are listed in this function. Called by VERN and manipulated by ZBRAK and ZBRENT, this function allows the implicit series of Eqs. (3-2), (3-8), (3-11), and (3-14) to be solved.

A2.7 Function MAKO

The vertical acceleration length equations are listed and executed in this function. Called by VERN and driven by

MIDPNT, this function performs the numerical integration of Eq. (3-17).

A2.8 Subroutine MIDPNT [36]

This subroutine is a numerical integration routine which computes the n^{th} stage of refinement of an extended midpoint integration rule. When it is called with n=1, the routine will return the crudest estimate for the integrated function. However, subsequent calculations with n=2,3,... (in that sequential order) improves the accuracy and can be easily performed in a DO LOOP. A convergence criterion is employed to halt the loop process when sufficient accuracy is achieved. As input, the subroutine needs:

1.) The lower and upper limits of integration.

2.) The stage of refinement, n.

3.) A integral function to operate on.

The routine returns to its caller the numerical value for the integral function at each stage of refinement, until sufficient accuracy is achieved.

A2.9 Subroutine OTTO

OTTO is used to calculate the pressure drop across an orifice plate. Thus, it is used in Part I of MOWGLI to verify that the "ideal" plates which are calculated by DRAC actually will provide the desired pressure drop. OTTO is also used in Part II to account for the presence of any currently existing

orifice plates in the pipeline distribution system.

As input, this subroutine requires:

1.) The pipe diameter in which the plate resides.

2.) The diameter of the plate opening.

3.) The superficial air velocity.

Then, using the series of equations presented in Chapter 4 (Eqs. (4-7) through (4-15)), the pressure drop across the plate is calculated. This value is then returned to MOWGLI.

A2.10 Function TREX

The horizontal, fully-accelerated particle speed expressions are listed in this function. Called by HOWIE and manipulated by ZBRAK and ZBRENT, this function allows the implicit series of Eqs. (3-2), (3-8), (3-12), and (3-15) to be solved.

A2.11 Function VLAD

This function is utilized by subroutine DRAC to calculate the orifice plate sizes which will provide the pressure drops required in Part I of MOWGLI. Due to the root-finding technique needed to solve Eqs. (4-7) through (4-15) for the plate opening diameter, DRAC calls ZBRAK and ZBRENT to determine the solution.

A2.12 Subroutine ZBRAK [36]

ZBRAK is a root-finding subroutine that divides an

interval into N equal parts and determines over which of these regions a zero-crossing of the function occurs. As input, it requires the following:

1.) Number of regions, N, to examine

2.) The interval of operation

3.) The function to be solved

It then returns to its caller the bracketed regions over which the zero-crossings occur.

A2.13 Function ZBRENT [36]

This function is used by the caller of ZBRAK to determine the exact solution of a function in the regions of zero-crossings provided by ZBRAK. ZBRENT utilizes Brent's method, which is a combination of bisection and inverse quadratic interpolation that converges upon the solution of a function in the neighborhood of a zero-crossing. The following input is required:

1.) The zero-crossing interval (supplied by ZBRAK).

2.) The maximum number of iterations to perform.

3.) The desired accuracy of the solution to the function.

4.) The function to be solved.

Since ZBRENT is an inherent part of a given routine which has called ZBRAK, its output is received by that same routine.

APPENDIX 3 - Gas Friction Factor

The pressure drop equations presented in Chapter 3 of this thesis make use of the gas friction factor, f_g. This coefficient effects the magnitude of the pressure loss experienced by the flow due to frictional resistance along the pipe walls. Thus, it depends upon the pipe geometry, air flow Reynolds number, and the surface roughness of the pipe material. Fox & McDonald [28] graphically present the Moody [37] data for the relative roughness, e/D, of common pipeline materials in *new* condition. The relative roughness value is then used in conjunction with the Reynolds number to graphically determine the friction factor for fully-developed flow in circular pipes, also based upon the data of Moody.

For this thesis, the following pipeline materials were considered: Commercial Steel, Wrought Iron, Cast Iron, Galvanized Iron, and Asphalted Cast Iron. The computer code developed in Chapter 5 requires the input of one of these materials for the calculation of the gas friction factor. Using curve-fits for the Moody data, the following equation is utilized by the program:

$$f_g = 0.25\left[\log\left(\frac{e/D}{3.7} + \frac{5.74}{Re^{0.9}}\right)\right]^{-2.0} \qquad \text{(A3-1)}$$

Thus, for each calculation which requires this factor, the

pipe diameter of the section and its superficial air velocity are needed. The relative roughness value depends upon the type of pipeline material, as given in the table below.

MATERIAL TYPE	ROUGHNESS (feet)
Commercial Steel	0.00015
Wrought Iron	0.00015
Galvanized Iron	0.00050
Cast Iron	0.00085
Asphalted Cast Iron	0.00040

Along with the Reynolds number, Eq. (A3-1) is solved using the appropriate roughness value, e, and dividing it by the pipe diameter (in feet).

APPENDIX 4 - Tabulated Data for Chapter 6

This information pertains to the sensitivity analysis in Chapter 6. For each case considered, the following variables are listed:

m coal = Coal mass flow rate
m air = Air mass flow rate
Yi coal = Coal mass fraction
Dev. = Coal flow deviation
A/F = Air-to-fuel ratio

The baseline values are:

Pipe Number	m coal [lbm/s]	m air [lbm/s]	Yi coal	Dev. [%]	A/F Ratio
1	2.9998	6.3510	0.2500	-0.0067	2.1171
2	2.9999	6.3510	0.2500	-0.0033	2.1171
3	3.0002	6.3510	0.2500	0.0067	2.1169
4	3.0001	6.3510	0.2500	0.0033	2.1169

A4.1 Variations in Operating Parameters

A4.1.1 Air Temperature=145°F

Method I

Pipe Number	m coal [lbm/s]	m air [lbm/s]	Yi coal	Dev. [%]	A/F Ratio
1	3.0496	6.5610	0.2541	1.6537	2.1514
2	2.9946	6.5610	0.2495	-0.1813	2.1910
3	2.9375	6.5610	0.2448	-2.0837	2.2335
4	3.0183	6.5610	0.2515	0.6113	2.1737

Method II

Pipe Number	m coal [lbm/s]	m air [lbm/s]	Yi coal	Dev. [%]	A/F Ratio
1	2.7782	6.6094	0.2315	-7.3933	2.3790
2	3.1221	6.5295	0.2602	4.0697	2.0914
3	3.2617	6.5067	0.2718	8.7220	1.9949
4	2.8381	6.5877	0.2365	-5.3983	2.3212

A4.1.2 Air Temperature=155°F

Method I

Pipe Number	m coal [lbm/s]	m air [lbm/s]	Yi coal	Dev. [%]	A/F Ratio
1	3.0265	6.4543	0.2522	0.8823	2.1326
2	2.9949	6.4543	0.2496	-0.1717	2.1551
3	2.9722	6.4543	0.2477	-0.9257	2.1715
4	3.0065	6.4543	0.2505	0.2153	2.1468

Method II

Pipe Number	m coal [lbm/s]	m air [lbm/s]	Yi coal	Dev. [%]	A/F Ratio
1	2.7719	6.5019	0.2310	-7.6023	2.3456
2	3.1170	6.4233	0.2597	3.8990	2.0608
3	3.2706	6.4209	0.2725	9.0187	1.9632
4	2.8405	6.4806	0.2367	-5.3153	2.2815

A4.1.3 Air Temperature=175°F

Method I

Pipe Number	m coal [lbm/s]	m air [lbm/s]	Yi coal	Dev. [%]	A/F Ratio
1	2.9764	6.2510	0.2480	-0.7853	2.1002
2	3.0043	6.2510	0.2504	0.1440	2.0807
3	3.0276	6.2510	0.2523	0.9193	2.0647
4	2.9917	6.2510	0.2493	-0.2780	2.0895

Method II

Pipe Number	m coal [lbm/s]	m air [lbm/s]	Yi coal	Dev. [%]	A/F Ratio
1	2.7628	6.2971	0.2302	-7.9057	2.2792
2	3.1017	6.2210	0.2585	3.3910	2.0057
3	3.2827	6.1993	0.2736	9.4243	1.8884
4	2.8527	6.2765	0.2377	-4.9097	2.2002

A4.1.4 Air Temperature=185°F

Method I

Pipe Number	m coal [lbm/s]	m air [lbm/s]	Yi coal	Dev. [%]	A/F Ratio
1	2.9494	6.1540	0.2458	-1.6857	2.0865
2	3.0015	6.1540	0.2501	0.0493	2.0503
3	3.0605	6.1540	0.2550	2.0153	2.0108
4	2.9886	6.1540	0.2491	-0.3790	2.0591

Method II

Pipe Number	m coal [lbm/s]	m air [lbm/s]	Yi coal	Dev. [%]	A/F Ratio
1	2.7602	6.1995	0.2300	-7.9920	2.2460
2	3.0919	6.1246	0.2577	3.0640	1.9808
3	3.2864	6.1032	0.2739	9.5460	1.8571
4	2.8615	6.1792	0.2385	-4.6183	2.1595

A4.1.5 25% Load (C.E. data)

Method I

Pipe Number	m coal [lbm/s]	m air [lbm/s]	Yi coal	Dev. [%]	A/F Ratio
1	0.8947	4.4730	0.2982	19.2893	4.9996
2	0.6646	4.4730	0.2215	-11.3893	6.7306
3	0.5967	4.4730	0.1989	-20.4360	7.4959
4	0.8440	4.4730	0.2813	12.5360	5.2996

Method II

Pipe Number	m coal [lbm/s]	m air [lbm/s]	Yi coal	Dev. [%]	A/F Ratio
1	0.6343	4.5076	0.2114	-15.4213	7.1060
2	0.7891	4.4531	0.2630	5.2080	5.6436
3	0.8881	4.4376	0.2960	18.4093	4.9968
4	0.6995	4.4928	0.2332	-6.7280	6.4225

A4.1.6 50% Load (C.E. data)

Method I

Pipe Number	m coal [lbm/s]	m air [lbm/s]	Yi coal	Dev. [%]	A/F Ratio
1	1.4989	5.4840	0.2498	-0.0767	3.6588
2	1.4636	5.4840	0.2439	-2.4293	3.7470
3	1.5068	5.4840	0.2511	0.4547	3.6395
4	1.5308	5.4840	0.2551	2.0513	3.5825

Method II

Pipe Number	m coal [lbm/s]	m air [lbm/s]	Yi coal	Dev. [%]	A/F Ratio
1	1.2735	5.5254	0.2123	-15.0973	4.3386
2	1.4133	5.4587	0.2355	-5.7833	3.8625
3	1.9730	5.4396	0.3288	31.5340	2.7570
4	1.3402	5.5074	0.2234	-10.6527	4.1093

A4.1.7 75% Load (C.E. data)

Method I

Pipe Number	m coal [lbm/s]	m air [lbm/s]	Yi coal	Dev. [%]	A/F Ratio
1	2.2929	6.0730	0.2548	1.9067	2.6486
2	2.2164	6.0730	0.2463	-1.4924	2.7400
3	2.2005	6.0730	0.2445	-2.1982	2.7598
4	2.2901	6.0730	0.2545	1.7836	2.6518

Method II

Pipe Number	m coal [lbm/s]	m air [lbm/s]	Yi coal	Dev. [%]	A/F Ratio
1	2.0709	6.1187	0.2301	-7.9622	2.9547
2	2.3195	6.0448	0.2577	3.0907	2.6060
3	2.4654	6.0236	0.2739	9.5733	2.4433
4	2.1442	6.0987	0.2382	-4.7018	2.8442

A4.1.8 25% Load (Constant A/F)

Method I

Pipe Number	m coal [lbm/s]	m air [lbm/s]	Yi coal	Dev. [%]	A/F Ratio
1	0.6858	1.5877	0.2286	-8.5613	2.3151
2	0.7904	1.5877	0.2635	5.3853	2.0088
3	0.8150	1.5877	0.2717	8.6680	1.9481
4	0.7088	1.5877	0.2363	-5.4920	2.2400

Method II

Pipe Number	m coal [lbm/s]	m air [lbm/s]	Yi coal	Dev. [%]	A/F Ratio
1	0.6590	1.5995	0.2197	-12.1320	2.4271
2	0.7917	1.5801	0.2639	5.5613	1.9959
3	0.8547	1.5746	0.2849	13.9653	1.8422
4	0.6945	1.5942	0.2315	-7.3947	2.2954

A4.1.9 50% Load (Constant A/F)

Method I

Pipe Number	m coal [lbm/s]	m air [lbm/s]	Yi coal	Dev. [%]	A/F Ratio
1	1.4243	3.1755	0.2374	-5.0460	2.2295
2	1.5658	3.1755	0.2610	4.3853	2.0281
3	1.5768	3.1755	0.2628	5.1187	2.0139
4	1.4340	3.1755	0.2390	-4.3980	2.2144

Method II

Pipe Number	m coal [lbm/s]	m air [lbm/s]	Yi coal	Dev. [%]	A/F Ratio
1	1.3221	3.1989	0.2203	-11.8633	2.4197
2	1.6068	3.1603	0.2678	7.1207	1.9668
3	1.6971	3.1492	0.2828	13.1380	1.8557
4	1.3741	3.1885	0.2290	-8.3953	2.3204

A4.1.10 75% Load (Constant A/F)

Method I

Pipe Number	m coal [lbm/s]	m air [lbm/s]	Yi coal	Dev. [%]	A/F Ratio
1	2.2501	4.7632	0.2500	0.0022	2.1169
2	2.3015	4.7632	0.2557	2.2876	2.0696
3	2.2467	4.7632	0.2496	-0.1462	2.1201
4	2.2018	4.7632	0.2446	-2.1436	2.1634

Method II

Pipe Number	m coal [lbm/s]	m air [lbm/s]	Yi coal	Dev. [%]	A/F Ratio
1	2.0186	4.7984	0.2243	-10.2853	2.3771
2	2.4210	4.7404	0.2690	7.5982	1.9581
3	2.4934	4.7238	0.2770	10.8182	1.8945
4	2.0671	4.7827	0.2297	-8.1311	2.3138

A4.2 Variation of Model Assumptions

A4.2.1 50 micron Particle Size

Method I

Pipe Number	m coal [lbm/s]	m air [lbm/s]	Yi coal	Dev. [%]	A/F Ratio
1	3.1421	6.3510	0.2618	4.7380	2.0212
2	3.0101	6.3510	0.2508	0.3360	2.1099
3	2.8407	6.3510	0.2367	-5.3097	2.2357
4	3.0071	6.3510	0.2506	0.2357	2.1120

Method II

Pipe Number	m coal [lbm/s]	m air [lbm/s]	Yi coal	Dev. [%]	A/F Ratio
1	2.7667	6.3979	0.2306	-7.7763	2.3124
2	3.2016	6.3206	0.2668	6.7187	1.9742
3	3.2503	6.2985	0.2709	8.3417	1.9378
4	2.7815	6.3769	0.2318	-7.2840	2.2926

A4.2.2 65 micron Particle Size

Method I

Pipe Number	m coal [lbm/s]	m air [lbm/s]	Yi coal	Dev. [%]	A/F Ratio
1	3.1544	6.3510	0.2629	5.1460	2.0134
2	3.0102	6.3510	0.2509	0.3403	2.1098
3	2.8284	6.3510	0.2357	-5.7217	2.2455
4	3.0071	6.3510	0.2506	0.2350	2.1120

Method II

Pipe Number	m coal [lbm/s]	m air [lbm/s]	Yi coal	Dev. [%]	A/F Ratio
1	2.7702	6.3979	0.2309	-7.6590	2.3095
2	3.2037	6.3206	0.2670	6.7910	1.9729
3	3.2460	6.2985	0.2705	8.2003	1.9404
4	2.7800	6.3769	0.2317	-7.3323	2.2938

A4.2.3 100 micron Particle Size

Method I

Pipe Number	m coal [lbm/s]	m air [lbm/s]	Yi coal	Dev. [%]	A/F Ratio
1	3.1357	6.3510	0.2613	4.5237	2.0254
2	3.0040	6.3510	0.2503	0.1330	2.1142
3	2.8473	6.3510	0.2373	-5.0887	2.2305
4	3.0130	6.3510	0.2511	0.4323	2.1079

Method II

Pipe Number	m coal [lbm/s]	m air [lbm/s]	Yi coal	Dev. [%]	A/F Ratio
1	2.7713	6.3979	0.2309	-7.6240	2.3086
2	3.1947	6.3206	0.2662	6.4910	1.9784
3	3.2489	6.2985	0.2707	8.2960	1.9387
4	2.7851	6.3769	0.2321	-7.1630	2.2897

A9/2.4 Roughness, e/D=0.00015

Method I

Pipe Number	m coal [lbm/s]	m air [lbm/s]	Yi coal	Dev. [%]	A/F Ratio
1	3.6114	6.3510	0.3010	20.3813	1.7586
2	3.1030	6.3510	0.2586	3.4320	2.0468
3	2.1842	6.3510	0.1820	-27.1950	2.9078
4	3.1014	6.3510	0.2585	3.3813	2.0478

Method II

Pipe Number	m coal [lbm/s]	m air [lbm/s]	Yi coal	Dev. [%]	A/F Ratio
1	3.4630	6.3979	0.2886	15.4323	1.8475
2	3.1480	6.3206	0.2623	4.9327	2.0078
3	2.4494	6.2985	0.2041	-18.3530	2.5714
4	2.9396	6.3769	0.2450	-2.0120	2.1693

A9/2.5 Roughness, e/D=0.0004

Method I

Pipe Number	m coal [lbm/s]	m air [lbm/s]	Yi coal	Dev. [%]	A/F Ratio
1	3.2607	6.3510	0.2717	8.6887	1.9478
2	3.0355	6.3510	0.2530	1.1847	2.0922
3	2.6664	6.3510	0.2222	-11.1213	2.3819
4	3.0374	6.3510	0.2531	1.2480	2.0909

Method II

Pipe Number	m coal [lbm/s]	m air [lbm/s]	Yi coal	Dev. [%]	A/F Ratio
1	3.0629	6.3979	0.2552	2.0967	2.0888
2	3.1168	6.3206	0.2597	3.8917	2.0279
3	2.9460	6.2985	0.2455	-1.8010	2.1380
4	2.8744	6.3769	0.2395	-4.1870	2.2185

A9/2.6 Roughness, e/D=0.0005

Method I

Pipe Number	m coal [lbm/s]	m air [lbm/s]	Yi coal	Dev. [%]	A/F Ratio
1	3.3481	6.3510	0.2790	11.6027	1.8969
2	3.0515	6.3510	0.2543	1.7173	2.0813
3	2.5565	6.3510	0.2130	-14.7843	2.4843
4	3.0439	6.3510	0.2537	1.4643	2.0864

Method II

Pipe Number	m coal [lbm/s]	m air [lbm/s]	Yi coal	Dev. [%]	A/F Ratio
1	3.1633	6.3979	0.2636	5.4440	2.0225
2	3.1217	6.3206	0.2601	4.0550	2.0247
3	2.8267	6.2985	0.2356	-5.7767	2.2282
4	2.8883	6.3769	0.2407	-3.7220	2.2078

A4.3 Variation of Bend Pressure Drop Correlation

A4.3.1 Schuchart

Method I

Pipe Number	m coal [lbm/s]	m air [lbm/s]	Yi coal	Dev. [%]	A/F Ratio
1	2.5609	6.3510	0.2134	-14.6383	2.4800
2	3.4134	6.3510	0.2844	13.7783	1.8606
3	3.4940	6.3510	0.2912	16.4660	1.8177
4	2.5318	6.3510	0.2110	-15.6063	2.5085

Method II

Pipe Number	m coal [lbm/s]	m air [lbm/s]	Yi coal	Dev. [%]	A/F Ratio
1	2.3954	6.3843	0.1996	-20.1530	2.6652
2	3.4496	6.3405	0.2875	14.9867	1.8380
3	3.6570	6.3131	0.3048	21.9010	1.7263
4	2.4980	6.3559	0.2082	-16.7347	2.5444

A4.3.2 Mason & Smith

Method I

Pipe Number	m coal [lbm/s]	m air [lbm/s]	Yi coal	Dev. [%]	A/F Ratio
1	3.7189	6.3510	0.3099	23.9630	1.7078
2	2.2720	6.3510	0.1893	-24.2680	2.7954
3	2.1989	6.3510	0.1832	-26.7023	2.8882
4	3.8102	6.3510	0.3175	27.0073	1.6668

Method II

Pipe Number	m coal [lbm/s]	m air [lbm/s]	Yi coal	Dev. [%]	A/F Ratio
1	2.2759	6.6248	0.1897	-24.1383	2.9109
2	3.1512	6.0973	0.2626	5.0413	1.9349
3	4.2283	6.0754	0.3524	40.9433	1.4368
4	2.3446	6.5963	0.1954	-21.8467	2.8134

A4.4 Clean Air Assumption

Pipe Number	m coal [lbm/s]	m air [lbm/s]	Yi coal	Dev. [%]	A/F Ratio
1	2.6881	6.3510	0.2240	-10.3963	2.3626
2	3.1584	6.3510	0.2632	5.2797	2.0108
3	3.3510	6.3510	0.2793	11.7013	1.8952
4	2.8025	6.3510	0.2335	-6.5847	2.2662

VITA

The author was born January 20, 1969 to Alice and Charles Curran, and was raised in Philadelphia, PA. He attended Father Judge High School in Philadelphia, and graduated in 1986 as class valedictorian.

In the Fall of 1986, the author enrolled in the College of Engineering and Science of Lehigh University. He received the Bachelor of Science degree in mechanical engineering from Lehigh in May of 1990.

Upon graduating, the author accepted a research assistantship with Lehigh's Energy Research Center and began graduate studies in Lehigh's mechanical engineering department. He will receive the Master of Science degree in mechanical engineering in May of 1992, and hopes to pursue an engineering career in the field of energy systems and power production.

END

OF

TITLE